Crafting Nanostructured Neural Interfaces with Hydrogel Particles

A Dissertation Presented for the

Doctor of Philosophy

Degree

The University of Tennessee, Knoxville

Emily Ann Morin

August 2017

Copyright © 2017 Emily Ann Morin

All rights reserved.

To my parents and sister,

Ann, Dave, & Olivia

and to Michael.

ACKNOWLEDGEMENTS

Above all, I would like to express my sincere gratitude to my advisor, Dr. Wei He, who, beyond everything, taught me patience. I would also like to thank my committee members, Dr. Madhu Dhar, Dr. Andy Sarles, and Dr. Xiaopeng Zhao for their critical contributions to my research.

I am especially thankful to Dr. John Dunlap for his constant technical support and for creating a welcoming environment at the University of Tennessee-Oak Ridge National Lab Joint Institute for Advanced Materials.

My gratitude is extended to Dr. Scott Lenaghan for his technical assistance and mentorship, Dr. Libby Barker for her mentorship, Dr. Bin Zhao for his technical and equipment assistance, Dr. Anming Hu for allowing me to use his Inkjet printing equipment, Dr. Ryan Fuierer from Asylum Research for his help with AFM analysis, Mr. Daniel P. Graham from the machine shop, Mr. Doug Fielden for his support with lab equipment, and Mr. Gregory Jones from the safety office for providing constant technical support. I am also thankful to Ms. Carla Lawrence, Ms. Tonya Brewer, Ms. Tracy Lee, Ms. Kam Manuel, Ms. Kathy Williams, Ms. Janet Carnes, Mr. Frank Holiway, and Mr. Randy Stooksbury for their administrative support.

Many thanks to my labmates, collaborators, and all those who helped me with my dissertation work and throughout graduate school: Dr. Lu Huang, Dr. Shuangcheng Tang, Dr. Larissa Capeletti, Ms. Katie Lou Rogers, Dr. Roger Wright, Dr. Wenxin Fu, Mr. Yongchao Yu, Dr. Graham Taylor, Dr. Guru Venkatesan, Dr. Mary-Anne Nguyen, Dr. Kimberly Sheldon, Mr. Trevor Grieco, Mr. Michael LaCour, Mr. Ian Zellar, and Mr. Mark Gragston, Mr. Andrew Kaminsky. Finally, I would like to thank my parents, sister

and friends for providing me with love and constant encouragement.

My final appreciation goes to the National Science Foundation (NSF) for funding support (CAREER Award DMR-1055208), the Program for Excellence and Equity in Research funded by NIGMS of the National Institutes of Health - IMSD training grant to the University of Tennessee-Knoxville under Award No. R25-GM086761, and the Center for Materials Processing at the University of Tennessee-Knoxville.

ABSTRACT

Central nervous system neural device functionality hinges on effective communication with surrounding neurons. This depends on both the permissiveness of the device material to promote neuron integration and the ability of the device to avoid a chronic inflammatory response. Here, a facile approach has been developed exploring the multiple functionalities of hydrogel particles to provide cues to impart neural integration for such materials. Three distinct, yet interconnected tasks were undertaken: investigating hydrogel particle-modified substrate neuron integration and central nervous system inflammatory response, investigating guided hydrogel particle adsorption, and investigating hydrogel particles as local reservoirs for counteracting adverse effects from oxidative species.

The potential of hydrogel particle modification on planar substrates and subsequent cell response to such substrates was investigated. The particle adsorption process can be tuned to control particle surface density by varying the adsorption time and the concentration of the original colloidal suspension. Using the PC12 cell line and primary cortical neurons derived from chick embryo, the particle-adsorbed surface readily supported robust cell adhesion and differentiation. For central nervous system inflammatory cell types NIH 3T3, RAW 264.7, and A172, the hydrogel particle-modified substrates elicited cell adhesion, sustained cell metabolic activity, while RAW 264.7 and A172 cells did not morphologically appear activated.

Hydrogel particles were investigated as directional cues for neuron adhesion and growth. PC12 cells preferentially adhered to HP-patterned regions of LbL-primed substrates. PC12 cell neurite outgrowth did not preferentially extend along the edge of

stripe patterns, which may be due to selected pattern width and spacing.

Potential of hydrogel particles to provide local therapeutic utility to combat oxidative stress was investigated with the neuroprotective antioxidant resveratrol. Results demonstrated that resveratrol could be loaded into free and surface-adsorbed hydrogel particles. The loaded resveratrol remained bioactive overtime and could provide antioxidant activity to PC12 cells following an oxidative stress trigger.

Collectively, these results help lay the groundwork to design the hydrogel particle system for future in vitro and in vivo investigations to ultimately realize stable long-term neural device communication.

TABLE OF CONTENTS

CHAPTER ONE INTRODUCTION AND LITERATURE REVIEW 1

1.1 Cell Response to Central Nervous System Neural Implants 2

1.1.1 Neuron Integration 3

1.1.2 Astroglial Reactivity Attenuation 5

1.2 Characteristics of Hydrogel Particles and Their Potential for Nanostructured Neural Interfaces 6

1.2.1 Size Considerations 6

1.2.2 Charge Considerations 7

1.2.3 Mechanical Properties 8

1.2.4 Responsiveness 10

1.2.5 Guided Particle Adsorption 11

1.3 Vision 12

1.4 Scientific Gaps and Objectives 13

1.4.1 Scientific Gaps 13

1.4.2 Research Objectives 14

1.5 Document Overview 15

CHAPTER TWO ADSORPTION OF CATIONIC HYDROGEL PARTICLES ONTO SOLID PLANAR SURFACES AND EFFECTS ON NEURONAL AND GLIAL CELL RESPONSES 16

2.1 Neuronal Integration Towards Hydrogel Particle-Modified Solid Planar Substrate 16

2.1.1 Introduction 16

2.1.2 Materials and Methods 19
2.1.2a Cationic Hydrogel Particle Synthesis and Characterization 19
2.1.2b Deposition of Particles on Planar Substrates and Characterization ... 19
2.1.2c PC12 Cell Culture 21
2.1.2d Primary Cortical Neuron Culture 23
2.1.2e Statistics 24
2.1.3 Results and Discussion 24
2.1.3a Hydrogel Particle Adsorption on Planar Substrates 24
2.1.3b Surface Wettability 35
2.1.3c Effects on Neuronal Cell Adhesion 38
2.1.3d Effects on Neuronal Cell Differentiation 40
2.1.3e Response of Primary Cortical Neurons to Adsorbed Hydrogel Particles 47
2.1.4 Conclusions 50
2.2 Central Nervous System Foreign Body Response Towards Hydrogel Particle-Modified Solid Planar Substrate 51
2.2.1 Introduction 51
2.2.2 Materials and Methods 54
2.2.2a Preparation and Characterization of Hydrogel Particle-Modified Planar Substrates 54
2.2.2b NIH 3T3 Cell Culture 54
2.2.2c RAW 264.7 Cell Culture 56
2.2.2d A172 Cell Culture 59

2.2.2e Statistics 60
2.2.3 Results and Discussion 60
2.2.3a Fibroblast Adhesion 60
2.2.3b Fibroblast Proliferation 63
2.2.3c Macrophage Adhesion 66
2.2.3d Macrophage Proliferation, Pro-Inflammatory Tumor Necrosis Factor-Alpha Expression, and HLA-DR expression 66
2.2.3e Astrocyte Adhesion 73
2.2.3f Astrocyte Proliferation and Glial Fibrillary Acidic Protein Expression 73
2.2.4 Conclusions 79
2.3 Cell-Cell Influences of Primary Cortical Neurons and A172 Cells on Hydrogel Particle-Modified Solid Planar Substrate 80
2.3.1 Introduction 80
2.3.2 Materials and Methods 81
2.3.2a Primary Cortical Neuron and A172 Co-Culture 81
2.3.2b Statistics 82
2.3.3 Results and Discussion 83
2.3.3a Cell Density 83
2.3.3b Cell-Cell Association 86
2.3.4 Conclusions 89
2.4 Conclusions and Future Work 89
CHAPTER THREE GUIDED PARTICLE ADSORPTION FOR DIRECTIONAL NEURONAL GROWTH 91

3.1 Introduction 91
3.2 Materials and Methods 92
3.2.1 Microfluidic Printing Technique 92
3.2.2 Microcontact Printing Technique 94
3.2.3 Microextrusion Printing Technique 94
3.2.4 PC12 Cell Culture 97
3.3 Results and Discussion 98
3.3.1 Microfluidic Printing Technique 98
3.3.2 Microcontact Printing Technique 100
3.3.3 Microextrusion Printing Technique 103
3.4 Conclusions and Future Work 103
CHAPTER FOUR CONTROLLED RELEASE OF THERAPEUTICS FROM SURFACE-ADSORBED HYDROGEL PARTICLES FOR LOCALIZED NEUROPROTECTION 107
4.1 Introduction 107
4.2 Materials and Methods 108
4.2.1 Loading Capabilities of Free Hydrogel Particles 108
4.2.2 Loading Capabilities of Surface-Adsorbed Hydrogel Particles 109
4.2.3 Bioactivity of Free and Surface-Adsorbed Hydrogel Particles 110
4.2.4 PC12 Cell Culture 111
4.2.5 Statistics 113
4.3 Results and Discussion 114
4.3.1 Loading Capabilities of Surface-Adsorbed Hydrogel Particles 114

4.3.2 Resveratrol Loading into Hydrogel Particles in Suspension.....116
4.3.3 Characterization of Resveratrol-Loaded Surface-Adsorbed Hydrogel Particles 120
4.3.4 Surface Interaction of Neuron and Resveratrol-Loaded Hydrogel Particles 120
4.3.5 Neuroprotective Effect of Resveratrol-Loaded Surface-Adsorbed Hydrogel Particles 127
4.4 Conclusions and Future Work.....132
CHAPTER FIVE CONCLUSIONS AND RECOMMENDATIONS.....133
LIST OF REFERENCES 136
VITA.....148

LIST OF FIGURES

Figure 1 The ECM guides axons of maturing neurons during development toward their proper targets (figure from [17]). 4

Figure 2 Scale illustrating the elastic modulus of natural brain and man-made materials (figure from [45]). 9

Figure 3 Chemical structure and physical appearance of aqueous dispersion of the HPs (left) as well as their intensity-average hydrodynamic size distribution (middle) and zeta potential in water (right).....26

Figure 4 Scanning electron micrographs of the LbL and LbL/HP finished samples.....27

Figure 5 Scanning electron micrographs of various LbL-primed surfaces. 29

Figure 6 Adsorbed HP height (left) and corresponding modulus (right), (red line in above images corresponds to analyzed data in graph below).....30

Figure 7 Scanning electron micrographs and schematic of LbL/HP-coated silicon substrate before and after insertion into agarose hydrogel.....31

Figure 8 Number density of adsorbed HPs and the surface area coverage by HPs as a function of (A) HP suspension concentration and (B) incubation time for adsorption (*p < 0.01). Insets: binary images of representative scanning electron micrographs. 32

Figure 9 PEGDE particle intensity-average hydrodynamic size distribution (left) and zeta potential in water (right). 34

Figure 10 Scanning electron micrographs of the LbL/HP and LbL/PEGDE surfaces displaying similar particle surface coverage. 36

Figure 11 Water contact angle measurements and representative photographs (side view) of water droplets on plain silicon and silicon with various surface

modifications. 37
Figure 12 Representative phase contrast images of PC12 cell adhesion and quantitative adherent cell density on various surfaces (*p < 0.01, compared to glass)..39
Figure 13 Live/dead images of PC12 cells attached to LbL/HP and LbL/PEI-modified surfaces (Viable cells: green, Damaged cells: red).....41
Figure 14 Quantitative adherent PC12 cell density on LbL/PEGDE and control substrates with representative phase contrast images (*p < 0.05, compared to glass, error reported as ± standard deviation). 42
Figure 15 PC12 cell morphology after 48 h of culture in NGF-supplemented media (72 h of culture total) on (A-D) the LbL/HP surface and (E-H) the LbL/PEI control surface. (A, E) Phase contrast images; (B, F) fluorescent images of cells stained for α-tubulin (green), actin filaments (red), and nuclei (blue); (C, D, G, H) scanning electron micrographs of fixed cells.....44
Figure 16 Percentages of PC12 cells at various differentiation stages following 48 h of culture in NGF-supplemented media (72 h of culture total) on the LbL/HP and LbL/PEI surfaces. Fluorescent images of cells stained for α-tubulin (green) and nuclei (blue) represent typical cell morphology at the corresponding stage. The total number of cells analyzed was 679 for the LbL/HP sample and 618 for the LbL/PEI sample. 46
Figure 17 Response of primary chick cortical neurons to the LbL/HP surface. (A-C) Phase contrast images of cells at (A) 24 h, (B) 48 h, and (C) 72 h of culture. (D) Fluorescent staining of cells after 72 h culture (α-tubulin, green; nuclei, blue). (E, F) Scanning electron micrographs of cells fixed at 72 h of culture.

.....48
Figure 18 Phase contrast images of chick cortical neurons on the LbL/PEI surface at (A) 24 h, (B) 48 h, and (C) 72 h of culture. 49
Figure 19 Quantitative 4 h NIH 3T3 cell adhesion density on LbL/HP and control substrates (*p < 0.05, compared to silicon) with representative fluorescent images of the cells stained for actin filaments (red) and nuclei (blue). 61
Figure 20 Representative phase contrast images of NIH 3T3 cells on LbL/HP and control substrates for 1 – 3 days of culture. 64
Figure 21 WST-1 assay quantified metabolic activity of NIH 3T3 cells for 1 – 3 days in culture on LbL/HP and control substrates (*p < 0.05, compared to glass at each time point). 65
Figure 22 Quantitative 2 h RAW 264.7 cell adhesion density on LbL/HP and control substrates with representative fluorescent images of the cells stained for actin filaments (red) and nuclei (blue). 67
Figure 23 (A) TNF-α secretion and (B) quantification of total protein for RAW 264.7 cells cultured for 1 – 3 days on silicon and LbL/HP silicon substrates (*p < 0.05, **p < 0.01 compared to silicon at each time point). (C) Representative SEM images of RAW 264.7 cells cultured for 1 – 3 days on silicon and LbL/HP silicon substrates. 69
Figure 24 Percent RAW 264.7 cells expressing elevated HLA-DR signal after 48 h with representative images (HLA-DR: red, nuclei: blue) (*p < 0.05, compared to glass + LPS).....70
Figure 25 Scanning electron micrographs of Day 3 LbL/HP substrate before and after

total protein cell lysis assay. 72
Figure 26 Quantitative 4 h A172 cell adhesion density on LbL/HP and control substrates (*p < 0.05, compared to silicon) with representative fluorescent images of the cells stained for actin filaments (red) and nuclei (blue). 74
Figure 27 Representative phase contrast images of A172 cells on LbL/HP and control substrates for 1 – 3 days of culture. 75
Figure 28 WST-1 assay quantified metabolic activity of A172 cells for 1 – 3 days in culture on LbL/HP and control substrates. 76
Figure 29 (A) Representative fluorescent images (GFAP: green, nuclei: blue) and processed inverted gray scale images of A172 cells on glass and LbL/HP glass substrates after 3 days in culture. (B) GFAP expression quantified as average fluorescent intensity per cell. 78
Figure 30 Representative fluorescent images of primary chick cortical neurons and A172 cells on LbL/HP and control substrates over 3-day co-culture (GFAP: red, α-tubulin: green, nuclei: blue). 84
Figure 31 Primary chick cortical neuron adherent cell density on LbL/HP and control substrates for 3-day co-culture (*p < 0.05, compared to glass at each time point). 85
Figure 32 A172 adherent cell density on LbL/HP and control substrates for 3-day co-culture (*p < 0.05, compared to glass at each time point). 87
Figure 33 Percent primary chick cortical neuron association with A172 cells after 4 h co-culture (*p < 0.01, compared to glass for each condition). 88
Figure 34 Schematic of microfluidic printing device fabrication process and technique. 93

Figure 35 Schematic of microcontact printing device technique. 95
Figure 36 Schematic of microextrusion printing device technique. 96
Figure 37 Microfluidic printing technique phase contrast images of (A) HP-patterned surface edge, (B) PC12 cells near HP-patterned surface edge after 24 h and (C) NGF-induced PC12 cells near HP-patterned surface edge after 72 h. Yellow dashed line signifies HP-pattern edge.....99
Figure 38 Microcontact printing technique (A) SEM image of LP record master template, (B) fluorescent image of FITC-BSA (green) patterned substrate, and (C) phase contrast image of HP-patterned substrate. Yellow dashed line signifies pattern edge.....101
Figure 39 Microcontact printing technique (A) phase contrast image of PC12 cells on HP-patterned surface after 24 h and (B,C) NGF-induced PC12 cells on HP-patterned surface after 72 h. Yellow dashed line signifies HP-pattern edge. 102
Figure 40 Microextrusion printing technique (A) photograph of patterned dyed alginate-PSS ink, (B) phase contrast image of HP-patterned surface edges, and (C) SEM image of HP-patterned surface edge. Yellow dashed line signifies HP-pattern edge.....104
Figure 41 Microextrusion printing technique (A,B) phase contrast images of NGF-induced PC12 cells near HP-patterned surface edge after 72 h and (C,D,E) SEM images of NGF-induced PC12 cells near HP-patterned surface edge after 72 h. Yellow dashed line signifies HP-pattern edge. 105
Figure 42 Fluorescent images of LbL/HP and LbL/PEI-modified planar silicon substrates

after incubation in nile red solution. 115
Figure 43 Intensity-average hydrodynamic size distribution of blank (HP) and RES-loaded HPs (RES HP) in water. 117
Figure 44 Chemical structure of RES. 118
Figure 45 Activity of RES-loaded HPs and controls reacted with DPPH. 119
Figure 46 Stability of free RES and RES loaded to HPs over time (*p < 0.05, comparison between samples at each time point). 121
Figure 47 Representative scanning electron micrographs of unloaded LbL/HP and RES-loaded LbL/HP substrates. 122
Figure 48 Representative 3D and 2D topographical images of silicon LbL/HP and RES-loaded LbL/HP substrates with line profile analysis (line profile analysis corresponds to the 2D image red line). 123
Figure 49 Activity of unloaded LbL/HP and RES-loaded LbL/HP substrates. 124
Figure 50 Water contact angle measurements and representative photographs (side view) of water droplets on RES-loaded LbL/HP and control substrates. ..125
Figure 51 Representative phase contrast images of PC12 cell adhesion and quantitative adherent cell density on RES-loaded LbL/HP surfaces and controls after 24 h. 126
Figure 52 Percent PC12 cell damage as a function of H_2O_2 concentration with representative phase contrast images. Scanning electron microscope image of LbL/HP substrate incubated in 1.05 mM H_2O_2 for 2 h (inset). 128
Figure 53 (A) Quantification of metabolically active PC12 cells after treatment for 2 h. Representative phase contrast images of cell morphology (B) -H_2O_2; -RES,

(C) +H_2O_2; -RES, (D) +H_2O_2; +RES (free), (E) +H_2O_2; +RES (LbL/HP). (*p < 0.05, compared to no treatment).....130

Figure 54 (A) Quantification PC12 cells presenting DCF signal after treatment for 2 h. Representative fluorescent (DCF: green) and phase contrast overlaid images of cells (B) -H_2O_2; -RES, (C) +H_2O_2; -RES, (D) +H_2O_2; +RES (free), (E) +H_2O_2; +RES (LbL/HP). (*p < 0.05, compared to no treatment). 131

CHAPTER ONE

INTRODUCTION AND LITERATURE REVIEW

Implantable brain devices and brain-computer interfaces have the ability to improve the quality of life for patients with neurological disorder like Parkinson's and epilepsy, and to provide independence to paralyzed individuals. For a recording microelectrode, like in the case of use with a paralyzed patient, the device functions by recording action potentials extracellularly from several neurons [1]. These devices can range from single units to arrays of up to 100 units. The electrode surface is typically tens of μm across and a few mm in length, such a length is significant in improving recording sensitivity by reaching the high action potential producing large pyramidal cells in layer V of the motor cortex [1]. In regards to device material and shape, the devices are typically fabricated from a rigid, sometimes semiconductive material with tip geometry that provides insertion capability into cortical tissue without device compromise. The conductive recording sites are either along or at the tip of the electrode shank and must provide a high signal-to-noise ratio and a low impedance measuring 500 kΩ – 2 MΩ for non-thin-film electrodes and 10 kΩ – 50 kΩ for thin-film electrodes (both at 1 kHz) [2].

Even with such optimization, these abilities are contingent upon successful integration of the manmade device material with neural tissue. Specifically, hydrogel particles (HPs) have multiple tunable features and favorable properties, making them a great candidate to investigate as a potential integration technology. In the following sections, the biological events relevant to neural interfacing applications, existing interfacing strategies, and the potential of HP agents as such interfacing agents will be

discussed in depth.

1.1 Cell Response to Central Nervous System Neural Implants

For implanted neural devices, a number of events that take place in the time scale of seconds to several months contribute to short- and long-term device failures. First, when the device is implanted into the brain it passes through the fibroblast-containing meningeal layers. These cells can migrate down the device shaft and form the base of the future astroglial scar surrounding the implant [3, 4]. These cells once stimulated, can pose a physical and physiological barrier to neuron-device communication through expressed extracellular matrix (ECM) molecules, chemorepellent expression, or through facilitation with other cells [3, 5, 6]. Upon remaining device insertion into the brain, neurons in the direct insertion path are physically damaged, while neurons in the surrounding vicinity suffer greatly due to the events described in detail below [7].

Furthermore, as the device is inserted, blood vessels are severed and pathologically recruit blood-borne monocyte-derived macrophages toward the stab-wound site. Once in its final location, the device interfaces with glial cells such as astrocytes, whose typical function is to help support neuron function both mechanically and chemically, and microglia cells, whose activated identity is identical to that of the monocyte-derived macrophages pathologically recruited from the damaged vessels with leaky blood brain barrier. These non-neuronal cells display certain physical and physiological characteristics once activated like hypertrophy, proliferation, migration, and cytokine and soluble factor secretion that can ultimately cause device functionality complications [8, 9]. These events reduce integration of the device with surrounding

neurons in multiple ways. Initially, reactive microglia contribute to increased oxidative stress in the environment through production of reactive oxygen species (ROS) [10-12], which can lead to a host of other cytokine release prompting damage to neurons [7, 13, 14]. Besides this chemical damage to neurons, the formation of the astroglial scar, which is caused mainly by astrocytes forming a fibrous tissue encapsulation surrounding the implant, physically cuts off communication of surrounding neurons with the functional device areas. This prevents neuron-device coupling or close neuron communication within the critical limit of 50 μm of the device, thereby reducing signal sensitivity until there is none.

1.1.1 Neuron Integration

Traditionally, rigid neural implant materials, such as silicon, are not adhesive to neurons due to material chemistry [15] and high elastic modulus [16]. Given that neurons are the designated target cell of neural implants, enabling direct coupling between neurons and implants will enhance the performance of neural implants. Promoting neuron adhesion is the fundamental feature of successful integration of neurons with biomaterials. In the developing nervous system, favorable anchorage points for neuron adhesion and neurite extension are provided by ECM molecules secreted from cells (Figure 1) [17]. It is important to engineer neuron-coupling strategies that take note of the neuron's biological adhesion cues noted above. Natural cell-secreted molecules like laminin, which play a critical role in the developing and regenerating CNS [18], have been used to promote neuron adhesion and to coat neural device surfaces [19-21]. For example alternating layers of polyelectrolyte and laminin on silicon substrates did not alter the device electrical impedance and provided a

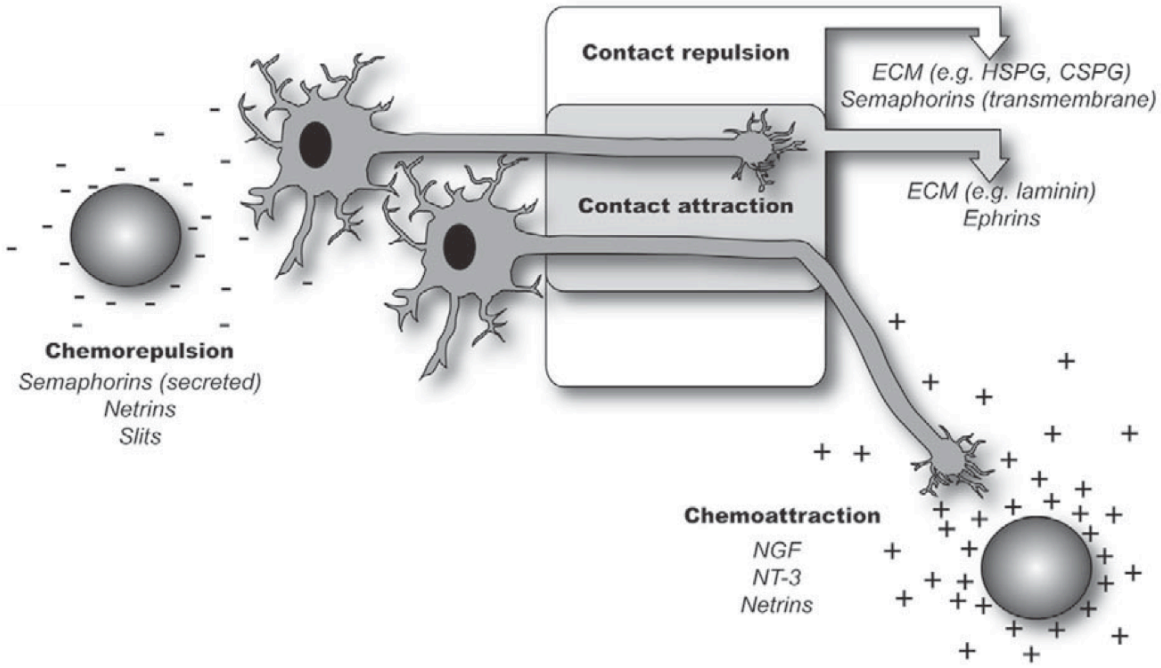


Figure 1 The ECM guides axons of maturing neurons during development toward their proper targets (figure from [17]).

permissive surface for neuron cell adhesion and differentiation [21]. However, for a purely synthetic and tunable polymer system, cationic functional groups on a polymer surface can provide similar neuron adhesive functions, if not better, to their natural counterparts [22-24]. Since at physiological pH 7.4 cell membranes carry a negative charge, many positively charged polymer surfaces, for example ones containing amine groups such as poly-L-lysine (PLL), are considered biologically adhesive surfaces that support cell adhesion through electrostatic interactions [25].

1.1.2 Astroglial Reactivity Attenuation

Numerous surface modification strategies have been investigated to mitigate long-term astroglial scarring effects from reactive central nervous system (CNS) cells. These include chemical, topographical, and drug delivery approaches. For example, mechanically adaptive implants were engineered to mitigate the mechanical mismatch of brain-implant interfaces [26]. Based on an curcumin antioxidant-loaded poly(vinyl alcohol) polymer, the researchers were interested in employing synergistic benefits from both the mechanically favorable material and local therapeutic delivery. Although higher neuronal survival was found after 4 weeks in an in vivo rat model, long-term 12-week models showed no differences from control implants. In a systemic approach, Potter et al. investigated resveratrol (RES) antioxidant delivery prior to and on the day of rat microelectrode implantation surgery [27]. After two weeks post-implantation, neuron density was enhanced near the electrode interface and oxidative species accumulation was reduced in RES-treated groups compared to control groups, however after 4 weeks post-implantation RES-treated and control groups were indistinguishable. Comparably, microgel-coated neural electrodes presented reduced astrocyte and microglia adhesion

in in vitro studies, however they did not significantly alter neuron density near the electrode interface or reduce microglial response for long-term in vivo rat studies [28].

1.2 Characteristics of Hydrogel Particles and Their Potential for Nanostructured Neural Interfaces

To this date, many polymer systems have been investigated for improving the integration of neurons with materials not permissive to neuron adhesion [21, 29-31]. However, this short-term complication of low neuron integration along with other long-term complications has not been suitably resolved together. HPs have many tunable characteristics such as size, charge, and mechanical properties. Versatile HPs are worth investigating as a surface modification strategy for such neural interfacing problems. Below outlines the important fundamentals of these structures.

1.2.1 Size Considerations

One of the fundamental features of HPs is their small and tunable size. One-pot processing methods of HPs based on polyetheramine and bisepoxide can yield sizes from 200 nm to 1 μm. This is accomplished simply by varying the reactant concentration [32]. Studies have shown that cells on surfaces with features ranging from tens to hundreds of nm in size have distinct differences in morphology dependent on the feature size and spacing, which has been theorized as due to the generation of cell anisotropic stresses [33]. Furthermore, surface feature size modifications have also been implicated in directed cell differentiation [34]. Particle diameter has effects on macrophage cellular uptake, where it was found that microspheres were most likely taken up by macrophages when in the 1.0 – 3.0 μm diameter range [35, 36]. As the intended function of the HPs requires their presence on the interface surface (i.e. cell

adhesion and therapeutic drug delivery), it is important to minimize the risk of phagocytosis by macrophages.

Sub-micron sized HPs' large surface area-to-volume ratio makes them an ideal candidate for multivalent bioconjugation that could allow for active targeting to specific cells [37]. Additionally, this same feature has imparted favorable properties in improving signal sensitivity and electrical coupling between the electrode device surfaces and cells. Particularly, coatings of platinum nanostructured grass, taking advantage of its high surface area due to both size and shape, reduced impedance of electrodes compared to conventional coatings [38]. In a similar fashion, nanoporous gold surfaces obtained reduced electrical impedance likely due to both increased effective surface and enhanced neuron-surface coupling [39].

1.2.2 Charge Considerations

HPs can have cationic, anionic, or zwitterionic charge characteristics based on their chemical compositions [40-42]. The zeta potentials of these particles can be altered simply based on the type of monomers used for HP preparation as well as the reaction conditions. As charge and cytotoxicity are closely related, it is important to pay careful attention to this particle characteristic. For example, Tang et al. investigated HP reaction condition effects on surface charge and subsequent cellular interactions [43]. In these in vitro studies, cytotoxicity of HPs towards a macrophage cell line was found to be dose and surface charge dependent. Reducing cationic surface charge to under +50 mV improved biocompatibility with cells. Specifically for neuron adhesion, cationic charge is preferred and should be high enough to promote electrostatic interactions with cells without being so great as to reduce biocompatibility or neurite extension.

1.2.3 Mechanical Properties

The crosslinking density of polymer chains comprising the HPs impacts its mechanical properties, where for a lower cross-linking density the particle will exhibit a lower stiffness [44]. Stiffness is a significant factor that has been found to influence cell behavior [17]. In particular, neurons have been shown to prefer softer substrates of several hundred Pa, similar to that of neural tissue (Figure 2), while astrocyte growth is suppressed on very soft substrates [16]. Furthermore, in co-cultures neurons only grew independently of astrocytes on soft polyacrylamide and fibrin gels (several hundred Pa) compared to hard polyacrylamide and fibrin gel substrates (9 kPa and 2.1 kPa, respectively) [16]. It is important to note in this study that a surface modification of the gel with laminin was used to promote cell adhesion. Rao and coworkers developed a polyethylene glycol-containing polyurethane (PU) hydrogel coating to promote neuron integration on neural devices [30]. Again for in vitro studies, substrates were coated with a cell adhesion-promoting polymer. PC12 neuron-like cells found the PU-coated substrate more favorable and had an increased neurite number and extension length compared to the uncoated substrate control. From in vivo studies, it was concluded that glial fibrillary acidic protein (GFAP) expression, a reactive astrocyte cell marker when upregulated, was reduced in cells on PU-coated surfaces compared to the uncoated control surface, although surface chemistry was not controlled. This highlights the importance of considering the combined mechanical and chemical properties of the cell-sensing interface to support desired cell responses.

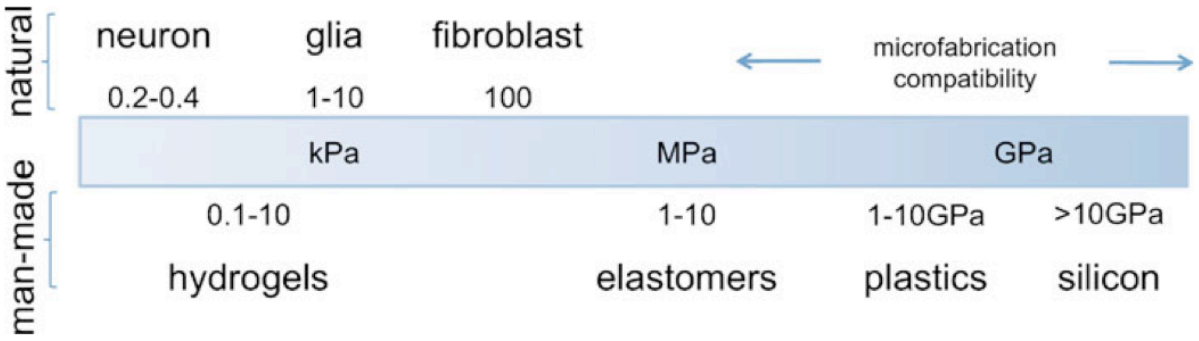


Figure 2 Scale illustrating the elastic modulus of natural brain and man-made materials (figure from [45]).

1.2.4 Responsiveness

Environmental stimuli-responsive polymers have been extensively explored in research today. Key features of nano- and micro-sized polymer delivery systems include responses to small changes in environmental cues, localized delivery to stimuli-producing areas, and time dependent delivery during stimuli production [46]. Drug loading for particles fabricated in the absence of drugs usually involves simple assembly mechanisms of non-covalent interactions such as hydrophobic interactions, hydrogen bonding, or electrostatic interactions [47]. Additionally, HPs can be prepared from numerous responsive polymer types like widely used poly(N-isopropylacrylamide) (PNIPAM) for temperature responsiveness [48, 49], vinylpyridine polymers for pH responsiveness [50], or polymers containing thiol/disulfide linkages for reduction and oxidation responsiveness [51]. Specific polymer chemistry contributes to the triggered swelling, shrinking, or degradation of particles to release a therapeutic agent of interest [52]. In recent years, researchers are looking to technology like HPs to impart local delivery of therapeutic agents. Although HPs are investigated extensively as injectable carriers for drugs [53], little has been studied regarding their localized delivery capabilities when immobilized to surfaces. In one report by McGillicuddy and co-workers, relatively hydrophilic N-isopropylacrylamide and hydrophobic N-tert-butylacrylamide based microgels were used as intravascular stent surface coatings to control delivery of fluvastatin [54]. In this method the drug-loaded microgels were incorporated into a copolymer matrix of similar components and stent wires were dip-coated in the microgel containing solution. The authors were able to fine-tune drug delivery diffusion kinetics based upon the relative hydrophobicities of the polymer ratios

of the microgel and matrix and elude drug for up to the entirety of a 60-day study.

1.2.5 Guided Particle Adsorption

HPs can also be exploited to create patterned features on a device surface to direct neural growth. In the developing nervous system besides chemotactic cues, topographical cues direct neuronal cell adhesion and development [55, 56]. For example, neuron and axons migrate along the tracts of glial cells, and neurons in the medulla oblongata have been found to migrate in the direction along fibers [57, 58]. Although parallel contact guidance is most often observed, perpendicular and guidepost axon guiding has also been reported [59]. Fabricated guidepost-like cues have been exploited in a variety of ways to alter cell morphology and direct cell growth.

Recently, nano- and micro-sized pillars have been investigated as guideposts for neuron adhesion and growth, and the cues were found to direct neurite extension based on the size and spacing of the pillars [60-63]. Although pillar features were able to influence neuron development, in these studies an additional element consisting of a coating of a cationically charged polymer, PLL, was used to facilitate attachment of cells to the surface. Pillar topography has also been implicated in directing astroglial cell attachment and growth [64]. Pillar features of 500 nm to 2.0 μm dimensions were fabricated using photolithography and etching techniques on silicon wafers. In vitro studies showed astroglial cell line preferred pillar regions over smooth regions [64].

Fabricated polymer surfaces with channels of various heights, widths, and spaces have also been successful in directing neuron development [57]. Using lithography methods Su et al. found channel-like patterned substrates imparted the longest neurite lengths and lowest cell velocity and migration compared to pillar and

planar substrates [65]. Furthermore, Johansson et al. found that axons tended to extend on shallow channel-like patterned ridges (100 nm high) instead of in the groove portion between ridges [66].

With modification of the size and spacing of particles, channel-like patterns can be fabricated to enable investigation of the control of populations of cells or cell processes towards or away from specific areas on a surface. Recently, HPs have been printed into such channel conformations. Peng and co-workers developed a *cool microcontact printing* technique, taking advantage of thermosensitive PNIPAM microgels [67]. In this method, PNIPAM microgel monolayers on a substrate were removed by contact with a cooled polydimethylsiloxane (PDMS) patterned mold. This procedure mechanism removed interfacing particles due to cold condensed water on the PDMS mold and the lower critical solution temperature of the particles. This technique is limited to the PDMS template design. Similar PNIPAM striped surfaces were printed and investigated for cell sheet harvesting [68]. Results showed fibroblast cells preferentially adhered to cationically charged polymer spaces between the PNIPAM microgels, as intended.

1.3 Vision

Neural interfaces have the potential to improve the quality of life for individuals suffering from neurological diseases and disorders, and to provide favorable conditions for experimental neuronal cultures for scientific research. Specifically, it is crucial that neuron adhesion on these abiotic entities is guaranteed, since neuron adhesion bears a significant effect on all other aspects of neural function. It has been found that the modification of many factors such as topography, charge, and stiffness can all influence

neural cell adhesion [57, 69, 70]. Additionally, it has been suggested that a combination of these multiple factors could have a synergistic benefit towards promoting cell adhesion [17]. Here we propose utilizing a versatile cationic HP system, tunable in multiple features, including a reservoir function for therapeutic delivery, to act as a "liaison" between neurons and non-adhesive abiotic biomaterials for neural interfaces. HPs have a three-dimensional polymer chain structure that, for this purpose, affords them favorable biocompatible, mechanical, and responsive properties [71, 72]. The versatility of HPs makes them a great candidate to investigate for enhancement of neuron interactions with artificial materials. Therefore, this research is targeted to advance the understanding of the synergistic effects and feasibility of a multi-functional polymeric HP system for neuro-integrative materials.

1.4 Scientific Gaps and Objectives

1.4.1 Scientific Gaps

Several significant scientific gaps have been identified via the above literature review:

Gap 1: There are insufficient investigations regarding CNS cell responses towards topographical patterns constructed directly from HPs. Additionally, the synergistic effects of charge and topographical influences on such cell types could help drive future multifunctional therapies for neural devices.

Gap 2: Existing literature does not directly use HPs as cues for neuron adhesion and neurite extension paths. Instead to promote neuron integration with specific topographical cues, there is typically a required separate surface covering of a cationically charged polymer. Therefore, HPs will provide information on a combined

direct approach to promote guided neuron growth, which is beneficial considering neurons only communicate with particular functional areas of neural devices.

Gap 3: Current treatments to promote integration of neurons onto planar surfaces and current treatments to promote local protection of neuron health are generally independent. Therefore, a need exists to combine both beneficial neural integration and local therapeutic delivery into one technology to further benefit functionality and long-term use of neural devices.

1.4.2 Research Objectives

Objective 1 (addressing Gap 1)**:** It is hypothesized that the cationic nature of our developed HPs will promote adhesion of neuronal cells to the originally non-adhesive substrates in a manner similar to that of other commonly used cationic polymers for adhesion induction in in vitro neuronal cell cultures. Therefore, the first research objectives are to develop HP-modified planar substrates and quantitatively and qualitatively investigate neuron cell responses and CNS inflammatory cell responses towards such surfaces.

Objective 2 (addressing Gap 2)**:** It is hypothesized that HPs can be used as contact guidance cues to direct PC12 cell adhesion preferentially to HP-patterned regions and to direct neurite outgrowth along the edge of HP-stripe patterns. Therefore, the second research objectives are to guide HP adsorption onto planar surfaces and to impart directional adhesion and growth of neurons via HP regions.

Objective 3 (addressing Gap 3): It is hypothesized that surface-adsorbed HPs are a feasible system to encapsulate therapeutic agents, mitigate oxidative molecules, and promote neuron health. Therefore, the third research objective is to investigate the

potential of surface-adsorbed HPs, loaded with RES, as local reservoirs for counteracting adverse effects from oxidative species.

1.5 Document Overview

So far this introductory chapter has provided the motivation and relevant prior research on the importance of integration of devices for neural applications and the significant role HPs could contribute to this matter. Chapter 2 presents a detailed examination into neural and CNS inflammatory cell responses towards HP-modified planar substrates. Chapter 3 discusses various methods for adsorbing HPs onto planar substrates in a guided manner and the effects on neuron interaction. Chapter 4 provides an investigation into the potential of surface-adsorbed HPs as local reservoirs for counteracting adverse effects from oxidative species. Each of these three research chapters is arranged with their own introduction, materials and methods, results and discussion, and conclusion sections. The overall research conclusions and future research recommendations are provided in chapter 5.

CHAPTER TWO

ADSORPTION OF CATIONIC HYDROGEL PARTICLES ONTO SOLID PLANAR SURFACES AND EFFECTS ON NEURONAL AND GLIAL CELL RESPONSES

2.1 Neuronal Integration Towards Hydrogel Particle-Modified Solid Planar Substrate

The following chapter section is based primarily on a manuscript entitled “Facile Use of Cationic Hydrogel Particles for Surface Modification of Planar Substrates Toward Multifunctional Neural Permissive Surfaces: An in Vitro Investigation” with the following authors Emily A. Morin, Shuangcheng Tang, Katie Lou Rogers, and Wei He published by ACS Applied Materials and Interfaces 2016, 8(8), pp 5737–5745. Emily A. Morin designed and performed the experiments, conducted the data analysis, and drafted the manuscript. Dr. Shuangcheng Tang prepared the HP and assisted in particle characterization. Katie Lou Rogers assisted in sample preparation. Dr. Wei He financially supported this work as well as assisted in designing the experiments, analyzing the data, and revising the manuscript.

2.1.1 Introduction

The use of manmade, abiotic materials to electrically interface with neural tissues has great implications for both basic neuroscience research and clinical interventions for neurological disorders and neural tissue repair [73-77]. For example, microfabricated thin-film penetrating electrodes based on silicon substrate for neural recording were used in conjunction with optogenetic technology to help researchers unveil the

fundamental role of a specific cortical layer in visual processing [78], whereas clinical significance of neural recording for paralyzed human patients was first demonstrated when a tetraplegic patient achieved volitional control of a computer cursor with neural signals recorded from the patient's motor cortex using an implanted micromachined, silicon-based array of electrodes [79]. Regardless of the nature of the intended applications, an intimate physical coupling between the abiotic material and the surrounding neural tissue is highly desirable as it will benefit longevity and reliability of the neural interface [80, 81]. Toward such goal, many strategies have been explored, some of which aim at attenuation of glial scar response to the implant [82-85], while others focus on facilitating direct interactions between neurons and the implant [21, 86, 87]. The latter approach will inevitably boost the sensitivity of the electrical relay of information at the interface since neurons will be in direct physical contact with the abiotic materials. To realize neural permissiveness for materials that have found widespread use for neural interfacing research, much of the effort is directed toward modification of surface properties of materials, especially on surface chemistry and surface topography [88]. Notable examples include coating the materials with adhesive molecules such as polylysine [89] or polyethylenimine (PEI) [90] based on the premise that negatively charged lipids or polysaccharides present on mammalian cell membrane are attracted electrostatically to these positively charged polymers [91], as well as incorporation of micro/nanoscale topographical surface cues in a wide variety of forms such as pillars [92, 93], pores [39], cones [94], fibers [86], etc. Attempts to create these physical features are commonly enabled by advanced microfabrication technologies such as lithography [92], focused ion beam machining [95], laser ablation [94], and

electrospinning [86]. However, coatings of adhesion-mediating compounds are often needed to promote neuron adhesion to the topographically altered surfaces.

Here we explore a simple strategy to achieve a neural permissive surface exhibiting both chemical and topographical cues. The approach harnesses a basic phenomenon of electrostatically driven adsorption of charged colloidal particles on a solid substrate [96]. On one hand, the desired neuron adhesion chemical cue is provided by choosing positively charged particles. On the other hand, a topographical cue is naturally fulfilled by the physical presence of adsorbed particles on the substrate. In this study, a colloidal HP system recently developed by our group was applied [32, 43]. These particles were formed readily in water by “click” reaction between monomers of bisepoxide and polyetheramine. Because of the presence of amine groups, the particles are cationic in nature under physiological pH. Their size is in the submicron range and easily tunable by adjusting reaction conditions, allowing us to apply these particles as topographical cues at a length scale in line with subcellular structures such as filopodia [97]. Furthermore, such HPs are capable of encapsulating hydrophobic substances, a function that is of great value for therapeutic interventions. Taking advantage of the above characteristics, we show that the surface of synthetic substrates such as silicon, a material frequently used for neural interfacing applications, can be easily modified via cationic HP adsorption to support adhesion and differentiation of both neuron-like PC12 cells and primary cortical neurons.

2.1.2 Materials and Methods

2.1.2a Cationic Hydrogel Particle Synthesis and Characterization

The details of the HP preparation have been described elsewhere [32, 43]. Briefly, Jeffamine T-403 polyetheramine (Huntsman) and 1,3-butadiene diepoxide (BDE, Aldrich) were mixed at the molar ratio of 2:3 (Jeffamine/diepoxide) to a final monomer concentration of 15 wt% in water. The resulting solution was first incubated at 65 °C for 10 min before it was diluted to 0.5 wt% and further reacted for 30 min. In the case of using poly(ethylene glycol) diglycidyl ether (PEGDE, Aldrich) to substitute for BDE, the reaction of the 15 wt% mixture was extended to 15 min. The particles produced were purified via multiple rinsing by 18.2 M•Ω cm ultrapure water. The hydrodynamic diameter and zeta potential of the HPs were characterized using a Zetasizer nano-ZS system (Malvern Zetasizer Nanoseries, Malvern, UK).

2.1.2b Deposition of Particles on Planar Substrates and Characterization

Preparation: Both silicon wafers with a 100 nm-thick oxide layer and, for direct visualization of live cell culture, microscopy glass slides were included as test substrates. The substrates were first cleaned with acetone, ethanol, and deionized (DI) H_2O, respectively, to remove any organic and inorganic matter. After drying thoroughly, the clean substrates were immersed into a boiling piranha solution freshly prepared by mixing 30% hydrogen peroxide (H_2O_2, Fisher Scientific) with concentrated sulfuric acid (95.0−98.0%, Sigma-Aldrich) at a volume ratio of 1:3 (Caution: Piranha solutions should be handled with extreme care as they react violently with organic compounds.) The piranha-treated substrates were then washed extensively with DI H_2O. By adopting a layer-by-layer (LbL) assembly process, a precursor film was first adsorbed to prime the

surface for HP deposition. Solutions of branched PEI (MW = 25 000 g/mol, Aldrich) and poly(4-styrenesulfonic acid) (PSS) (18 wt% solution in water, Aldrich) were prepared to a concentration of 1 mg/mL (pH 7.4) using 1X phosphate-buffered saline (PBS) solution. Briefly, the layers were formed by alternating immersion of the test substrates in solutions of PEI and PSS for 10 min, respectively. Between each incubation, the substrates were rinsed with ultrapure water for 10 min to remove any excess polyelectrolytes. This process was repeated once to obtain $(PEI/PSS)_2$-primed substrates, denoted as LbL. Cationic HP deposition was achieved by incubating the LbL-primed substrates in HP suspensions with concentrations varying from 0.1 mg/mL to 0.5 mg/mL to 1 mg/mL for controlled periods of time up to 5 h. In the case of PEGDE particle deposition, LbL-primed substrates were incubated in PEGDE particle suspensions with concentrations varying from 1 mg/mL to 2 mg/mL for 10 min. The samples were then rinsed with ultrapure water, air-dried, and denoted as LbL/HP or LbL/PEGDE for further study.

Characterization: The HP deposition and distribution on the LbL/HP samples were characterized by a LEO 1525 scanning electron microscope (SEM, LEO Electron Microscope, Germany) or a Zeiss Auriga (Zeiss, Germany). To preserve surface morphology, the samples were examined directly without any conductive coating of gold. MATLAB processing of the obtained SEM images was performed to quantify HP density and percent area coverage on the sample surface.

For atomic force microscopy (AFM) characterization in air, silicon LbL/HP substrates were analyzed by force mapping in tapping mode with an AC240TSA-R3 (f = 70 kHz, k = 2 N/m) probe (Asylum Research, USA).

Sample surface wettability was measured by the sessile-drop contact angle method using a CAM-Plus contact angle goniometer (Cheminstruments, USA). Droplets of DI H_2O (3 µL) were carefully placed on the samples (n = 5), and the water contact angle was measured using the half angle method. For investigation into HP-modified surface insertion tolerance, samples were imaged with SEM before and after manual insertion into a relevant brain model of agarose hydrogel fabricated at 0.6% in 1X PBS [98].

2.1.2c PC12 Cell Culture

The PC12 cell line, from rat adrenal gland pheochromocytoma, was used at passages 3 – 10. The cells were maintained on T25 tissue culture flask in F-12K medium (ATCC) supplemented with 15% horse serum (HS) (Life Technologies), 2.5% fetal bovine serum (FBS) (Thermo Scientific), and 1% antibiotic-antimycotic (Anti/Anti) (Life Technologies). To pass, cells were detached from flasks by mechanical force via pipetting and dispersed through a 22G × ¾ needle multiple times to acquire individual cells.

Adhesion Study: To evaluate the ability of HP-coated substrates to support cellular adhesion, individual PC12 cells were acquired and seeded at a density of 5000 cells/cm^2 onto the LbL/HP glass substrates (n = 3) placed in a 35 mm dish. Uncoated glass and PEI-coated, LbL-primed glass substrates (LbL/PEI) were used as a negative and positive control, respectively. Following overnight attachment, cell medium was replaced with fresh medium to remove any unattached cells. Representative phase contrast images were then taken on each sample using a Zeiss Axio Observer A1 inverted microscope (Zeiss, Germany). The number of adhered cells on each sample

was quantified per 10, 10X images and averaged within each sample set.

Differentiation Study: To evaluate how HPs influence neuron differentiation and morphology, PC12 cells were seeded at a density of 10 000 cells/cm^2 onto LbL/HP silicon (n = 8) or glass samples placed in a 24-well plate. Cells were allowed to attach overnight, after which differentiation was induced by switching the medium to differentiation medium of supplemented F-12K culture medium with 1% HS, 0.2% FBS, 1% Anti/Anti, and 50 ng/mL 2.5 s nerve growth factor (NGF) (BD Biosciences). For immunocytochemistry studies, after 48 h of culture in NGF-containing medium, samples were washed with 1X PBS and fixed with 4% paraformaldehyde (Electron Microscopy Sciences) for 20 min at room temperature (RT) and then rinsed three times with 1X PBS. The cells were permeabilized with 0.1% Triton X-100 in 1X PBS for 5 min, followed by 30 min incubation in 4% goat serum (GS, Gibco) in 1X PBS to block nonspecific protein binding. To investigate neurite development, cells were labeled with monoclonal anti-α-tubulin primary antibody produced by mouse (Sigma-Aldrich) at 1:200 dilution in blocking solution for 1 h. Cells were then labeled with Alexa Fluor 488 goat antimouse IgG1 (γ1) secondary antibody (Life Technologies) at 1:100 dilution in 1X PBS or Alexa Fluor 594 phalloidin (Invitrogen) at 1:50 dilution in 1X PBS for 1 h. To counterstain for nuclei, cells were incubated in 3 μg/mL of Hoechst 33342 (Thermo Scientific) in 1X PBS for 20 min. Cells were washed between steps with 0.05% Tween 20 wash buffer. Samples were mounted with a fluoromount G (Southern Biotech) antifade mounting solution. Fluorescent images were collected using a Zeiss Axio Observer A1 inverted fluorescent microscope (Zeiss, Germany). ImageJ image analysis software (NIH, USA) was utilized for stage and neurite analysis. Cells were classified

into four distinct differentiation stages: Stage 0, attached cells with a round morphology and no extensions; Stage 1, cells exhibiting flattened, spread morphology as well as cells with minor protrusions no longer than the length of the cell body; Stage 2, cells extending neurite-like processes with the longest one being the length of the cell body; Stage 3, cells having at least one neurite-like process that is two lengths of the cell body or longer. No cells were categorized into more than one stage. Cells expressing at least one neurite the length of the cell body and not contacting any other cell's neurites were included in determining number of neurites per cell and branching. Branches were defined as processes extended 5 μm or farther away from the primary neurites [99]. Quantification of branching activity was done by dividing the total number of branch occurrences with the total neurite count.

Cell-substrate interactions were also qualitatively assessed using SEM. Samples from the differentiation study were washed with 1X PBS fixed with 3% gluteraldehyde (Electron Microscopy Sciences, USA) for 24 h at 4 °C, and underwent processes of dehydration using a series of ascending grades of ethanol washes (25, 50, 75, and 100%). To ensure a thorough removal of water, dehydration was continued by either critical point drying or incubation in a series of 100% ethanol and hexamethyldisilazane (HMDS) mixtures at ratios of 2:1, 1:1, and 1:2, followed by complete evaporation in 100% HMDS [100]. Samples were sputter-coated with gold for 20 s at 20 mA before SEM imaging.

2.1.2d Primary Cortical Neuron Culture

Cortical neurons were obtained from 7-day-old chicken embryo [101]. Forebrains of the embryo were dissected, minced into small pieces, and enzymatically dissociated

with 0.25% trypsin (Invitrogen) in 1X PBS for 20 min at 37 °C, followed by inactivation with culture medium of Dulbecco minimum essential medium DMEM (ATCC) containing 1% L-glutamine (Life Technologies), 10% FBS, and 1% Anti/Anti. A cell pellet was obtained after a brief centrifugation, and mechanical trituration using a fire-polished Pasteur pipet was applied to further dissociate the cells for seeding.

To determine the ability of the HP-coated sample to support primary neuron adhesion and growth, individual cortical neurons were seeded at a density of 50 000 cells/cm^2 onto LbL/HP samples placed in a 35 mm dish. The culture medium was replaced at 24 h to remove unattached neurons. Phase contrast images were taken every 24 h up to 72 h in total to monitor neuron attachment and neurite development. At the end of the 72 h culture, samples were qualitatively assessed using SEM and fluorescent staining following procedures described in the above PC12 cell differentiation study.

2.1.2e Statistics

Data were analyzed by the one-way analysis of variance (ANOVA) using a Tukey's post hoc test (SPSS statistics software). Differences were considered significant for $p < 0.05$. All data were reported as the mean ± standard error unless otherwise noted.

2.1.3 Results and Discussion

2.1.3a Hydrogel Particle Adsorption on Planar Substrates

Among the various types of HPs that have been reported to date, we selected the one prepared from monomers of bisepoxide and aliphatic polyetheramine largely because of the cationic characteristic of the resulting particles and the ease of

preparation [32, 43]. For neuronal cultures, it is widely shown that surface treatments of culture substrates with cationic polymers such as polylysine, polyornithine, or PEI can greatly improve neuron adhesion to the substrates [90, 102]. Thus, HPs carrying positive charges can provide a chemical-cue based strategy to modulate neuron adhesion. As shown in Figure 3, the prepared HPs used in this study have an average surface charge of +60 mV with intensity-average hydrodynamic diameter being 410 nm based on DLS measurements.

Prior to particle deposition onto the test substrates, a tetra-layer precursor film was constructed on the substrate using the electrostatically based LbL assembly technique. Specifically, the precursor film consisted of two bilayers of nondegradable PEI/PSS [$(PEI/PSS)_2$], where mechanistically each layer reverses the film charge by neutralizing the underlying layer and providing a charged surface for subsequent polyelectrolyte adsorption [103]. In this case the outer layer is PSS to make the surface negatively charged to accommodate subsequent adsorption of cationic HPs. The role of the precursor film is to prime the surface of the substrates and minimize any interference introduced by the inherent substrate surface charge heterogeneity. It is unlikely that the LbL modification would increase neural device impedance, as previously reported similar multi-bilayer films did not change probe impedance magnitude when measured at the applied biologically relevant neural activity frequency of 1 kHz [21].

Figure 4 shows SEM images of the dried, LbL-primed silicon surfaces before and after HP adsorption without any conductive gold coating. It can be observed that these cationic HPs readily adsorbed onto the featureless LbL-primed surface driven by

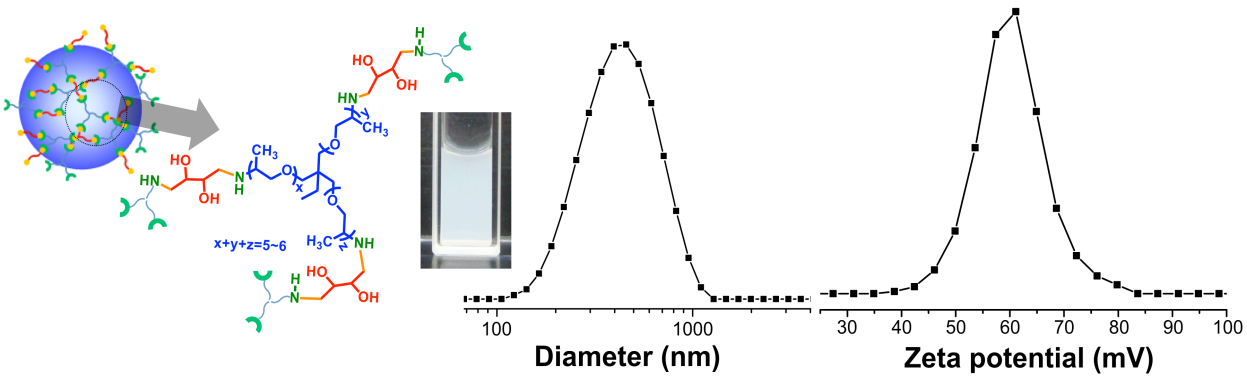


Figure 3 Chemical structure and physical appearance of aqueous dispersion of the HPs (left) as well as their intensity-average hydrodynamic size distribution (middle) and zeta potential in water (right).

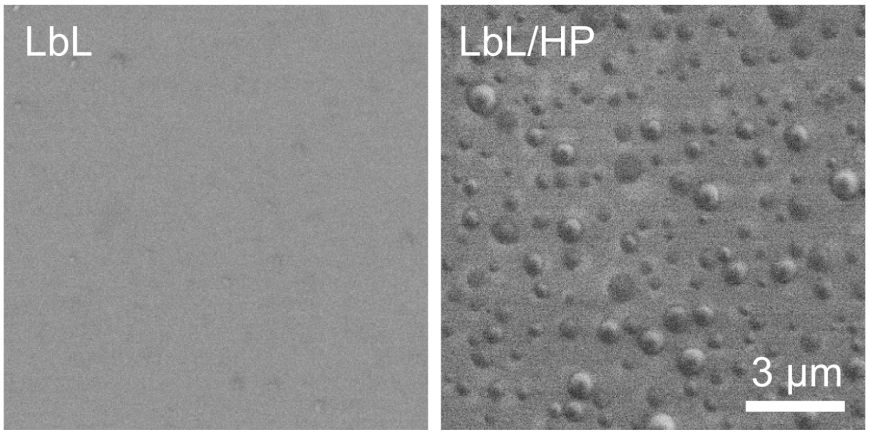


Figure 4 Scanning electron micrographs of the LbL and LbL/HP finished samples.

electrostatic interaction. It is also clear that the particles adsorbed to the surface in a random, yet uniform single layer coverage. Very little particle aggregation was observed, which can be attributed to lateral interparticle electrostatic repulsion originating from the positive charges carried by these HPs. Furthermore, because of the HP suspension being polydispersed (Figure 3), the resulting surface shows a diverse population of adsorbed HP varying in sizes. The HP can be adsorbed to a variety of LbL-primed common electrode material surfaces (Figure 5). Initial studies revealed that in air the adsorbed particle presents a modulus of around 150 MPa (Figure 6). Future research will determine the adsorbed particle modulus under physiological hydrated conditions. Additionally, the adsorbed HP is not removed upon insertion into a relevant brain model of agarose hydrogel (Figure 7).

We also examined the influence of HP suspension concentration and incubation time on its deposition on planar substrates. By keeping the incubation time consistent at 10 min, we noticed that the surface packing density of HPs increased as the HP suspension concentration increased from 0.1, to 0.5, and to 1 mg/mL (Figure 8A). The corresponding fractional surface area covered by the adsorbed HPs determined through image analysis also showed an increasing trend with the increase of HP suspension concentration (Figure 8A). Such a concentration effect can be easily explained by the number of particles available in the colloidal suspension for adsorption to the substrate. To examine the influence of incubation time, the HP suspension concentration was fixed at 1 mg/mL, and the substrates were allowed to incubate for 30 s, 10 min, and 5 h, respectively. As shown in Figure 8B, the density of HPs adsorbed to the surface is significantly different among all three time points, with the 30 s sample having the

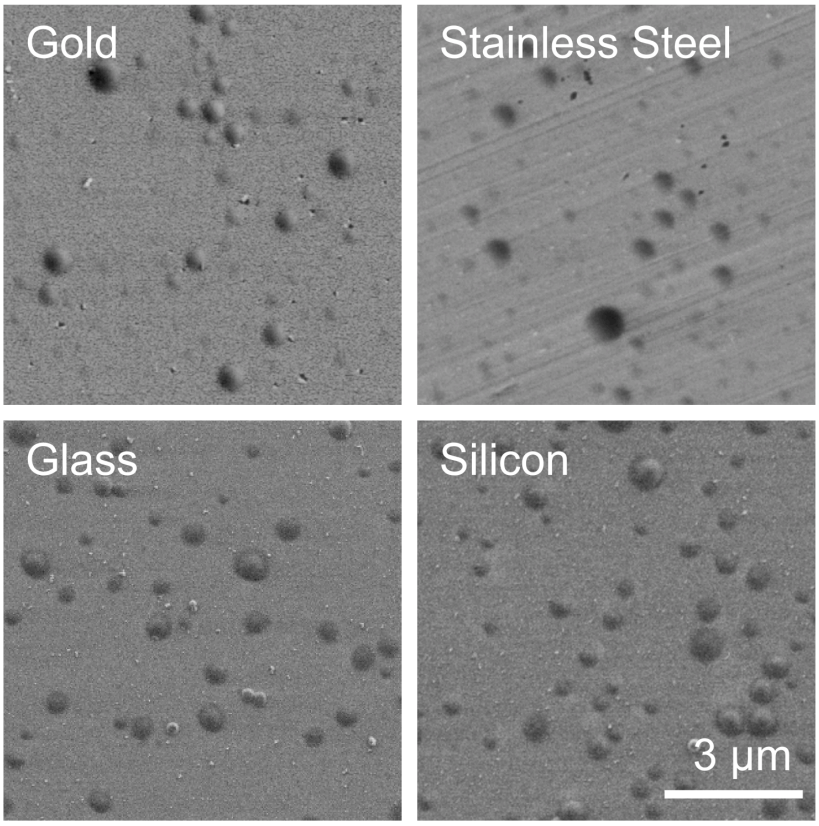


Figure 5 Scanning electron micrographs of various LbL-primed surfaces.

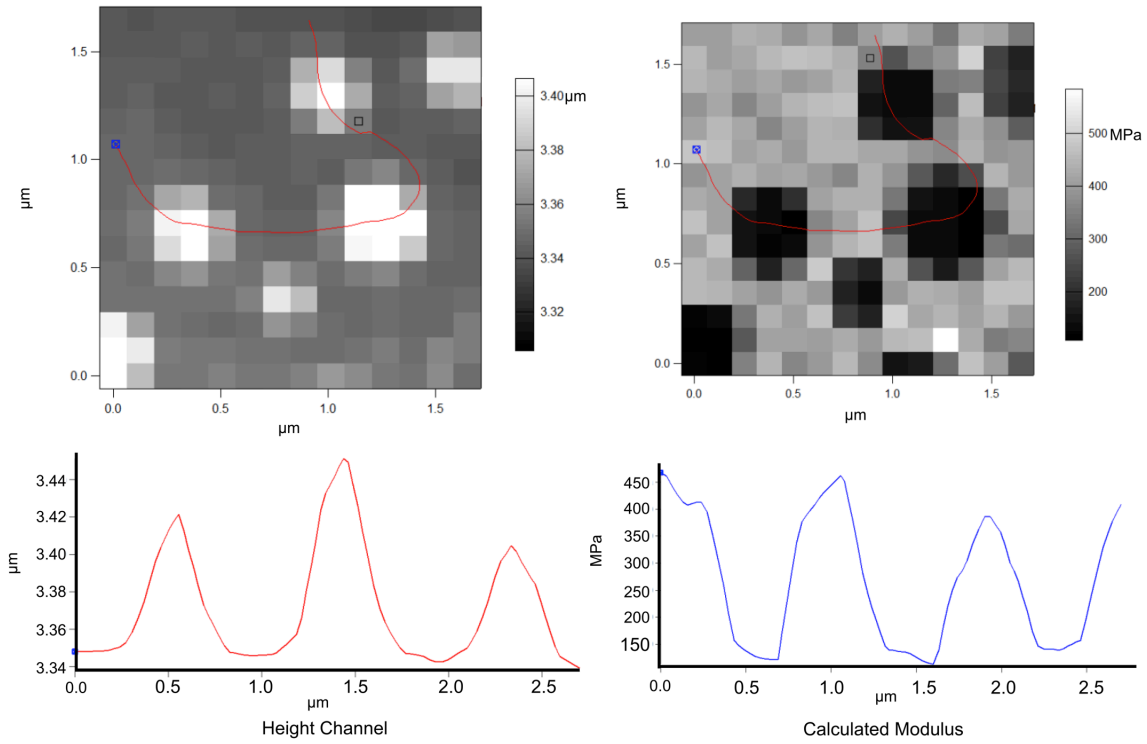


Figure 6 Adsorbed HP height (left) and corresponding modulus (right), (red line in above images corresponds to analyzed data in graph below).

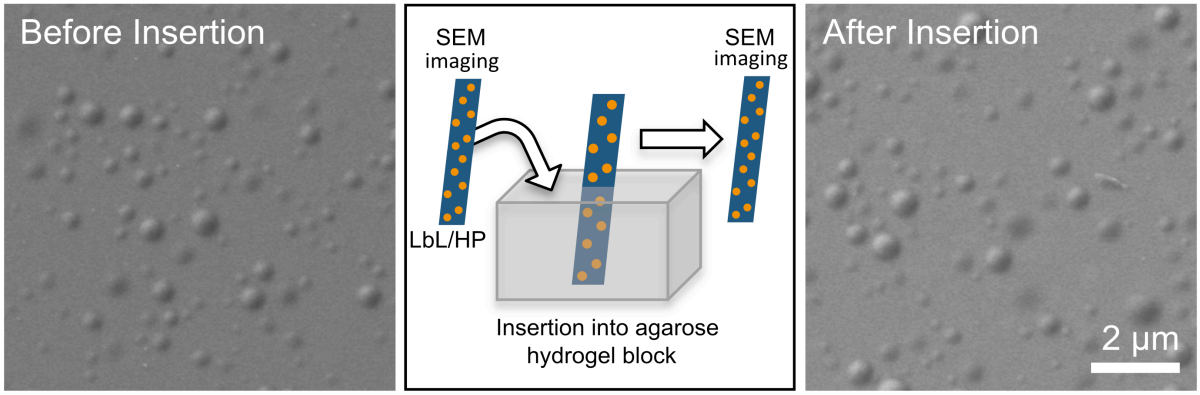


Figure 7 Scanning electron micrographs and schematic of LbL/HP-coated silicon substrate before and after insertion into agarose hydrogel.

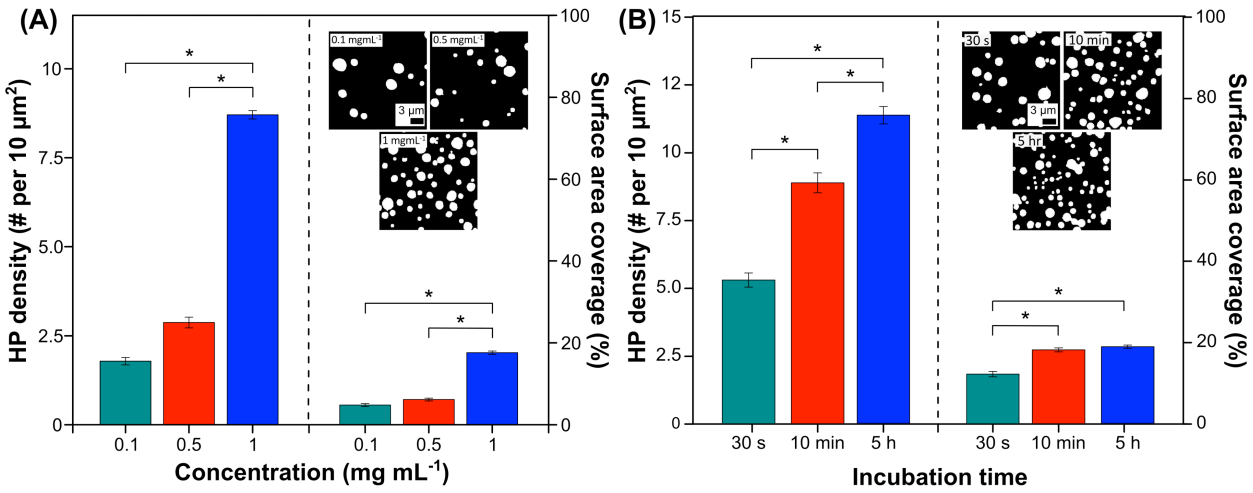


Figure 8 Number density of adsorbed HPs and the surface area coverage by HPs as a function of (A) HP suspension concentration and (B) incubation time for adsorption (*p < 0.01). Insets: binary images of representative scanning electron micrographs.

lowest density and the 5 h sample having the highest density. It also reflects the adsorption kinetics, where the initial adsorption is very fast, and it slows down when approaching the saturation limit due to the charged nature of these particles. This observation is consistent with the “random sequential adsorption” model commonly used to describe localized adsorption of colloidal particles at solid/liquid interfaces [104]. Image analysis revealed that the surface area covered by HPs adsorbed after 30 s of incubation was significantly smaller than those obtained after 10 min and 5 h incubation, likely due to the drastic difference in the number of HPs adsorbed onto the surface at various time points. It is interesting to note that despite the significantly higher number of HPs adsorbed after 5 h as compared to 10 min adsorption, there was no statistical difference in surface area coverage between these two groups. This can be explained by the polydispersed nature of the HP suspension. As incubation time increases from 10 min to 5 h, smaller HPs adsorb to the spaces between the already adsorbed particles [105], leading to an increase in the surface density of adsorbed HPs, but not significantly impacting the surface area coverage because they have a smaller comparative size to the other HPs. Collectively, these studies demonstrate that various levels of surface modification of planar substrates via adsorption of cationic HPs can be easily achieved with simple change of adsorption parameters.

Additionally, a predictably softer PEGDE particle was fabricated by substituting BDE with PEGDE and characteristically compared to the HP diameter and zeta potential. The PEGDE particle had an average surface charge of +53 mV with intensity hydrodynamic diameter of 590 nm based on DLS measurements, which was lower in charge and larger in average hydrodynamic diameter compared to the HP (Figure 9).

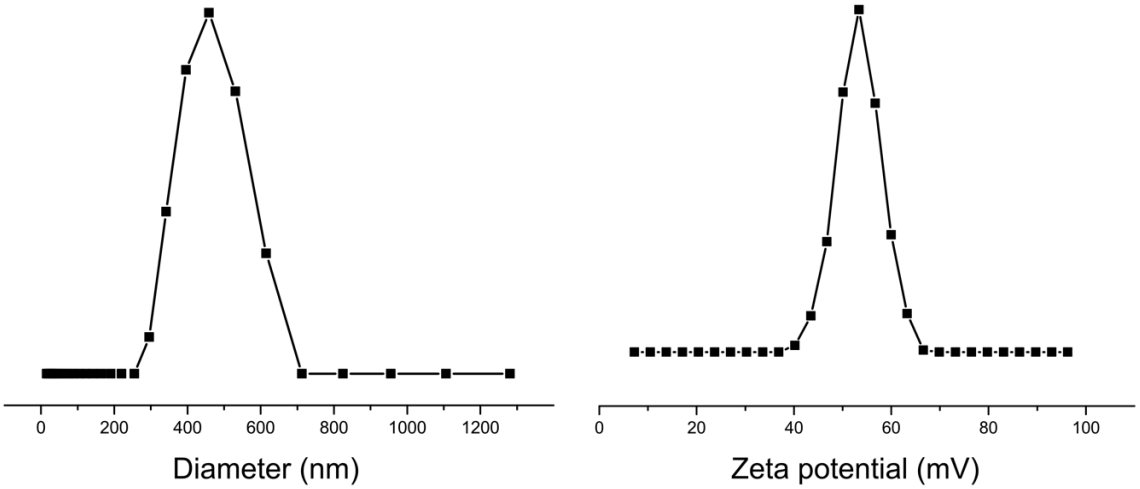


Figure 9 PEGDE particle intensity-average hydrodynamic size distribution (left) and zeta potential in water (right).

This larger diameter is most likely due to the longer PEGDE polymers compared to the HPs' BDE polymer chains. Also, the PEGDE polymer contains poly(ethylene glycol) (PEG) segments, which are known to be highly hydrophilic and most likely contributed to PEGDE particle diameter increase due to swelling. SEM images of Figure 10 revealed that the dehydrated PEGDE particles were on average smaller than the HP. This led to a higher PEGDE particle suspension concentration of 1.75 mg/mL required to impart the 18% particle surface coverage that matched the HP surface coverage used in cell studies with the HP-modified substrates.

2.1.3b Surface Wettability

Surface wettability plays a key role in cellular responses toward biomaterials [106]. Prior to cell culture, water contact angle measurements were conducted on various samples to investigate this surface characteristic. As shown in Figure 11, the unmodified clean silicon was moderately hydrophilic with water contact angle being 50.2 ± 6.8°. LbL priming drastically increased surface hydrophilicity evident from the decrease of contact angle to 10.0 ± 2.4° and the captured image of the droplet. Subsequent adsorption of HPs onto the LbL surface led to surface wettability similar to that of the plain silicon surface. This effect can be partially attributed to the adsorbed HP-induced surface topography, which is known to directly impact surface wettability [107]. As a control for later cell culture study, an additional PSS capping layer was introduced to the HP-adsorbed surface. The resulting LbL/HP/PSS surface was slightly more hydrophilic than the LbL/HP surface, which is consistent with the observation of LbL surface being more hydrophilic than the LbL/PEI surface. A similar finding was reported by Chen and co-workers where PSS adsorption lowers the water contact

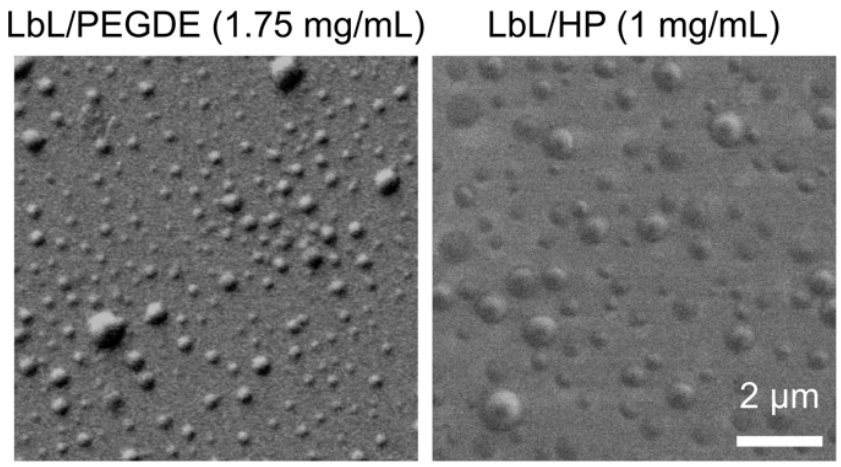


Figure 10 Scanning electron micrographs of the LbL/HP and LbL/PEGDE surfaces displaying similar particle surface coverage.

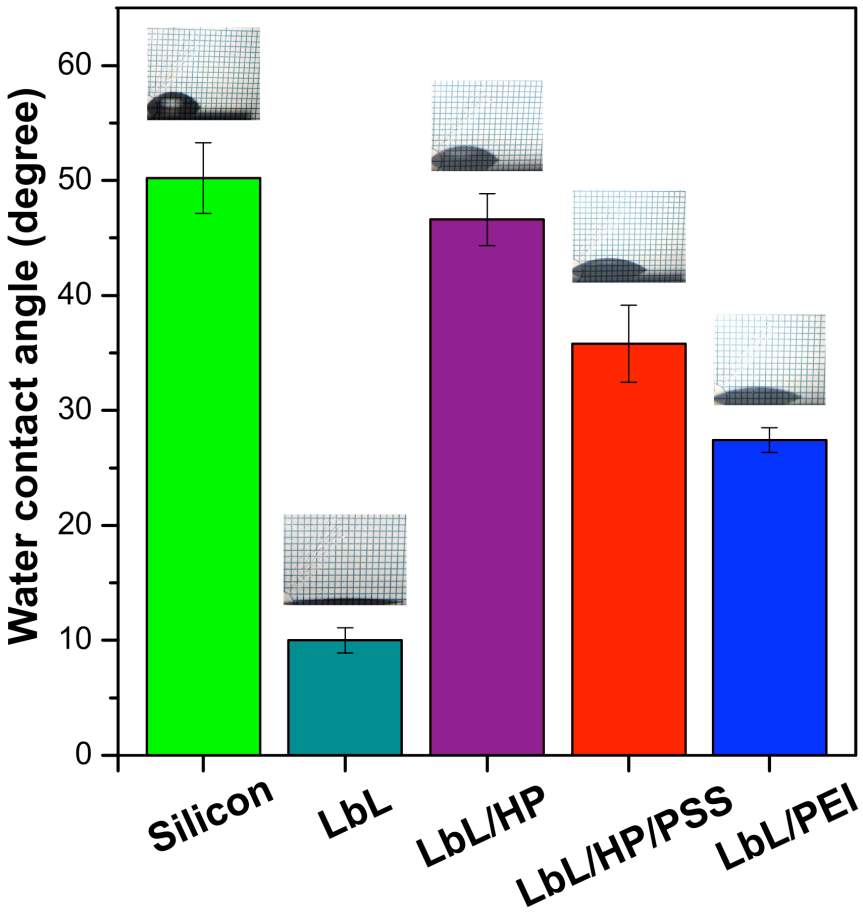


Figure 11 Water contact angle measurements and representative photographs (side view) of water droplets on plain silicon and silicon with various surface modifications.

angle of the surface, when surface wettability was monitored during the LbL assembly of PEI/PSS [108]. This phenomenon could be due to different polarity exhibited by sulfonated species and aminated species.

2.1.3c Effects on Neuronal Cell Adhesion

To examine if adsorbed cationic HPs can improve neuronal interaction with the planar substrates, we first investigated neuron adhesion. Our hypothesis was that the cationic nature of these HPs would promote adhesion of neuronal cells to the originally non-adhesive substrates in a manner similar to that of other commonly used cationic polymers for adhesion induction in in vitro neuronal cell cultures. A well-established PC12 cell line was used, and cell adhesion was analyzed following overnight culture on various surfaces. As shown by the phase contrast images in Figure 12, the unmodified bare surface showed poor support of PC12 cell attachment. In contrast, compared to the unmodified bare surface, a significant improvement in cell adhesion was observed on the LbL/HP-modified surface, with the average number of adherent cells almost 15-times that found on the bare surface (Figure 12). We attributed such improvement to the adsorbed cationic HPs not the underlying LbL layer because of the following observations: (1) LbL modification alone showed no enhancement in PC12 cell adhesion; and (2) when an additional anionic layer of PSS polymer was introduced to the LbL/HP-modified surface, the substrate became almost nonsupportive of cell adhesion like the bare surface. It suggests that the positively charged nature of HPs is the key to the observed cell adhesion promoting effect. This finding is in agreement with other studies using cationic polymer coatings as substrate pretreatments to improve PC12 cell adhesion [89, 109-111]. Although the adsorbed HPs also bring a change to

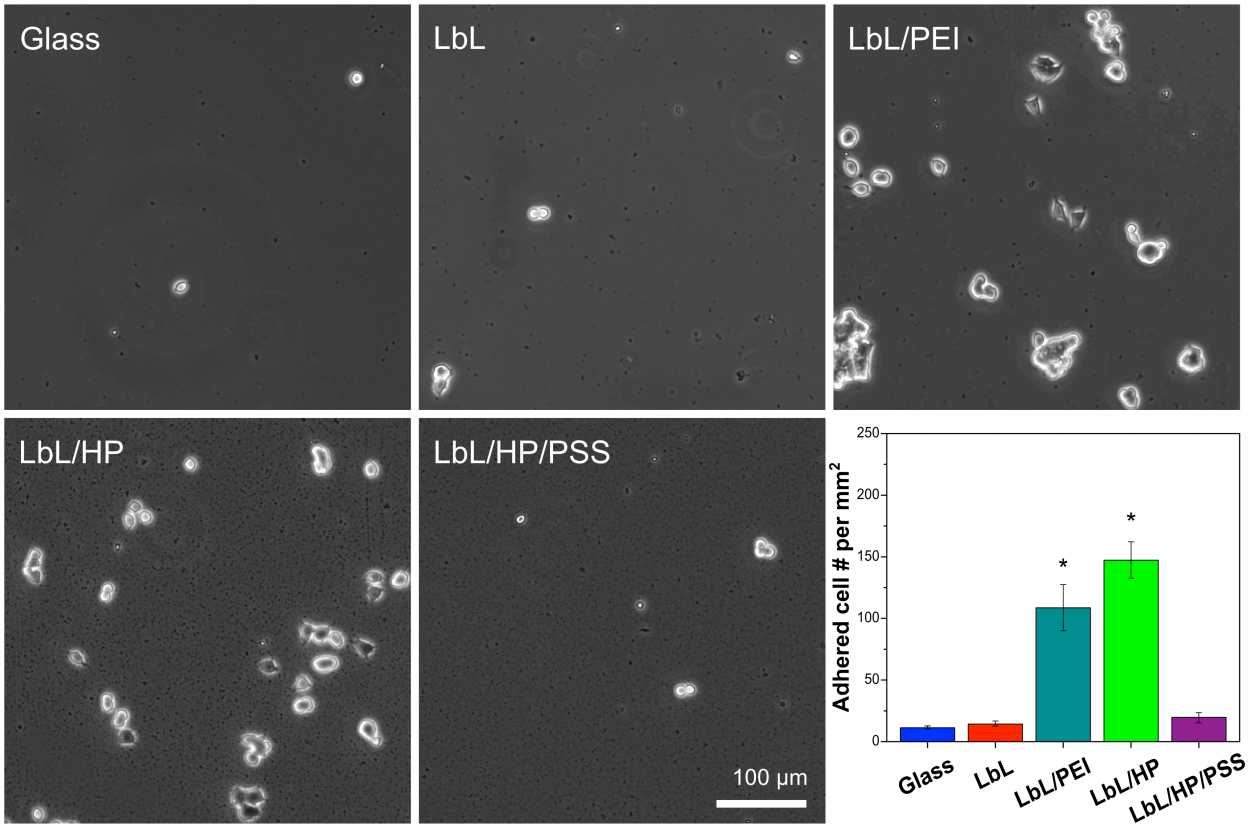


Figure 12 Representative phase contrast images of PC12 cell adhesion and quantitative adherent cell density on various surfaces (*p < 0.01, compared to glass).

the topographical characteristic of the substrate, this physical-based contribution to the enhancement of cell adhesion is insignificant. As seen from the LbL/PEI group, where the cationic polymer PEI was adsorbed on top of the LbL surface, the number of PC12 cells attached was statistically comparable ($p > 0.05$) with that on the LbL/HP surface (Figure 12). A live/dead assay was performed to assess the viability of the cells on the LbL/HP and LbL/PEI-modified surfaces, and the results showed predominantly living cells (Figure 13). This further confirms that the improved neuron adhesion mainly originates from the cationic feature of these HPs.

PC12 adhesion was also confirmed on the PEGDE particle-modified surface (Figure 14). Adhered cells on LbL/PEGDE substrates were polygonal shape with small extensions, similar to adhered cells on LbL/PEI substrates. Unlike with the LbL/HP/PSS surface, PC12 cells adhered on the LbL/PEGDE/PSS surface and displayed a round cell morphology with little to no extensions. This may be due to three different hypotheses: (1) there may be inadequate PSS coverage of the PEGDE particles due to potentially elevated particle swelling compared to the HP, allowing the cells to sense the underlying cationic charge of the particle, (2) there may be reduced particle stiffness due to the longer PEGDE substituted for the BDE segment, and (3) there may be altered surface topography due to possibly increased swelling properties of the PEGDE particle. The exact mechanism will be further elucidated in future studies.

2.1.3d Effects on Neuronal Cell Differentiation

Besides adhesion, it is also imperative to examine whether the adsorbed HPs support neuronal differentiation of the attached cells. PC12 cells are well known for their ability to differentiate into neurons when treated with NGF. Therefore, following

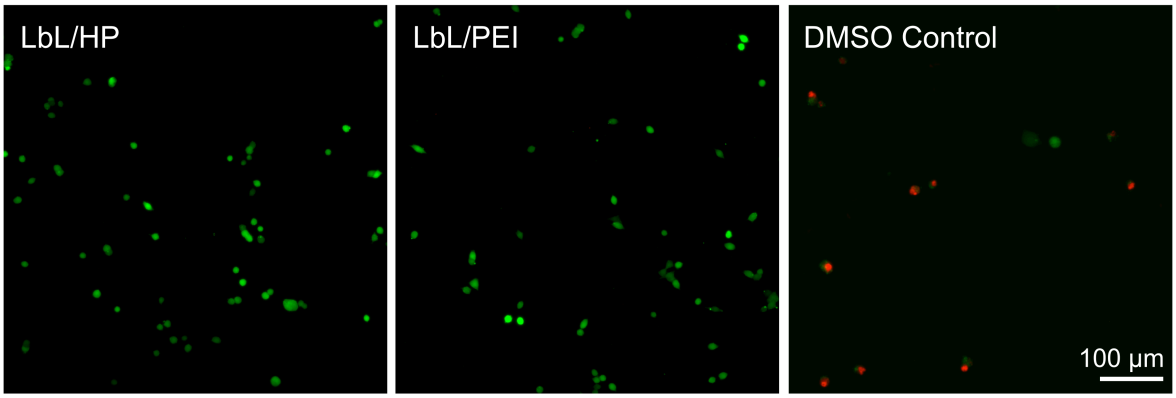


Figure 13 Live/dead images of PC12 cells attached to LbL/HP and LbL/PEI-modified surfaces (Viable cells: green, Damaged cells: red).

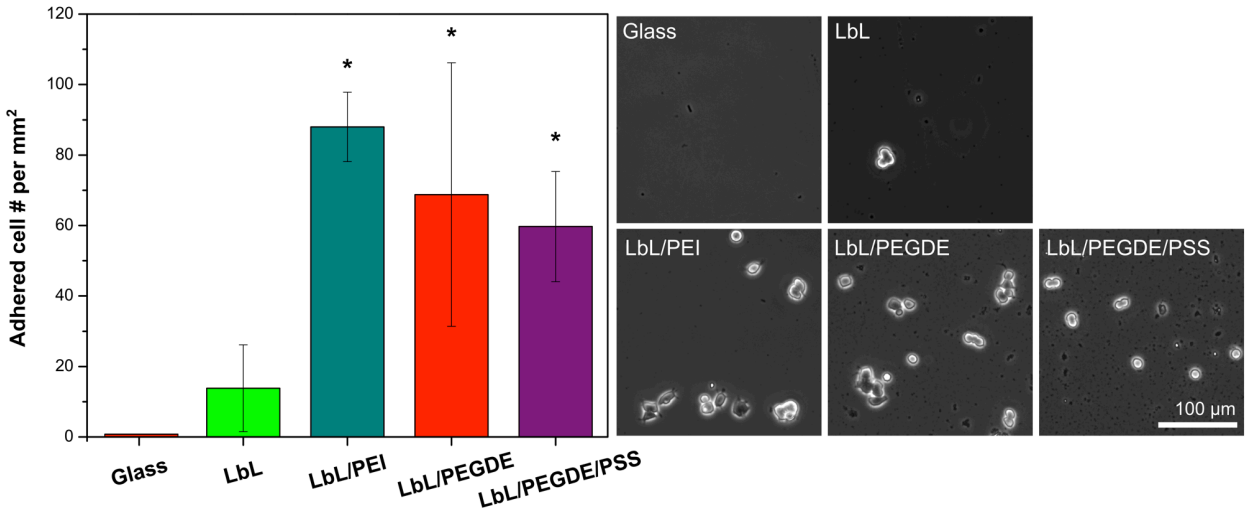


Figure 14 Quantitative adherent PC12 cell density on LbL/PEGDE and control substrates with representative phase contrast images (*$p < 0.05$, compared to glass, error reported as ± standard deviation).

overnight of initial cell culture, NGF-supplemented medium was used to induce PC12 differentiation for 2 days, and cell response was then evaluated. Both phase contrast and fluorescent images showed clear evidence of neurite outgrowth from PC12 cells attached on the LbL/HP-modified glass or silicon substrate (Figure 15A,B) as well as cells on the LbL/PEI control (Figure 15E,F). For neurite-bearing cells, actin-rich stains were noted mainly at the tips of extending neurites and their branches, whereas for cells lacking prominent neurites, actin stains were concentrated in fine protrusions stemming from the cell body (Figure 15B,F). To gain a closer view on the physical interactions between the differentiated cells and the underlying substrates, SEM was used on fixed cultures. On the LbL/HP surface, both cell body and neurite extensions were seen making direct contact with HPs (Figure 15C). Furthermore, numerous thin finger-like protrusions surrounding the growth cones were observed either navigating through the space between HPs or directly growing atop of HPs (Figure 15D). These morphological structures of cells, also known as filopodia, are important for neurons to survey their environments and guide neurite extensions [112]. The surface morphological feature created by adsorbed HPs was isotropic in nature. Therefore, the directionality of neurite trajectory appeared to be random and not greatly influenced by such surface HP cues (Figure 15C). For comparison, the physical interaction between cell and the LbL/PEI surface was examined in parallel under SEM (Figure 15G), and growth-cone filopodia were observed as well (Figure 15H).

The heterogeneity of PC12 cell morphology observed in this study prompted us to further classify the cells into four distinct differentiation stages: Stage 0, attached cells with a round morphology and no extensions; Stage 1, cells exhibiting flattened, spread

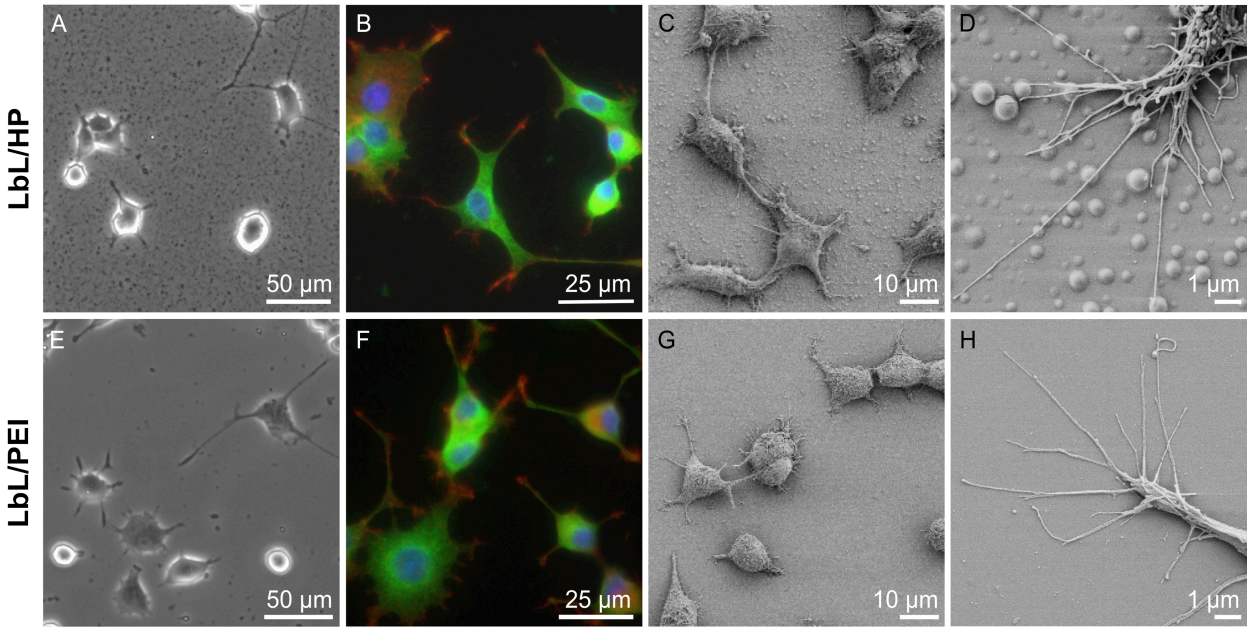


Figure 15 PC12 cell morphology after 48 h of culture in NGF-supplemented media (72 h of culture total) on (A-D) the LbL/HP surface and (E-H) the LbL/PEI control surface. (A, E) Phase contrast images; (B, F) fluorescent images of cells stained for α-tubulin (green), actin filaments (red), and nuclei (blue); (C, D, G, H) scanning electron micrographs of fixed cells.

morphology as well as cells with minor protrusions no longer than the length of the cell body; Stage 2, cells extending neurite-like processes with the longest one being the length of the cell body; Stage 3, cells having at least one neurite-like process that is two lengths of the cell body or longer. As shown in Figure 16, regardless of the substrates, nearly 31% of cells acquired NGF-induced, neurite-bearing phenotype, which is represented by Stage 2 and Stage 3 cells. Within each stage category, the percentages of cells on the LbL/HP surface and the LbL/PEI control surface were statistically comparable in spite of the two substrates being drastically different in surface morphology. Average number of neurites per cell and average occurrences of branching per neurite were quantified to be 1.63 ± 0.30 and 0.14 ± 0.06 for the LbL/HP sample and 1.55 ± 0.22 and 0.14 ± 0.08 for the LbL/PEI control (values reported as mean ± standard deviation). At first glance, these results appeared to oppose the general notion that physical features of culture substrates affect PC12 cell differentiation. For example, Bain et al. observed a higher percentage of differentiated PC12 cells on a polished GaN a surface with vertically grown GaN nanowires [113]. However, in a study reported by Su and co-workers, neurite outgrowth from PC12 cells cultured on Si wafer with square-arrayed nanopillars was promoted over those grown on nonpatterned plain Si wafer [65]. Although the present work showed PC12 cells exhibiting similar differentiation behaviors on the two morphologically different substrates, it is important to note that the LbL/HP surface and the LbL/PEI surface not only differ topographically, but also chemically. In general, the LbL/HP surface can be viewed as cationic HPs spaced by anionic PSS polymers, while the LbL/PEI surface presents cationic PEI polymers. The observed cell differentiation behavior is likely resulting from the interplays of physical

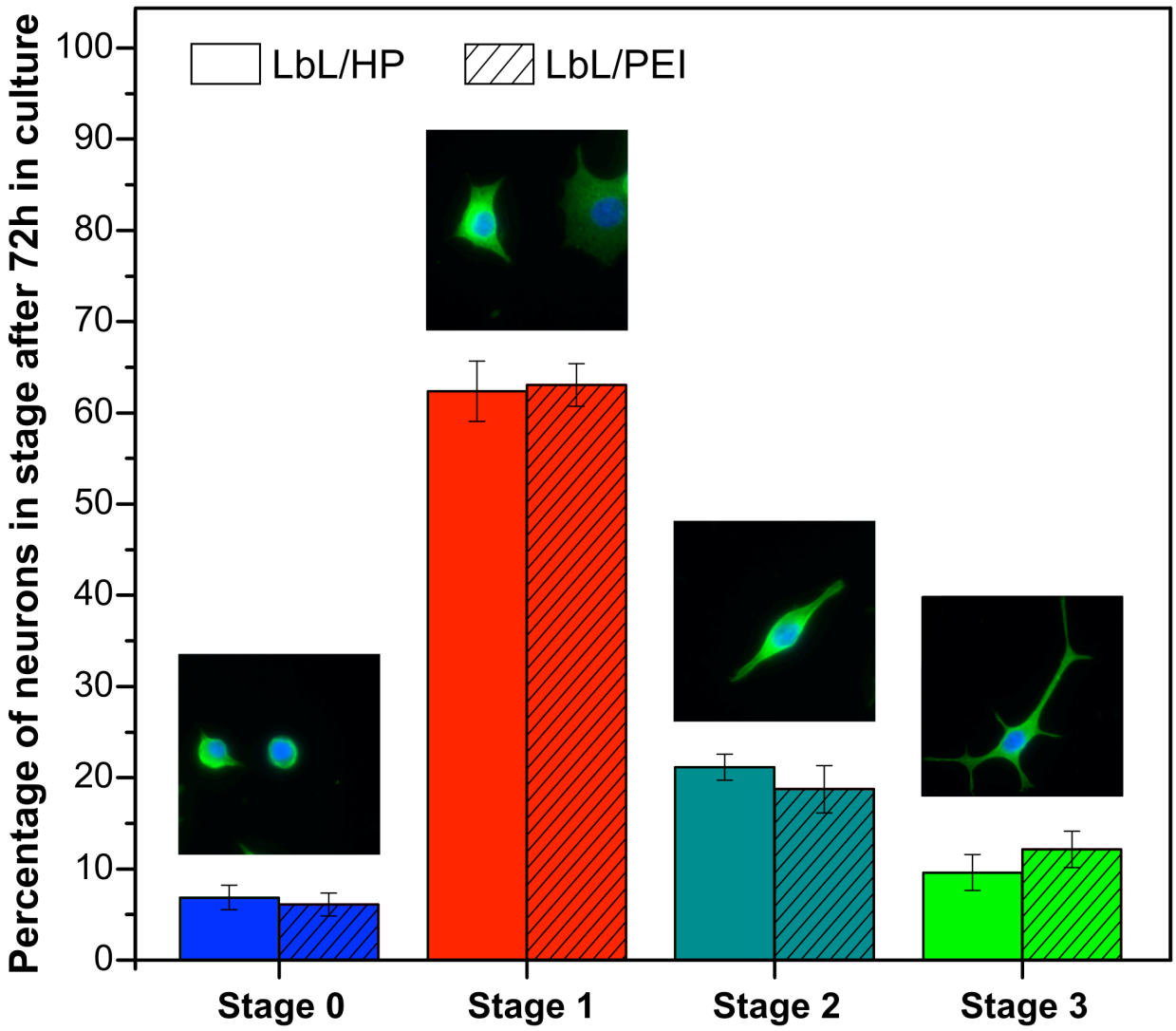


Figure 16 Percentages of PC12 cells at various differentiation stages following 48 h of culture in NGF-supplemented media (72 h of culture total) on the LbL/HP and LbL/PEI surfaces. Fluorescent images of cells stained for α-tubulin (green) and nuclei (blue) represent typical cell morphology at the corresponding stage. The total number of cells analyzed was 679 for the LbL/HP sample and 618 for the LbL/PEI sample.

and chemical surface cues, though the exact mechanisms behind such particle−cell interactions need to be further elucidated. Toward that end, elegant and sophisticated technologies, such as AFM [114, 115], could be adopted in the future to probe the strength of single cell adhesion to surfaces modified with HPs differing in size and surface charge. The information gained will also help tease apart contributions from each surface cue. Nevertheless, our findings demonstrate that the adsorbed HPs are supportive of neuronal differentiation of the attached PC12 cells.

2.1.3e Response of Primary Cortical Neurons to Adsorbed Hydrogel Particles

The promising findings from the PC12 cell studies have encouraged us to examine the response of primarily derived neurons to the HP-adsorbed surface. By using embryonic chick cortical neurons, we found that the HP-adsorbed surface was also supportive of cortical neuron adhesion and neurite outgrowth. Phase contrast imaging revealed that neurons attached in groups to the substrate after 24 h of culture (Figure 17A) and maintained such a group appearance throughout the 3-day incubation (Figure 17B,C). This response was different from that observed with the LbL/PEI control, where individual neurons adhered across the surface (Figure 18A) and gradually formed small clusters over time (Figure 18B,C). Neurite outgrowth was clearly progressing during the culture, from minor processes seen at 24 h (Figure 17A) to subsequent development of long neurites and establishment of cell-cell connections (Figure 17B,C). The neuritic nature of the extended processes was further visualized via immunostaining (Figure 17D), and SEM imaging allowed a direct view of the cell-substrate interaction, where cell bodies and neurites were commonly found growing

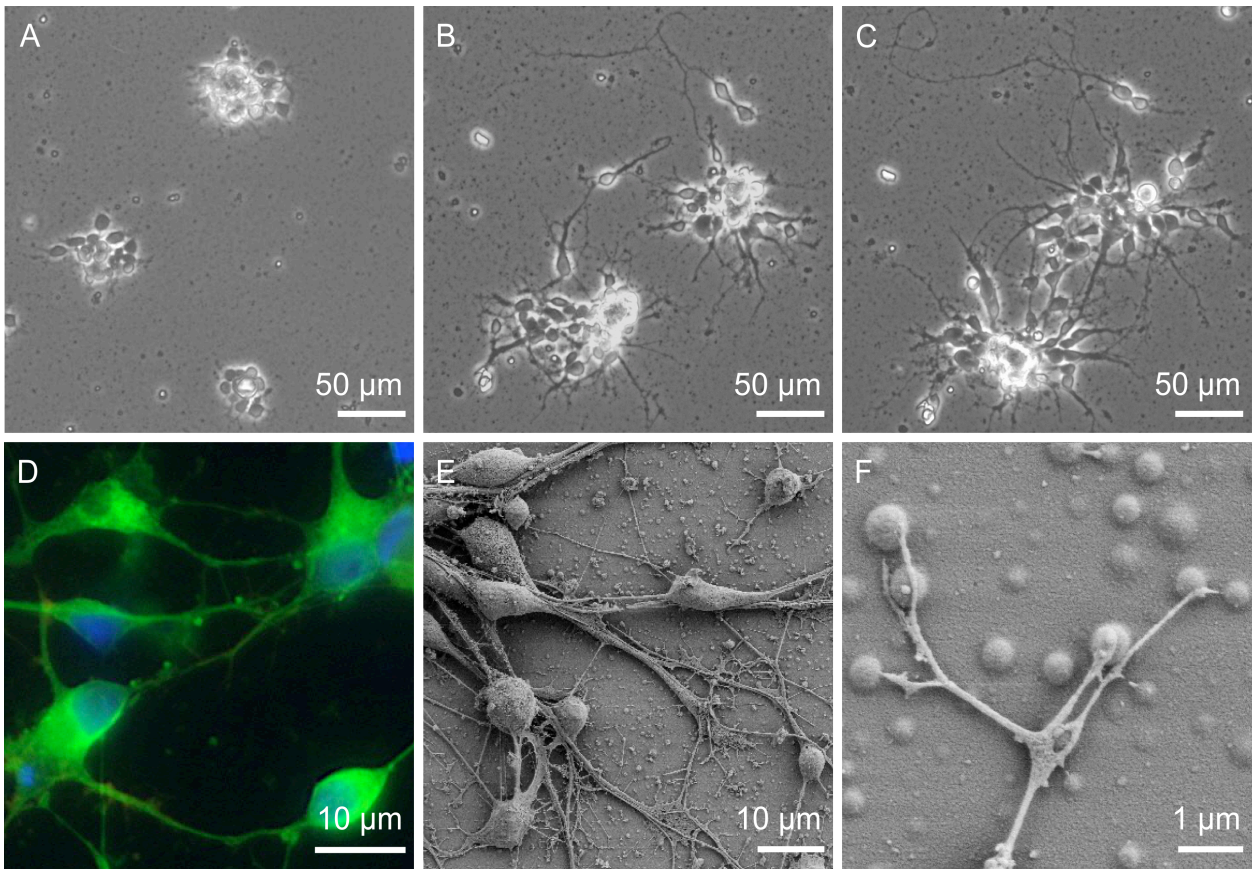


Figure 17 Response of primary chick cortical neurons to the LbL/HP surface. (A-C) Phase contrast images of cells at (A) 24 h, (B) 48 h, and (C) 72 h of culture. (D) Fluorescent staining of cells after 72 h culture (α-tubulin, green; nuclei, blue). (E, F) Scanning electron micrographs of cells fixed at 72 h of culture.

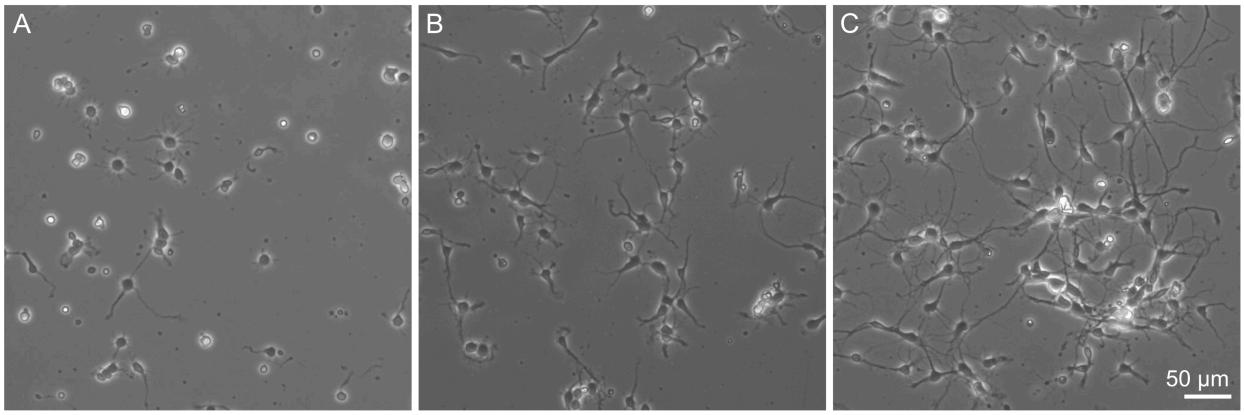


Figure 18 Phase contrast images of chick cortical neurons on the LbL/PEI surface at (A) 24 h, (B) 48 h, and (C) 72 h of culture.

directly in contact with or on top of the HPs adsorbed on the surface (Figure 17E,F). Collectively, these results further prove that a simple approach of adsorbing cationic HPs can improve neuronal interaction with planar substrates that are otherwise non-permissive to neurons.

2.1.4 Conclusions

In this study, we have presented an unprecedented simple and straightforward surface modification strategy of imparting neural permissiveness, a characteristic highly desirable for neural interfacing. By leveraging a unique epoxy-amine clicked HP system that we have recently developed and harnessing the basic phenomenon of electrostatically driven adsorption of charged colloidal particles on a solid substrate, a multifunctional surface integrating chemical cues, topographical cues, and reservoirs for hydrophobic compounds was achieved in a single step for the first time. The neural permissive feature of the modified surface was characterized in vitro with cultures of neuron-like PC12 cells and primary cortical neurons, both of which exhibited adhesion and differentiation. Collectively, these results substantiate the feasibility of creating easy to apply and scale up, low cost, adaptable, and multifunctional neuron interactive surfaces with herein developed approach. It is important to bear in mind the rapidly changing landscape of futuristic implantable neural prostheses, with increasing research efforts of developing ultrasmall neural implants. With the simplicity of our coating process and the previously shown versatility of preparing such cationic HPs with sizes down to the nanoscale, it is applicable to use the strategy presented here to facilitate long-term function of the next generation of devices. Future studies will exploit the hydrogel nature of our cationic particles and investigate whether particle stiffness can

be modified to our advantage to further modulate neuron response to the decorated surfaces. In addition, containment, release, and effectiveness of antioxidative biomolecules from the HP-adsorbed surfaces will be further investigated toward neural protection. The ultimate driving force is to advance the new multifunctional surface into clinical studies to gauge its practical potential in stabilizing the biotic/abiotic neural interface for reliable and long-term neural communication.

2.2 Central Nervous System Foreign Body Response Towards Hydrogel Particle-Modified Solid Planar Substrate

The following chapter section is based on a manuscript entitled “In Vitro Study of Central Nervous System Foreign Body Response Towards Hydrogel Particle-Modified Planar Substrate” with the following authors Emily A. Morin and Wei He that is under review after submission to the Journal of Biomedical Materials Research Part A. Emily A. Morin designed and performed the experiments, conducted the data analysis, and drafted the manuscript. Dr. Wei He financially supported this work as well as assisted in designing the experiments, analyzing the data, and revising the manuscript.

2.2.1 Introduction

Neural devices offer a promising solution to restore lost motor control or alleviate incapacitating symptoms for individuals suffering from traumatic brain injuries [1, 79] or neurological disorders like Parkinson’s disease [116, 117], epilepsy [118], or major depression [119]. Neural devices for such applications are implanted into the patient’s brain and interface with neural tissue. For the device to perform its intended function, such as recording and sending potentials from axons to externals devices or providing pulses of electrical stimulation, intimate communication with neighboring axons is

essential. To improve device efficiency, neuron adhesion and differentiation to the electrode must be pursued [120, 121]. However, common smooth electrode materials such as silicon [21, 122], platinum [123], and tungsten [124] that interface with the surrounding neural tissue are not permissive to such neuron integration.

A number of techniques have sought to improve device efficiency through direct neuron-device interaction. These efforts are typically directed towards surface chemistry and topographical modification. For example, cationic surface treatments such as polylysine [89] and PEI [90] promote neuron adhesion to a surface due to electrostatic interactions with cell membranes [125]. Topographical cues such as pillars [126] and grooves [127] have sought to direct axon growth and differentiation through cue shape, size, and spacing modifications.

Recently, our lab developed a system, that offers such charge and topographical cues, to promote neural growth on substrates typically non-permissive to neurons [128]. This system promotes neural cell adhesion mainly by providing cationic cues on the substrate surface through electrostatically adsorbed HPs. Furthermore, the adsorbed HPs hold a unique reservoir function, offering the potential for localized delivery of therapeutic agents beneficial for neural interfacing applications. While our results integrating neurons with HP-coated substrates were encouraging, little is known how non-neuronal cells would respond to such a modified surface. In particular, following neural device implantation, there are a few major cell types that comprise an inflammatory host response, which can form a dense fibrous capsule surrounding the implant and culminate in lost device function.

First, as the device is implanted into the brain it passes through the meningeal layers, which contain fibroblast that can migrate onto the device shaft [3, 4]. These stimulated cells and their elevated ECM expression can pose a physical barrier to neuron-device communication [3]. Moreover, they may negatively affect neurite outgrowth directly through potent chemorepellent expression [5] or indirectly through mediation with astrocytes [6]. As the device next advances in the highly vascularized brain, severed blood vessels pathologically recruit blood-borne monocyte-derived macrophages toward the implantation site. Once implanted in its final location in the brain, the device interfaces with glial cells such as astrocytes, that make up a majority of cells in this area, and microglia, whose activated function resembles that of the monocyte-derived macrophages pathologically recruited from the damaged vessels with leaky blood brain barrier. Reactive astrocytes are largely marked by cell hypertrophy, proliferation, migration, and an upregulation of GFAP [8]. Activated microglia can be recognized morphologically by their cell processes slightly retracting and thickening and physiologically by soluble factor secretion, cytokine secretion, and proliferation [9]. Specifically, cytokine secretion, as with pro-inflammatory cytokine tumor necrosis factor-alpha (TNF-α), may not impart damage to neurons directly but instead may act indirectly through synergistic interactions with other cytokines leading to cytotoxic nitric oxide production [11, 12] or through mediated interactions with non-neuronal cells [129]. These cells have the potential to reject the device and form a barrier, called a glial scar, obstructing it from nearby healthy tissue, specifically neurons, and thus tremendously reducing neuron-device communication. Therefore, when developing neural implant surfaces, it is important to study its effects on these various types of cells.

In the present work, the response of such inflammatory reactive cells towards the HP-modified surface was investigated in vitro. Specifically, the cells' initial interaction with the substrates was investigated using adhesion assays. To further probe the cells' response to the HP surface, indicators of cell reactivity like morphological changes, proliferation, and activation markers were evaluated. The findings of this study can help optimization of HP-based surface modification of neural implants toward improved performance.

2.2.2 Materials and Methods

2.2.2a Preparation and Characterization of Hydrogel Particle-Modified Planar Substrates

Preparation: Both silicon wafers with a 100-nm-thick oxide layer and microscopy glass slides (for direct visualization of live cell culture) were included as test substrates. Preparation of planar substrates has been described elsewhere [128]. LbL substrates with subsequent 10 min incubation in 1 mg/mL HP or PEI solution are denoted as LbL/HP or LbL/PEI, respectively.

Characterization: The HP deposition and distribution on the LbL/HP samples were characterized by a Zeiss Auriga SEM (Zeiss, Germany). In order to preserve surface morphology, the samples were examined directly without any conductive gold coating.

2.2.2b NIH 3T3 Cell Culture

NIH 3T3 fibroblast cells were used at passages 9 and 10. Cells were maintained in DMEM (ATCC) supplemented with 10% fetal calf serum (Thermo Scientific) and 1% penicillin/streptomycin (P/S) (Fisher Scientific) at 37 °C in a 5% CO_2 balanced-air

incubator. Medium was replaced every 2 – 3 days. To pass, cells were detached from the flask following trypsinization with 0.25% trypsin-ethylenediaminetetraacetic acid (EDTA) solution (Gibco).

Adhesion Study: To investigate cellular adhesion, individual fibroblast cells were acquired and seeded at a density of 10 000 cells/cm^2 onto the LbL/HP silicon substrates (n = 4) placed in a 24-well plate. Bare silicon, LbL, and LbL/PEI silicon substrates were used as controls. Following a 4 h attachment, the samples were prepared for immunocytochemistry visualization and quantification. Briefly, samples were washed with 1X PBS and fixed with 4% paraformaldehyde (Electron Microscopy Sciences) for 20 min at RT and then rinsed three times with 1X PBS. The cells were permeabilized with 0.1% Triton X-100 in 1X PBS for 5 min, followed by 30 min incubation in 4% GS (Gibco) in 1X PBS to block non-specific protein binding. Cells were then labeled with Alexa Fluor 594 phalloidin (Invitrogen) at 1:50 dilution in 1X PBS for 1 h. To counter stain for nuclei, cells were incubated in 3 µg/mL Hoechst 33342 (Thermo Scientific) in 1X PBS for 20 min. Cells were washed between steps with 0.05% Tween 20 wash buffer. Samples were mounted with a fluoromount G (Southern Biotech) antifade mounting solution. Fluorescent images were collected using a Zeiss Axio Observer A1 inverted fluorescent microscope (Zeiss, Germany).

Proliferation Study: A water-soluble tetrazolium salt (WST-1, Roche Applied Science, USA) assay was used to assess cell proliferation at 1, 2, and 3 days. Individual fibroblast cells were seeded at a density of 10 000 cells/cm^2 onto bare glass, LbL, LbL/HP, and LbL/PEI glass samples (n = 4) placed individually in wells of a 48-well plate. For each time point samples were transferred to a 48-well plate containing fresh

medium. WST-1 reagent was added to each well and incubated at 37 °C for 1.5 h protected from light. After mixing, supernatants were transferred to a 96-well plate and quantified using a plate reader to measure the solution absorbance at 440 nm against a blank control. Representative phase contrast images were taken for each sample using a Zeiss Axio Observer A1 inverted microscope (Zeiss, Germany) before beginning the WST-1 procedure.

2.2.2c RAW 264.7 Cell Culture

RAW 264.7 macrophage cells were used at passages 5 – 16. The cells were maintained in 100 mm non-tissue culture treated petri-dishes in DMEM supplemented with 10% FBS (Thermo Scientific) and 1% P/S at 37 °C in a 5% CO_2 balanced-air incubator. For medium renewal or passaging, cells were centrifuged, supernatant medium was removed, and cells were resuspended in fresh medium and subcultured or used for cell study.

Adhesion Study: To investigate cellular adhesion, individual macrophage cells were acquired and seeded at a density of 25 000 cells/well onto the LbL/HP silicon substrates (n = 3) placed individually in wells of a 48-well plate. Bare silicon, LbL, and LbL/PEI silicon substrates were used as controls. Following a 2 h incubation a live/dead staining assay was performed. Samples were rinsed with 1X PBS and incubated in a 1X PBS solution containing 2 μM calcein AM for 20 min at 37 °C. Calcein AM labeled cells were viewed under a Zeiss Axio Observer A1 inverted fluorescent microscope. Separate samples were prepared for qualitative cytoskeletal analysis following the fluorescent staining procedures described in the above NIH 3T3 cell adhesion study.

Activation Study: Production of pro-inflammatory TNF-α was quantified using a BD OptEIA mouse TNF enzyme-linked immunosorbent assay (ELISA) kit (BD Biosciences, USA). Following the assay procedure, 50 µL ELISA diluent was added to each well of an anti-mouse TNF monoclonal antibody pre-coated 96-well plate. 50 µL standards or collected sample medium (n = 4) were added to wells and incubated for 2 h at RT to allow binding of any present TNF to the immobilized antibody. After washing and aspirating, 100 µL biotinylated polyclonal anti-mouse TNF antibody was added to each well and incubated for 1 h at RT to produce an antibody-antigen-antibody sandwich. After washing and aspirating, 100 µL streptavidin-horseradish peroxidase conjugate was added to each well and incubated for 30 min at RT. The wells were again thoroughly washed, aspirated, and 100 µL TMB one-step substrate reagent was added to each well and incubated for 30 min at RT, which produced a blue color with intensity directly proportional to the amount of TNF present in the sample. 50 µL stop solution was added to each well and the plate was read at 450 nm and at 570 nm (λ correction).

To normalize pro-inflammatory cytokine secretion to cell number, cell samples were washed three times with 1X PBS, to remove interference from cell medium. To lyse, samples underwent three freeze/thaw cycles. 1X CyQUANT cell lysis buffer (Invitrogen, USA) was added to each sample and incubated for 5 min. Total protein content in the supernatant of centrifuged cell lysates was quantified using a Pierce Micro BCA Protein Assay Reagent Kit (Pierce, USA). Briefly, BCA working reagent was added to each sample, mixed, and incubated for 30 min at 37 °C protected from light. After cooling to RT, the absorbance value at 562 nm was recorded by a plate reader. As the total protein study quantifies amount of cells per sample per day, these results were

also indicative of cell proliferation behavior.

Cell proliferation and cell-substrate interactions were further qualitatively assessed using SEM. Samples cultured in parallel with the TNF-α secretion study were washed with 1X PBS, fixed with 3% gluteraldehyde (Electron Microscopy Sciences, USA) for 24 h at 4 °C, and underwent processes of dehydration using a series of ascending grades of ethanol washes (25, 50, 75, and 100%). Dehydration was continued by an incubation in a series of 100% ethanol and HMDS mixtures at ratios of 2:1, 1:1, 1:2, followed by evaporation in 100% HMDS. Samples were sputter-coated with gold for 20 s at 20 mA before SEM imaging.

To visualize HLA-DR, cells were seeded at a density of 10 000 cells/cm^2 onto bare glass or HP-modified glass substrates (n = 4) in a 24-well plate. After 24 h cell incubation, cell medium was replaced with fresh medium for non-treated bare glass and HP-modified glass substrates, with 5 µg/mL lipopolysaccharide (LPS, from *Escherichia coli* 0127:B8, Sigma-Aldrich) for stimulated bare glass control substrates, and incubated for 24 h. To improve staining visualization, the cells were fixed before they became confluent in ice-cold 100% methanol for 15 min at -20 °C and rinsed three times with 1X PBS for 5 min each. The samples were incubated for 30 min in 4% GS in 1X PBS to block non-specific protein binding. Cells were labeled with anti-HLA-DR [YE2/36 HLK] produced in rat (Abcam) at 1:100 dilution in 4% GS for 1 h, then labeled with Alexa Fluor 594 goat anti-rat IgG (H+L) secondary antibody (Invitrogen) at 1:200 dilution in 1X PBS for 1 h. Images were captured under the same imaging parameters.

2.2.2d A172 Cell Culture

A172 brain glioblastoma astrocyte-like cells were used at passages 4 – 9. Cells were maintained in DMEM growth medium supplemented with 10% FBS and 1% P/S at 37 °C in a 5% CO_2 balanced-air incubator. Medium was replaced every 2 – 3 days. To pass, cells were detached from the flask following trypsinization with 0.25% trypsin-EDTA solution.

Adhesion Study: To investigate cellular adhesion, individual astrocyte-like cells were acquired and seeded at a density of 10 000 cells/cm^2 onto the LbL/HP silicon substrates (n = 3) placed in a 24-well plate. Bare silicon, LbL, and LbL/PEI silicon substrates were used as controls. Following a 4 h attachment, the samples were prepared for quantification following the fluorescent staining procedures described in the above NIH 3T3 cell adhesion study.

Proliferation Study: Individual astrocyte-like cells were seeded at a density of 10 000 cells/cm^2 onto bare glass, LbL, LbL/HP, and LbL/PEI glass samples (n = 4) placed individually in wells of a 48-well plate. The WST-1 assay was prepared following the above NIH 3T3 proliferation study.

Activation Study: To quantify GFAP expression, an indicator, when overly expressed, of reactive astrocyte and A172 astrocyte-like cells, individual cells were seeded at a density of 10 000 cells/cm^2 onto bare glass and LbL/HP glass (n = 4) samples placed individually in wells of a 48-well plate and cultured for 3 days. Fluorescent staining procedures followed the above NIH 3T3 adhesion study. To investigate GFAP expression, cells were labeled with anti-GFAP produced in rabbit (Aldrich) at 1:500 dilution in 4% GS for 1 h, then labeled with Alexa Fluor 488 goat anti-

rabbit IgG (H+L) secondary antibody (Invitrogen) at 1:200 dilution in 1X PBS for 1 h. Images were captured under the same imaging parameters. GFAP intensity was calculated per image using ImageJ image analysis software (NIH, USA) by measuring, after background subtraction, the total pixel intensities divided by the cell count.

2.2.2e Statistics

Data were analyzed by the one-way ANOVA using a Tukey's post-hoc test (SPSS statistics software). Differences were considered significant for $p < 0.05$. All data were reported as mean ± standard deviation. Experiments were preformed in duplicate.

2.2.3 Results and Discussion

Previously, surface-adsorbed HPs have shown promising results promoting neuron integration onto typical neural device substrates that are non-adhesive to neurons. Nevertheless, for clinical applications it is well recognized that such neural devices encounter an array of cell types, beyond neurons, that impact the performance of the device. Therefore, it is critical to investigate how the HP-coated substrates influence behavior of cells that are characteristic of a CNS chronic tissue reaction.

2.2.3a Fibroblast Adhesion

In CNS in vivo implantation studies, meningeal fibroblasts have been shown to migrate from the meningeal layers down the neural device shaft [3, 4]. As fibroblast are anchorage-dependent cells it was imperative to first study their early adhesion to the substrates. Figure 19 shows the LbL, LbL/HP, and LbL/PEI silicon substrates incited fibroblast cellular adhesion to varying extents. The bare silicon substrate did not support adhesion. The LbL substrates had about 40% less adherent cell density as the LbL/HP substrates. Typical morphology of an adhered cell on the test substrates varied. The

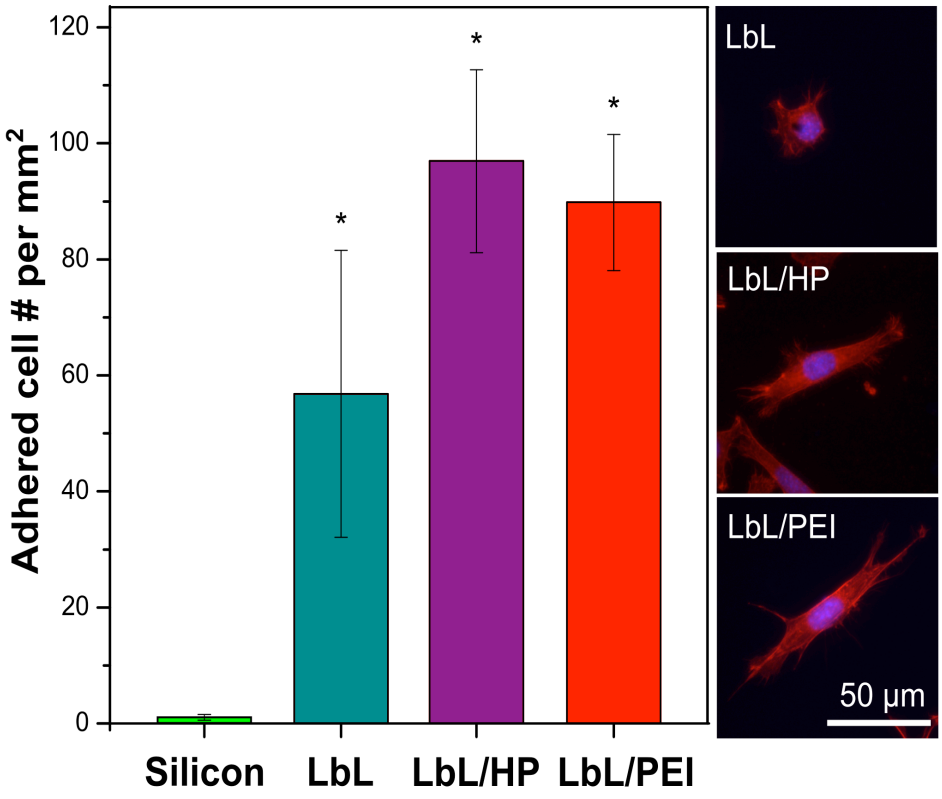


Figure 19 Quantitative 4 h NIH 3T3 cell adhesion density on LbL/HP and control substrates (*$p < 0.05$, compared to silicon) with representative fluorescent images of the cells stained for actin filaments (red) and nuclei (blue).

cells on the LbL surface were small and round with little to no extensions, while the cells on both the LbL/HP and LbL/PEI substrates had similar cell morphology with polarized spread cell bodies and multiple short filopodia extensions.

The fibroblast cell adhesion to the LbL/HP-coated silicon substrates is most likely a result of cationic charge contributions from the particles, as the cationic charged LbL/PEI control substrate also presented a similar density of adhered cells. This hypothesis is supported by the research of Webb et al. that under physiological pH, NIH 3T3 adhesion increased when cultured on cationic charge substrates compared to non-cationic charged substrates [130]. This outcome is not likely a result of surface hydrophilicity, as both bare silicon and LbL/HP had similar water contact angles, roughly 50º, yet exhibited drastically different cell adhesion densities. Although surface wettability in the moderate range of 50 – 60° water contact angle has shown maximal NIH 3T3 cell growth compared to other contact angles on the same polymer substrate [131], this was not the case for the bare silicon control substrate as it had almost no cell adhesion. Although baring similarities to Webb and coworkers' previous study where the substrates with an overall greater density of adhered cells appeared to have cells with more focal adhesion sites than their counterparts, it is interesting to note that the morphological characteristics of these adhered cells differed [130]. Cells adhering to the cationically charged LbL/HP and LbL/PEI substrates displayed a bipolar shape and higher aspect ratio, unlike Webb and coworkers' findings, compared to the LbL substrates that displayed round cells with little spreading.

2.2.3b Fibroblast Proliferation

Next, to investigate fibroblast-device interaction over time, proliferation of the fibroblast cells on the substrates was quantified. The phase contrast images of Figure 20 show for all substrate groups the cell density increased over time. After day 1 and 2, all four test substrates had similar cell morphologies consisting of polygonal shaped cell bodies with cell extensions of moderate length. The cells were evenly distributed on the samples. After day 3, it was microscopically determined that the cells on both the LbL/HP and LbL/PEI had reached confluence.

The metabolic activity of the cells on bare glass, LbL, LbL/HP, and LbL/PEI glass was evaluated over 3 days using a WST-1 assay. Figure 21 shows that, while the various substrates all supported fibroblast proliferation over time, the rate of proliferation varied greatly. The fibroblasts on the glass and LbL-primed glass samples proliferated at the slowest rates. Fibroblasts on both the LbL/HP and LbL/PEI reproduced at a similar elevated rate over time and were statistically different compared to the absolute metabolic activities of the cells on the glass samples at each time point.

The LbL/HP substrates had significantly greater cell proliferation compared the bare glass control substrates, and can thus be considered non-cytotoxic towards cultured fibroblast cells. On one hand, such fibroblast proliferation on functional areas of the device could diminish neural signal device communication. On the other hand, fibroblast proliferation with non-functional areas of the device could promote integration of the implant with surrounding tissue [3]. Micromotion of neural devices in vivo can be caused by physiological or external factors resulting in vibrational disturbances or physical device drift [132]. Strategies promoting device integration with surrounding

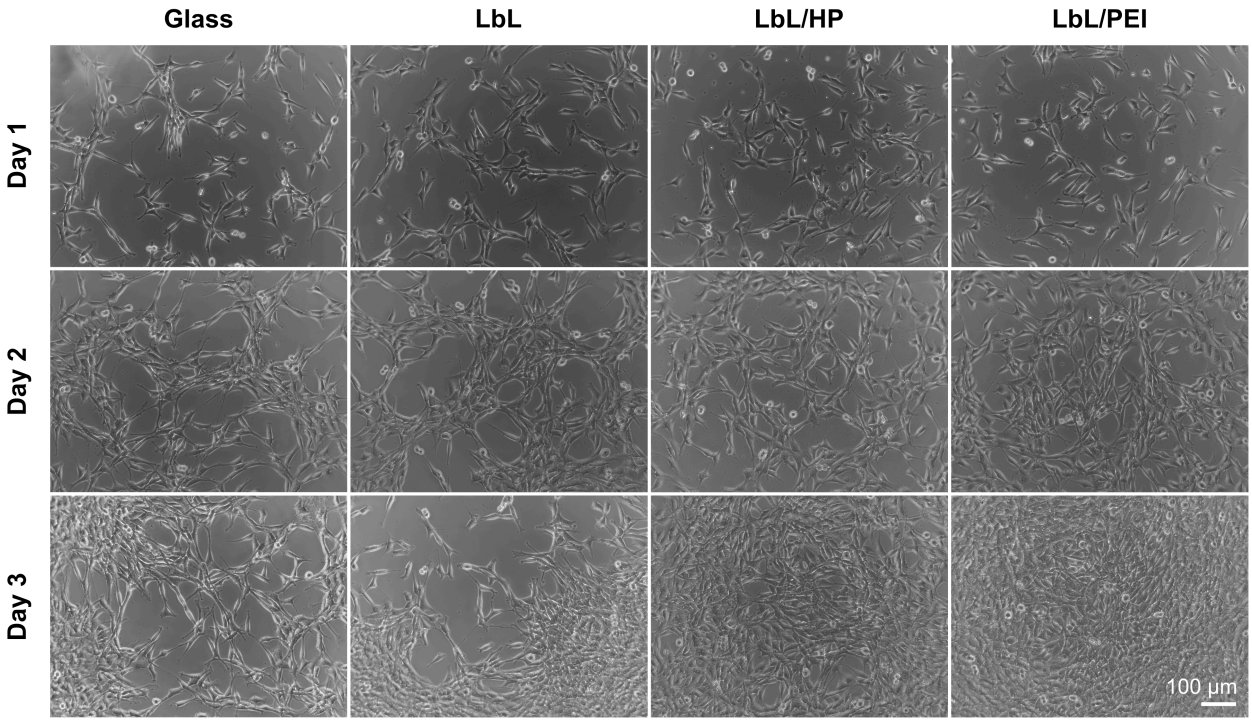


Figure 20 Representative phase contrast images of NIH 3T3 cells on LbL/HP and control substrates for 1 – 3 days of culture.

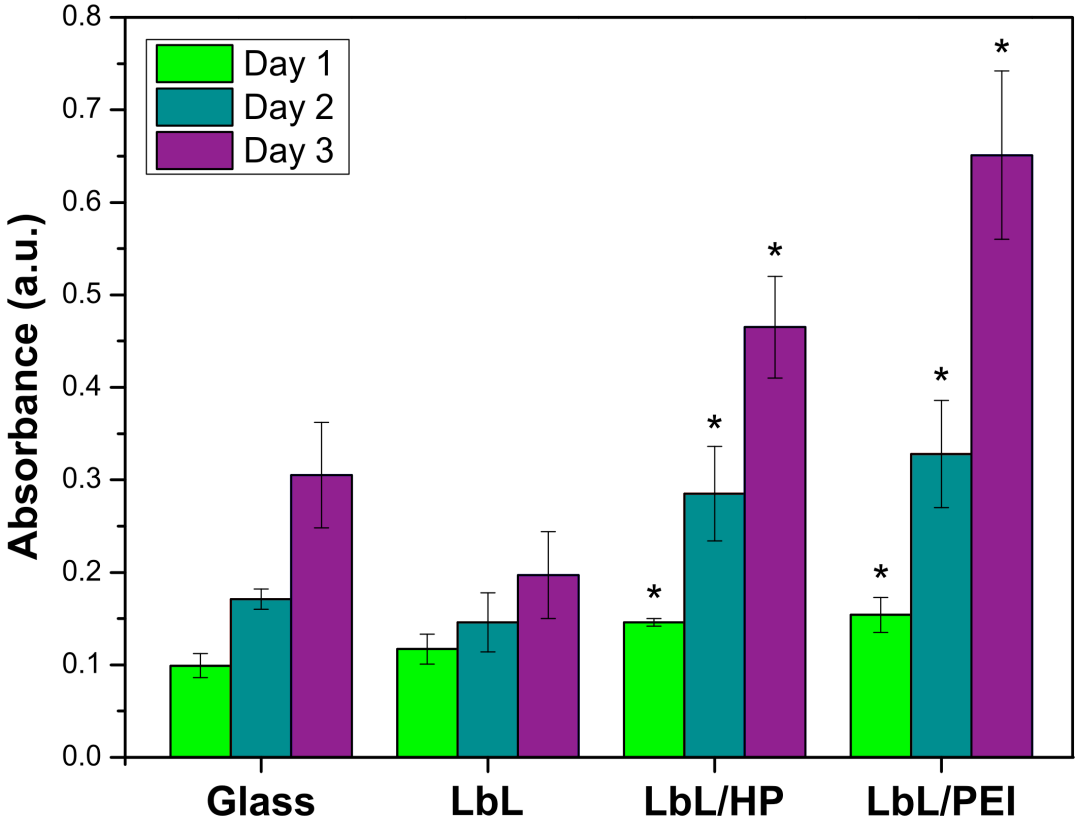


Figure 21 WST-1 assay quantified metabolic activity of NIH 3T3 cells for 1 – 3 days in culture on LbL/HP and control substrates (*$p < 0.05$, compared to glass at each time point).

neural tissue could reduce such micromotion and improve sensitivity and longevity of neural device recordings [133].

2.2.3c Macrophage Adhesion

Macrophages associated with chronically implanted neural devices originate from two distinct locations [134]. Participating in immune function, microglial cells in the CNS are functionally equivalent to macrophage cells in the peripheral tissue [135]. These cells can become activated following axonal injury induced by neural device implantation and can remain in an activated state of “frustrated phagocytosis” due to their inability to phagocytose the implant in the surrounding tissue [136]. Additionally, blood-borne monocyte-derived macrophages originate from the breach in the blood brain barrier upon device implantation [137] and secrete inflammatory factors that could compromise neuron health and device functionality [138]. A macrophage cell response to a CNS biomaterial is marked in part by adhesion, proliferation, morphological changes, and release of inflammatory factors [14]. Figure 22 shows the 2 h adhesion of RAW 264.7 macrophage cells on bare silicon, LbL, LbL/HP, and LbL/PEI silicon. The substrates all elicited adhesion with no significant difference of cell densities on LbL, LbL/HP, and LbL/PEI substrates compared to cells on bare silicon. Fluorescent cytoskeletal staining showed similar cell morphologies between sample groups, where all cells had small rounded bodies with short filopodia extensions.

2.2.3d Macrophage Proliferation, Pro-Inflammatory Tumor Necrosis Factor-Alpha Expression, and HLA-DR expression

The bare silicon and LbL/HP samples had a similar cell growth rate over 2 days as quantified by total protein concentration; however, by day 3 the LbL/HP samples had

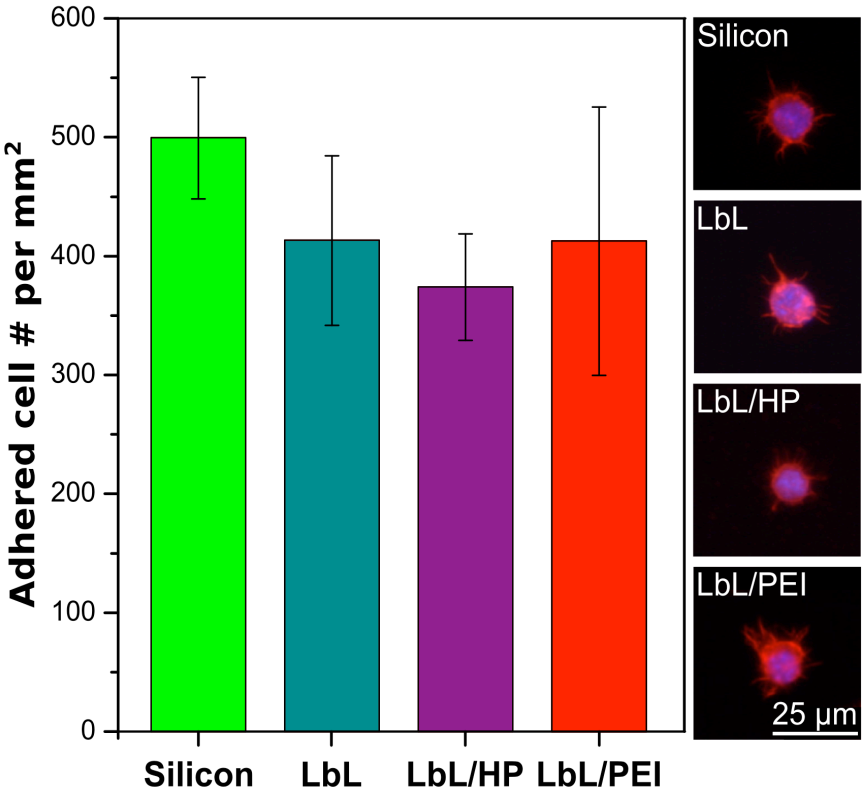


Figure 22 Quantitative 2 h RAW 264.7 cell adhesion density on LbL/HP and control substrates with representative fluorescent images of the cells stained for actin filaments (red) and nuclei (blue).

a significant increase in total protein concentration (Figure 23B). This result was supported by low magnification SEM images (Figure 23C). Magnified SEM images show the macrophage cells differed in morphology at the experimental time points. The cells on the silicon substrates displayed a spread cell body and polarized morphology with filopodia extensions and lamellapodia spreading, while the cells on the LbL/HP substrates displayed a mostly round cell body morphology with filopodia extensions making intimate contact with the surface-adsorbed HPs and little to no lamellapodia spreading.

The activation of macrophages was evaluated over 3 days by TNF-α quantification, total protein concentration quantification, HLA-DR expression, and SEM imaging. TNF-α, a pro-inflammatory cytokine marker, increased over time for both bare silicon and LbL/HP silicon samples, where the increase in TNF-α production over 3 days for the LbL/HP samples was significantly different compared to the bare silicon samples for each day (Figure 23A). Additionally, cells on unmodified and HP-modified substrates expressed significantly less elevated levels of HLA-DR, a commonly used marker for M1 macrophages [139], compared to LPS-stimulated macrophages on unmodified substrates (Figure 24).

On the bare silicon substrates, the polarized macrophage cell morphology corresponding with low TNF-α expression is consistent with previous research investigating pro-inflammatory activation of RAW 264.7 cells [140]. Although cells grown on LbL/HP substrates had increased proliferation and TNF-α expression over time compared to the bare silicon control, their morphology was rounded with thin filopodia extensions, which is distinctive from the mature morphology typically associated with

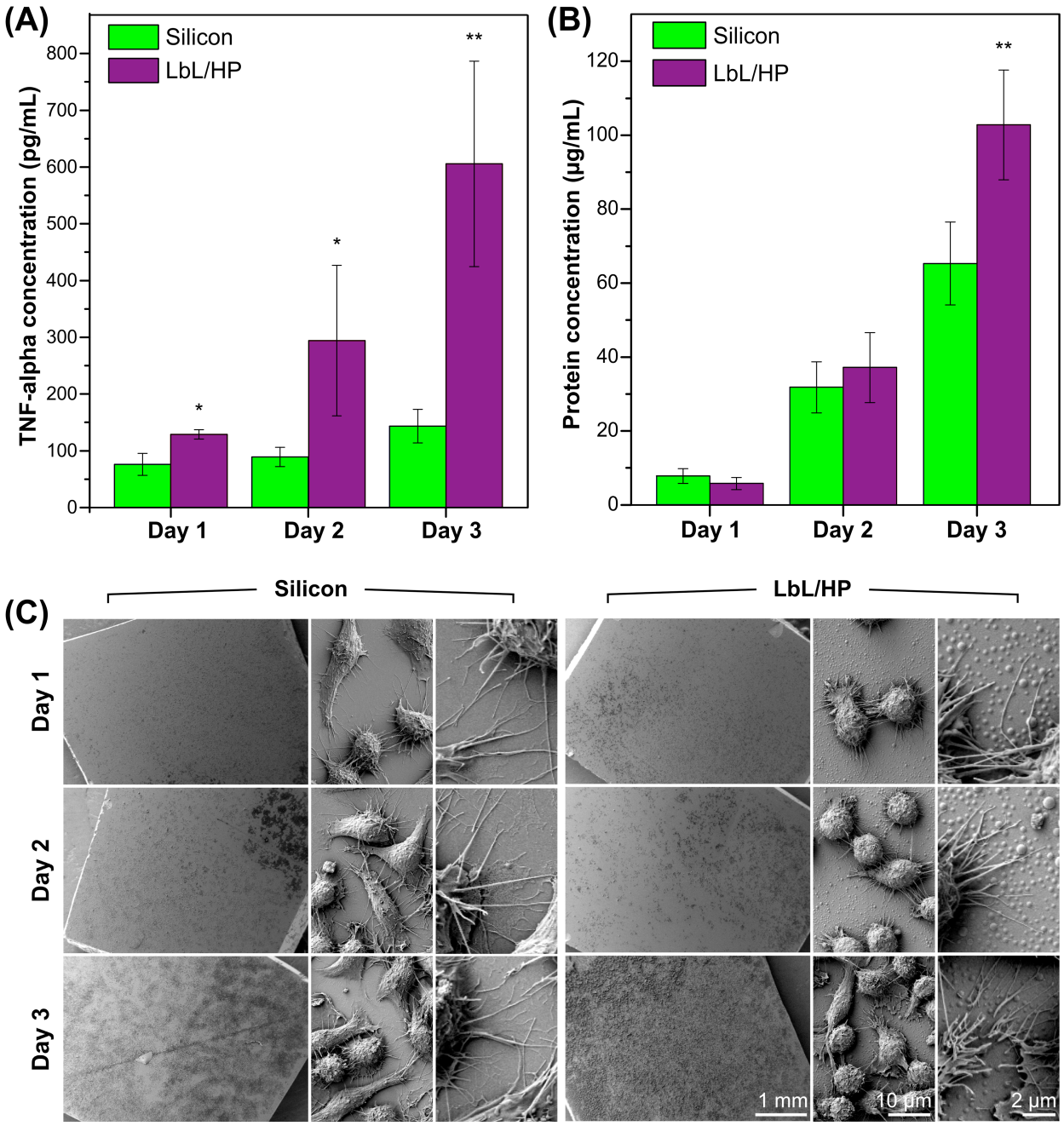


Figure 23 (A) TNF-α secretion and (B) quantification of total protein for RAW 264.7 cells cultured for 1 – 3 days on silicon and LbL/HP silicon substrates (*$p < 0.05$, **$p < 0.01$ compared to silicon at each time point). (C) Representative SEM images of RAW 264.7 cells cultured for 1 – 3 days on silicon and LbL/HP silicon substrates.

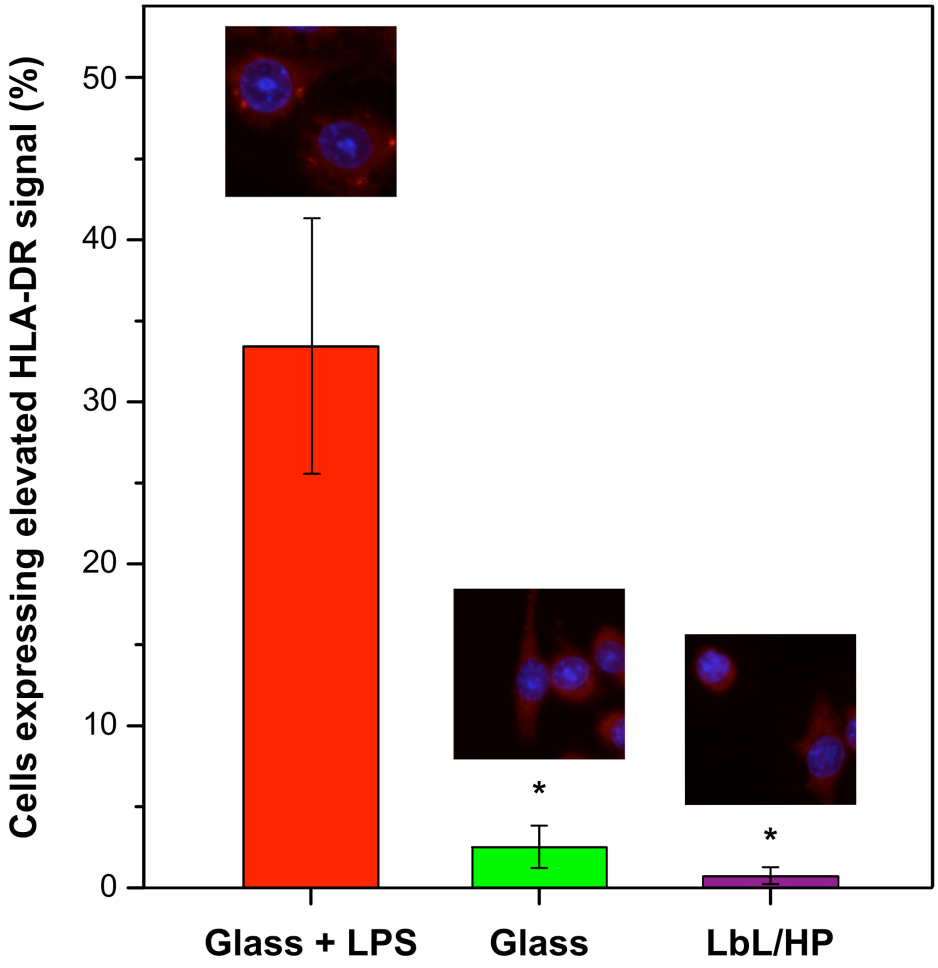


Figure 24 Percent RAW 264.7 cells expressing elevated HLA-DR signal after 48 h with representative images (HLA-DR: red, nuclei: blue) (*$p < 0.05$, compared to glass + LPS).

activated RAW 264.7 cells that are polygonal shaped with numerous thick pseudopodia [140, 141]. Proinflammatory cytokine interleukin-1 beta (IL-1β) expression was also quantified [data not shown]. However, concentrations for all experimental time points were lower than the assay detection sensitivity limit of 8 pg/mL. Whether the extent of TNF-α or IL-1β secreted from cells cultured on LbL/HP substrates would adversely impact survival of surrounding neural cells requires further investigations. Since HLA-DR marker can have a variable basal expression among macrophages [142], only the percentage of cells with a clear elevated signal was quantified. Cells on unmodified and HP-modified substrates had a low percentage of cells expressing elevated HLA-DR signal, about 2.5% and 1% respectively, compared to cells stimulated with LPS, about 33%. Unlike the RAW 264.7 cells of the unmodified and HP-modified samples which displayed a morphology similar to the cells from corresponding SEM images of the TNF-α study, many of the LPS-stimulated cells displayed a mature morphology of polygonal shape with several thick pseudopodia.

Regarding phagocytosis, macrophages can engulf both free and surface associated microbes [143], however to our knowledge there is no work for comparison investigating macrophage phagocytosis of surface-adsorbed polymeric particles. Following the total protein assay, which removed cells from the substrate surface during the cell lysis step, it allowed us to determine via SEM imaging whether HPs remained adsorbed to the substrate surface. Observation of these images revealed the macrophage cells did not phagocytose the surface-adsorbed HPs during the course of the culture (Figure 25), which seems probable as the particles' diameter is smaller than the free particle size range typically phagocytosed by macrophages [36]. This finding is

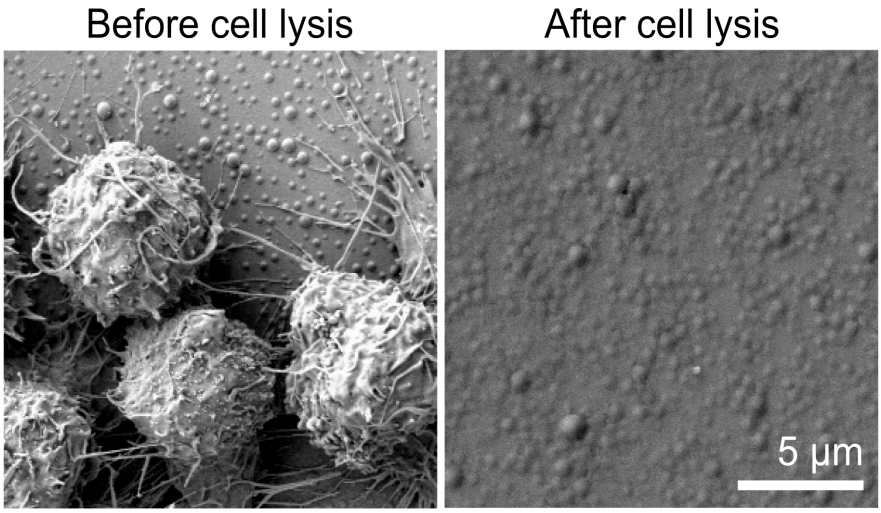


Figure 25 Scanning electron micrographs of Day 3 LbL/HP substrate before and after total protein cell lysis assay.

encouraging, considering that one of the intended functions of the adsorbed HPs is to serve as reservoirs for localized release of therapeutics.

2.2.3e Astrocyte Adhesion

Figure 26 shows the 4 h A172 cell adhesion evaluated for bare silicon, LbL, LbL/HP, and LbL/PEI silicon samples. LbL/HP and LbL/PEI substrates prompted astrocyte-like cell adhesion and had a significantly greater density of adhered cells compared to bare silicon. This result may be due to the cationic charge of the HPs, as the cationically charged LbL/PEI surface had a statistically greater cell adhesion density than the bare silicon and a similar average density to the LbL/HP substrates. The morphology of the cells was drastically different among sample groups. The few cells supported by the silicon and LbL-primed silicon substrates had small, round cell bodies with few polarized cell extensions. LbL/HP-supported cells had larger spreading cell bodies with many defined extensions and LbL/PEI-supported cells had spread cell bodies with lamellapodia spreading but few to none defined cell body extensions.

2.2.3f Astrocyte Proliferation and Glial Fibrillary Acidic Protein Expression

Astrocyte cells constitute the majority of the glial cells in the CNS and are a principal component of the glial scar. Reactive astrocytes are characterized by a number of attributes including enhanced proliferation, migration, and an upregulation of GFAP.

Cell growth on substrates was evaluated by phase contrast imaging over 3 days (Figure 27). The cells on each sample had evenly distributed densities that increased in number over time. Cells on bare glass, LbL/HP, and LbL/PEI glass samples had reached confluence after 3 days of culture. Figure 28 shows the cell metabolic activity

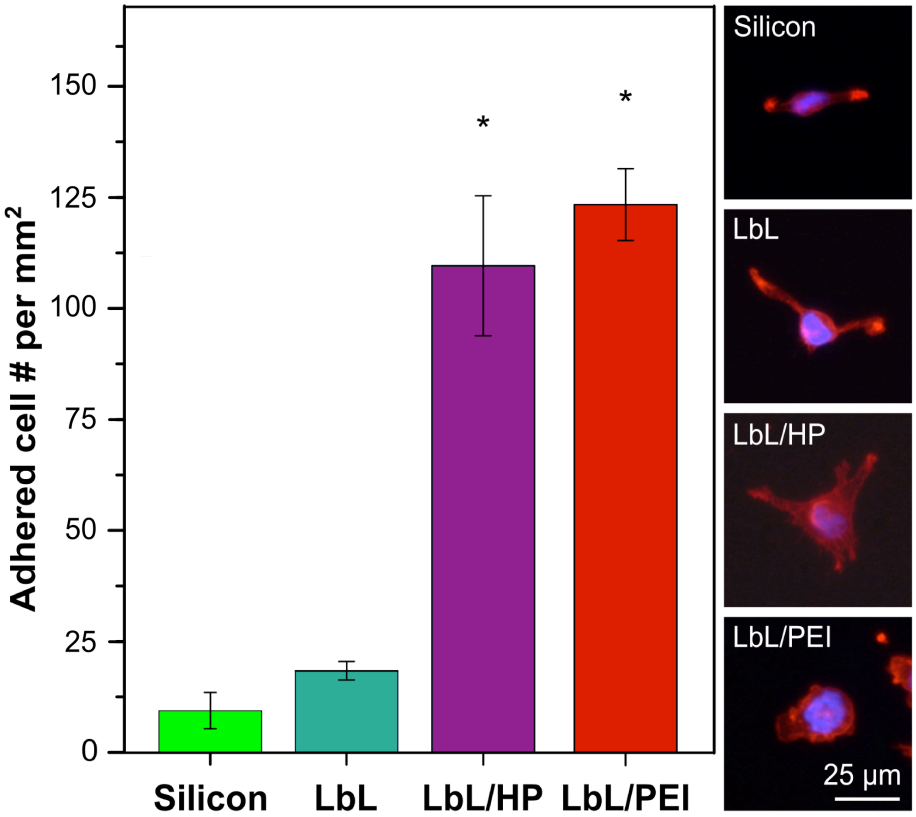


Figure 26 Quantitative 4 h A172 cell adhesion density on LbL/HP and control substrates (*p < 0.05, compared to silicon) with representative fluorescent images of the cells stained for actin filaments (red) and nuclei (blue).

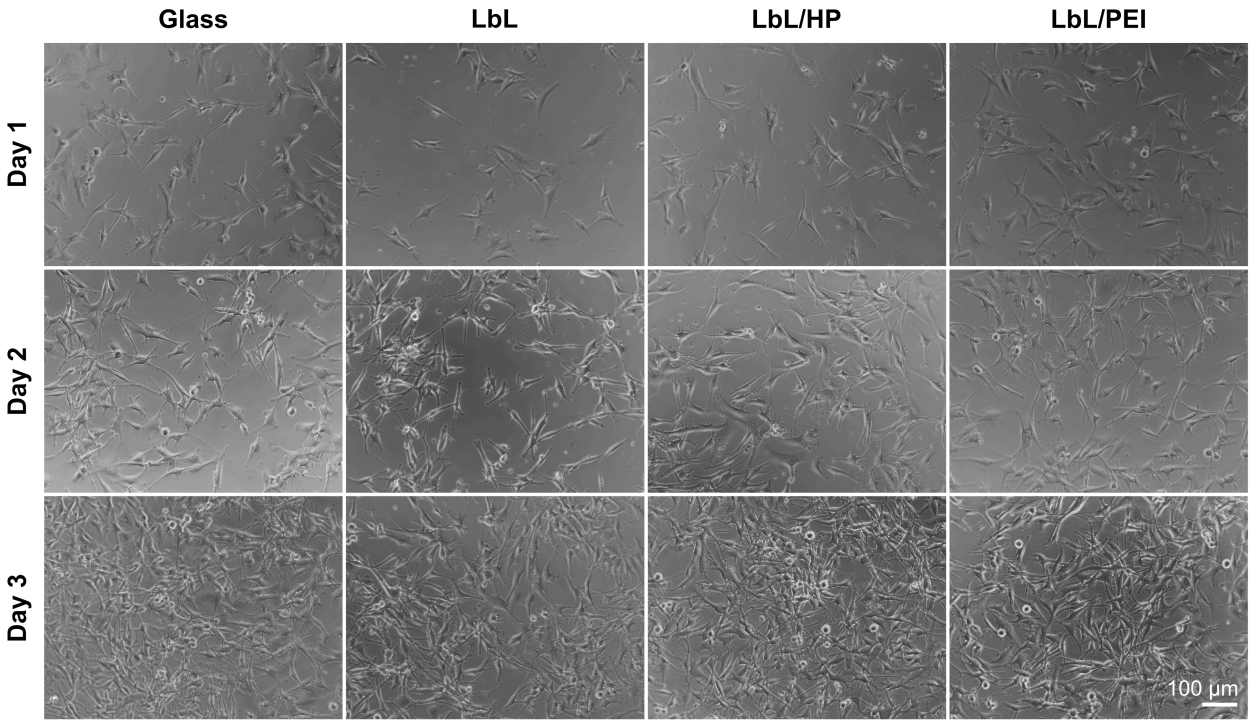


Figure 27 Representative phase contrast images of A172 cells on LbL/HP and control substrates for 1 – 3 days of culture.

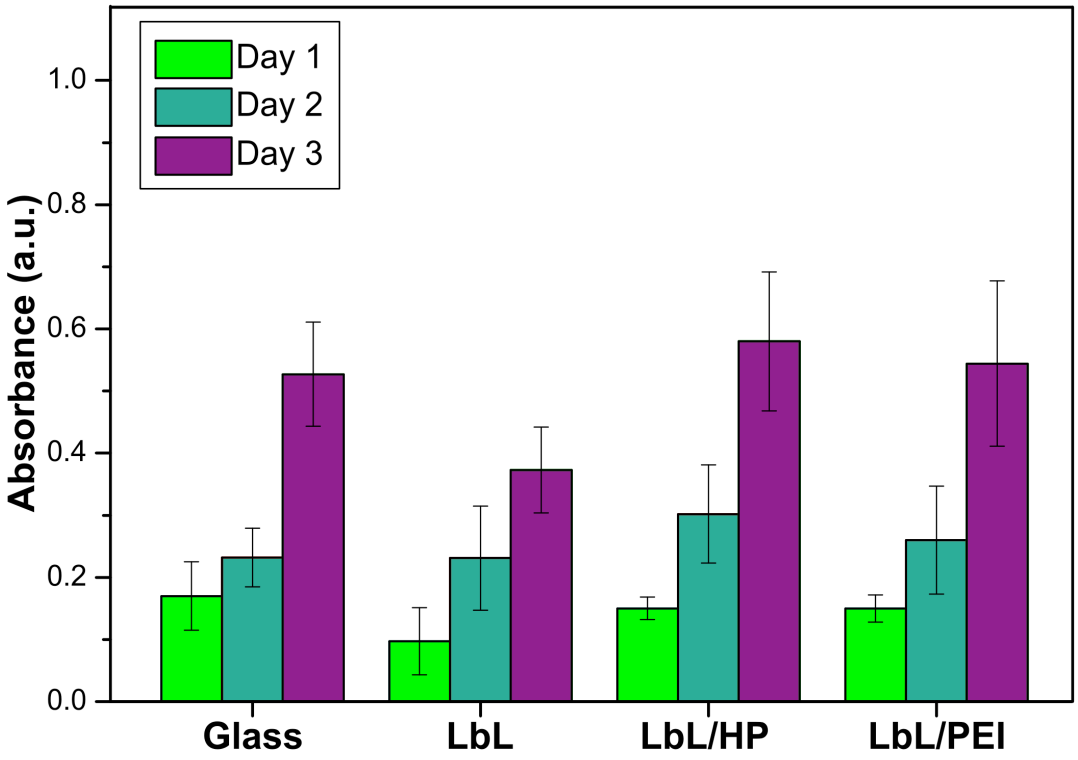


Figure 28 WST-1 assay quantified metabolic activity of A172 cells for 1 – 3 days in culture on LbL/HP and control substrates.

on the various substrates increased overtime. Compared to glass, the extent of increase at each day was statistically similar.

Astrocyte-like cell reactivity was evaluated by analyzing GFAP content per cell on the LbL/HP glass and bare glass control samples. Figure 29 representative images show similarities between astrocyte-like cell body morphology on each sample group after 3 days in culture. Astrocyte-like cells on both sample groups had comparable cell morphologies, where there was a combination of thin polarized cells and highly spread cells (Figure 29A). The fluorescent signal of the cells appeared similar between the two groups with uniform fluorescent intensity along both the cell bodies and cell extensions. Both bare glass and LbL/HP glass samples had a similar average and distribution of the quantified fluorescence per cell (Figure 29B).

Over time the cells on the LbL/HP substrates mainly displayed a spindle shape, which is consistent with typical healthy, undifferentiated A172 cells [144]. Considering astrocyte activation, GFAP distribution has correlations with astrocyte shape, motility, and differentiation, where differentiated astrocytes display higher concentrations of GFAP compared to undifferentiated cells [145]. The GFAP distribution in cells adhered to both the bare glass and LbL/HP-coated glass was finely granular and diffuse throughout the cell cytoplasm, which is consistent with other spindle shaped astrocyte cells [145]. The weak GFAP signal could be a result of basal GFAP levels in the astrocyte-like cells. It is noteworthy to indicate that the A172 cell line has been reported as an alternative of primary astrocytes [146], however other significant aspects of the inflammatory response, including hypertrophic phenotype and inflammatory factor secretion, are important to obtain using primary mouse astrocytes. This will improve our

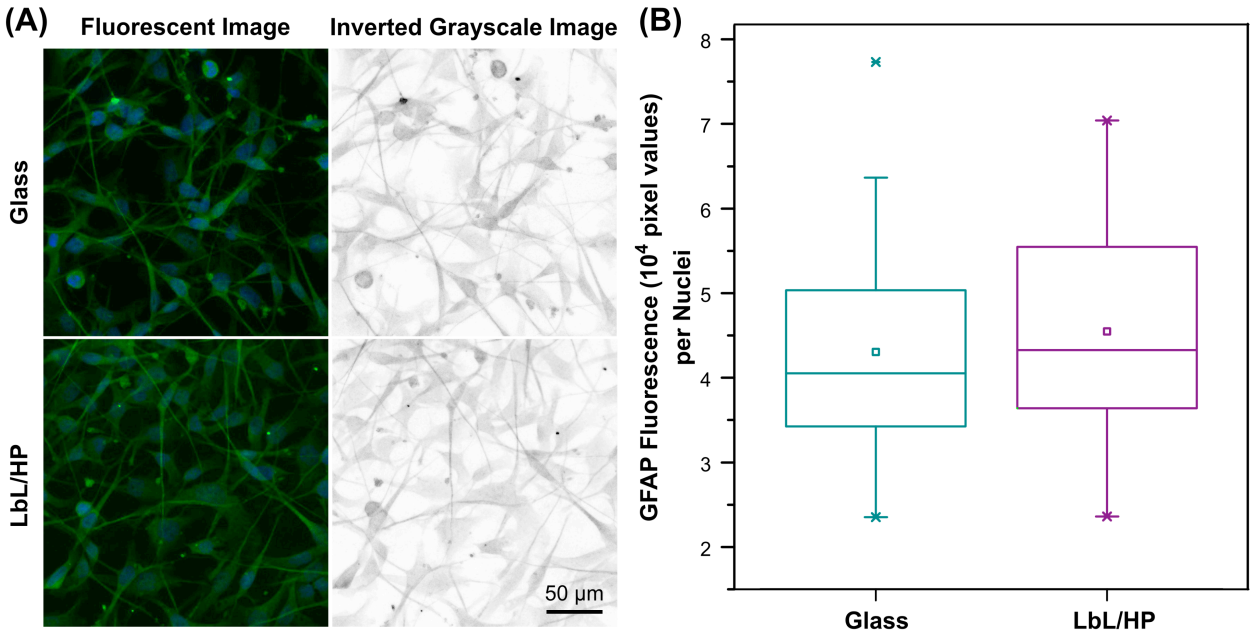


Figure 29 (A) Representative fluorescent images (GFAP: green, nuclei: blue) and processed inverted gray scale images of A172 cells on glass and LbL/HP glass substrates after 3 days in culture. (B) GFAP expression quantified as average fluorescent intensity per cell.

understanding of astrocyte inflammatory responses towards the HP-modified surface. The presence of astrocyte-like cells attaching and proliferating on the LbL/HP substrates does not necessarily imply detrimental consequences, as astrocyte proximity to neurons often bears physiological significance. It is well known that without astrocytes, important neuron and vascular bridge structures would be divided [147]. Nevertheless, with the original intention of developing the LbL/HP surface for direct engagement with neurons, the proliferative activity of astrocyte on such a surface should be further modulated to allow the modified surface to remain available for direct neuron access.

2.2.4 Conclusions

In an effort to understand CNS inflammatory cell response towards HP-modified surfaces, NIH 3T3 fibroblast, RAW 264.7 macrophage, and A172 astrocyte-like cells were evaluated in vitro. None of the cell types were vitally damaged by the HP-modified surface and remained metabolically active over the course of 3-day investigations. Such an outcome could be beneficial to promote integration of non-functional areas of a neural device and prevent micromotion and its negative effects on device function. Cultured on the LbL/HP substrates, RAW 264.7 cells expressed detectable levels of pro-inflammatory cytokine TNF-α but displayed a morphology unlike that of typical activated RAW 264.7 cells. A172 astrocyte-like cells largely displayed an undifferentiated morphology and expressed a mild amount of GFAP after 3 days, which may be a basal amount. Furthermore, the surface-adsorbed HPs hold the unique potential to further benefit the interfacing of neural devices as localized delivery agents of therapeutic biomolecules. Future research will be based on these findings to refine

the strategy of surface modification of neural implants with adsorbed HPs to improve stability, sensitivity, and longevity of neural devices.

2.3 Cell-Cell Influences of Primary Cortical Neurons and A172 Cells on Hydrogel Particle-Modified Solid Planar Substrate

2.3.1 Introduction

In the CNS astrocytes and neurons are intimately associated. Astrocytes play a large role in brain homeostasis that implicate them in both neuroprotection and neurodegeneration [148]. Neurons and astrocytes are also significantly associated in proximity and in direct contact of developing and adult CNS tissue. For example, neurons in direct contact with astrocytes, either with their cell body or neurites, responded to calcium waves propagation in stimulated contacting astrocytes [149]. Furthermore, cell-cell contact of astrocytes and neurons is associated with synaptogenesis [150].

As previously mentioned, astrocytes can impede neuron integration with neural devices through physiological changes that contribute greatly to the glial scar [14]. In a mechanical lesion mouse cortical co-culture model, neurons were able to migrate and develop neurites in proximity with inhibited reactive astrocytes and under permissive conditions of laminin [151]. It is important to study close involvement of neurons and astrocytes when developing neural implant surfaces, as their interaction with each other and such devices bear a large part in device functionality.

2.3.2 Materials and Methods

2.3.2a Primary Cortical Neuron and A172 Co-Culture

Cortical neurons were obtained from 7-day-old chicken embryo [101]. Forebrains of the embryo were dissected, minced into small pieces, and enzymatically dissociated with 0.25% trypsin (Invitrogen) in 1X PBS for 20 min at 37 °C, followed by inactivation with culture medium of DMEM (ATCC) containing 1% L-glutamine (Life Technologies), 10% FBS, and 1% Anti/Anti. A cell pellet was obtained after a brief centrifugation, and mechanical trituration using a fire-polished Pasteur pipet was applied to further dissociate the cells for seeding.

A172 brain glioblastoma astrocyte-like cells were used at passages 9 – 18. Cells were maintained in DMEM growth medium supplemented with 10% FBS and 1% P/S at 37 °C in a 5% CO_2 balanced-air incubator. Medium was replaced every 2 – 3 days. To pass, cells were detached from the flask following trypsinization with 0.25% trypsin-EDTA solution. Before co-culture incubation, cells were pretreated with cortical neuron medium for several days.

Cell Density Quantification: To determine the preferred adhesion of neuron and A172 cells on HP-coated samples (n = 4) individual A172 cells were seeded at a density of 10 000 cells/cm^2 onto LbL/HP cleaned glass, and LbL/PEI samples, placed in individually in a 48-well plate. To this, individual cortical neurons were seeded at a density of 50 000 cells/cm^2. For the 72 h samples, the culture medium was replaced at 24 h to remove unattached cells.

For immunocytochemistry studies, at the end of the predetermined time periods 4, 24, and 72 h, samples were washed with 1X PBS and fixed with 4%

paraformaldehyde (Electron Microscopy Sciences) for 20 min at RT and then rinsed three times with 1X PBS. The cells were permeabilized with 0.1% Triton X-100 in 1X PBS for 5 min, followed by 30 min incubation in 4% GS (Gibco) in 1X PBS to block nonspecific protein binding. To distinguish between neurons and A172 cells, neurons were labeled with monoclonal anti-α-tubulin primary antibody produced by mouse (Sigma-Aldrich) at 1:200 dilution and A172 cells were labeled with anti-GFAP produced in rabbit (Aldrich) at 1:500 dilution in blocking solution for 1 h. Neurons were then labeled with Alexa Fluor 488 goat antimouse IgG1 (γ1) secondary antibody (Life Technologies) at 1:100 dilution and A172 cells were labeled with Alexa Fluor 594 goat anti-rabbit IgG (H+L) secondary antibody (Invitrogen) at 1:200 dilution in 1X PBS for 1 h. To counterstain for nuclei, cells were incubated in 3 μg/mL of Hoechst 33342 (Thermo Scientific) in 1X PBS for 20 min. Cells were washed between steps with 0.05% Tween 20 wash buffer. Fluorescent images were collected using a Zeiss Axio Observer A1 inverted fluorescent microscope (Zeiss, Germany). ImageJ image analysis software (NIH, USA) was utilized for cell counting. Samples were mounted with a fluoromount G (Southern Biotech) antifade mounting solution.

For cell association quantification, neuron body and extensions not touching any part of A172 cells were classified as “off”, neuron body or extensions partially on or touching any A172 cells were classified as “partial”, and neuron body completely on top of A172 cells were classified as “on”.

2.3.2b Statistics

Data were analyzed by the one-way ANOVA using a Tukey’s post-hoc test (SPSS statistics software). Differences were considered significant for $p < 0.05$. All data

were reported as mean ± standard deviation. Experiments were performed in duplicate.

2.3.3 Results and Discussion

2.3.3a Cell Density

To examine how cortical neurons and A172 cell interact together with the various substrates, the cell density was quantified via fluorescent images after 4, 24, and 72 h in culture. Although not intentionally, both cell types produced a green signal, as the A172 cells were non-specifically stained with the Alexa Fluor 488 goat antimouse IgG1 (γ1) secondary antibody. The neurons were not however non-specifically stained with the Alexa Fluor 594 goat anti-rabbit IgG (H+L) secondary antibody, and therefore the neurons were easily distinguished from the A172 cells, as they produced no red signal. The cell density of both neuron and A172 cells increased over time, albeit at differing rates, while the astrocyte extension and neurite extension lengths also visually appeared to increase in size over time (Figure 30). After the initial 4 h adhesion LbL/PEI samples had the highest number of cortical neurons (Figure 31). This is most likely due to the cationic charge of the LbL/PEI substrate, which has been found to favor neuron attachment [101]. The density of neurons on the LbL/HP and glass substrates increased over time, while neuron density on the LbL/PEI remained constant. By the end of 72 h all three samples had similar adhered neuron densities. It is possible the most of the adhered neurons on the LbL/PEI substrates differentiated rapidly upon adhering to the substrate, while many of the adhered neurons on the LbL/HP substrates may have proliferated for dozens of hours before differentiating or did not differentiate at all. This is not unusual, as previous research has found that embryonic cortical neurons [152] and hippocampal neurons [153] can proliferate on polymer-coated substrates for

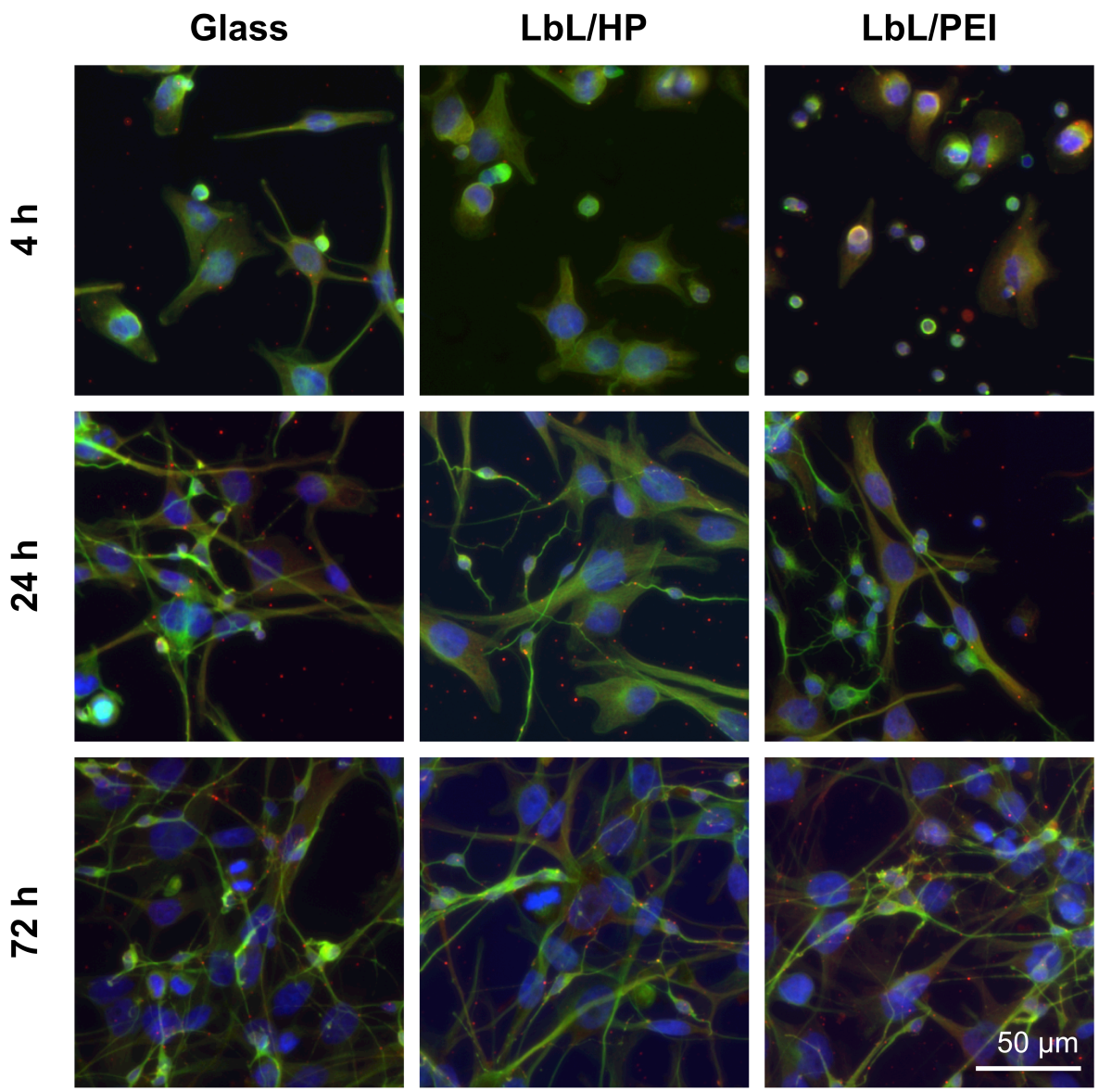


Figure 30 Representative fluorescent images of primary chick cortical neurons and A172 cells on LbL/HP and control substrates over 3-day co-culture (GFAP: red, α-tubulin: green, nuclei: blue).

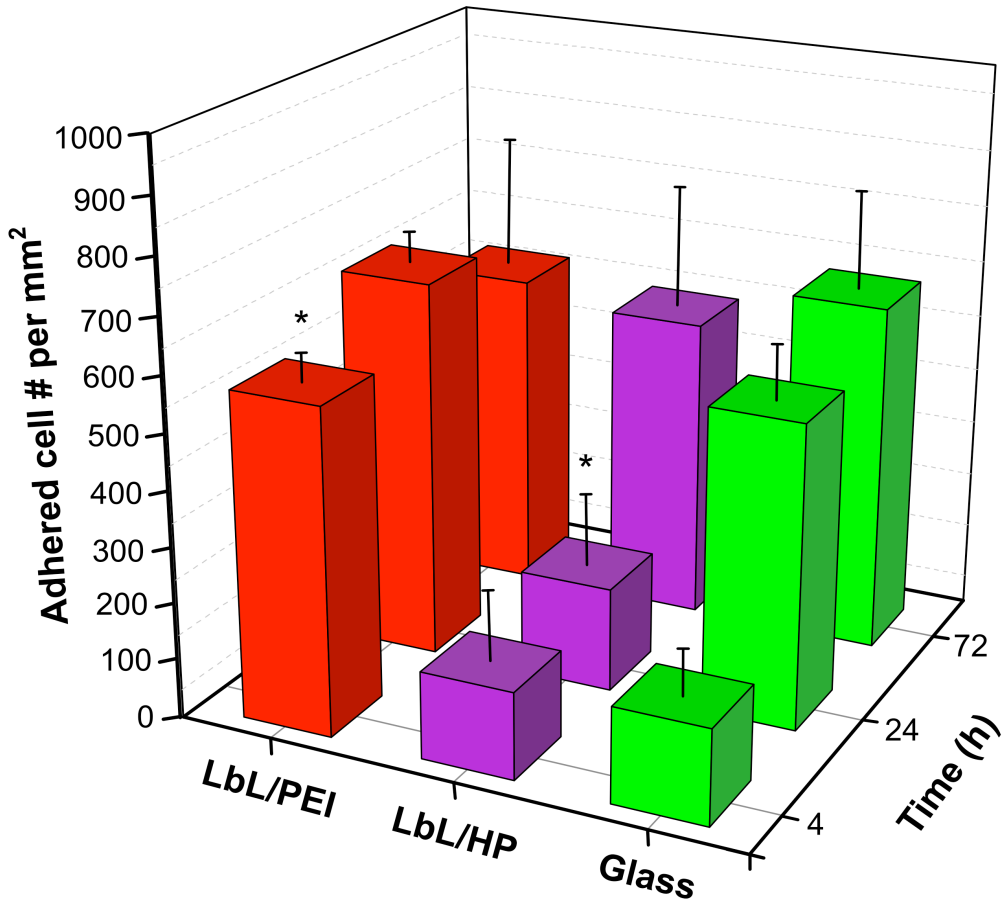


Figure 31 Primary chick cortical neuron adherent cell density on LbL/HP and control substrates for 3-day co-culture (*$p < 0.05$, compared to glass at each time point).

several days. It is possible the density increase of neurons on glass substrates from 4 to 24 h may also be due to proliferation or to a slow rate of neuron adhesion to the substrate. It has also been found that distinctive cationic polymer substrates can elicit different degrees of neuronal maturation [154]. Over time the majority of cortical neuron cell bodies tended to congregate together with their neurites forming extensive networks (Figure 30). This is in agreement with typical behavior of differentiated cortical neurons [101].

Conversely with A172 cell initial adhesion, all samples types had similar cell density after 4 h (Figure 32). The A172 cell adhesion density on LbL/HP and LbL/PEI was about 120 cells/mm^2, which is similar to previous studies of monoculture A172 cells (Figure 26) on like substrates. After 24 h, A172 cells on both LbL/HP and LbL/PEI substrates adhered in lower number compared to cells on glass substrates. A172 cell density on all sample types increased over time. It is possible the neurons on the LbL/HP surface may have an effect on mitigating A172 proliferation, however more extensive research is needed to confirm this.

2.3.3b Cell-Cell Association

Besides cell density, it is important to examine the association of the cell types with one another. Figure 33 shows the amount of neurons associated with the A172 cells after 4 h. It was challenging to distinguish cell association after this time point, since the cell extensions were long and typically encountered several cells. This type of cell interwoven network behavior has been seen before in other neuron-astrocyte direct contact co-cultures on cationically charged polymer substrates [155]. Compared to glass, cortical neurons on the LbL/HP and LbL/PEI samples had on average a

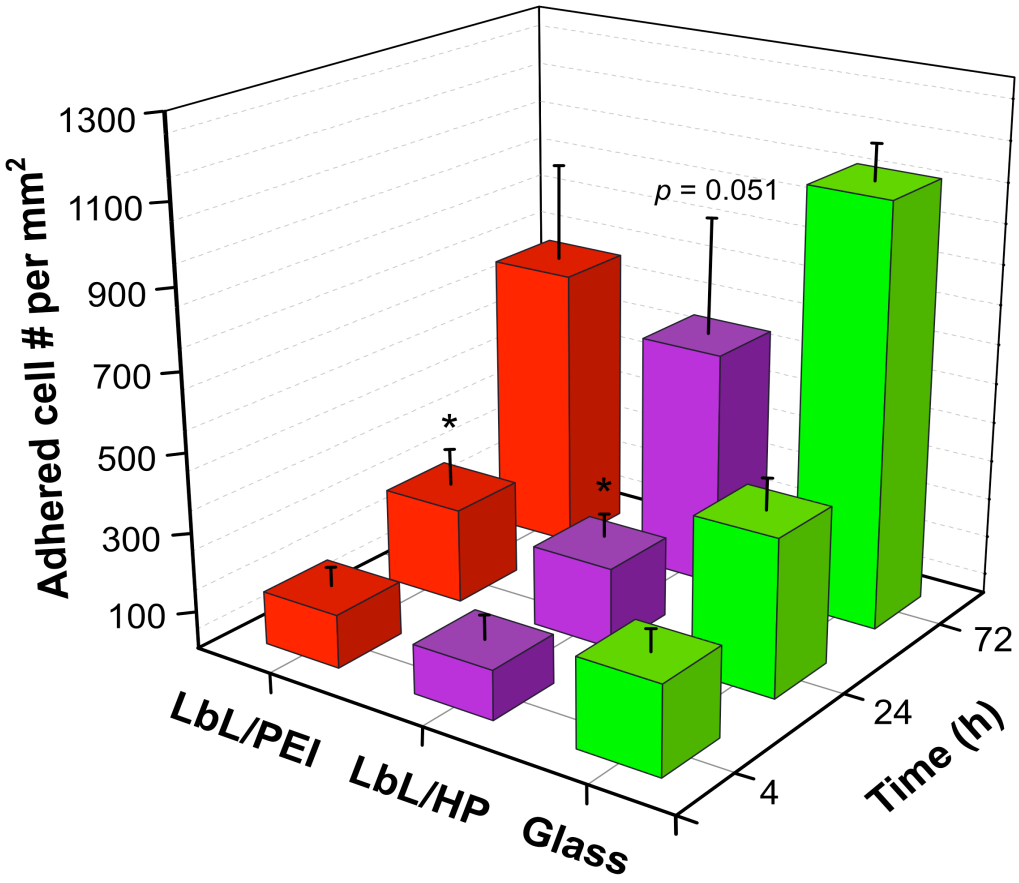


Figure 32 A172 adherent cell density on LbL/HP and control substrates for 3-day co-culture (*$p < 0.05$, compared to glass at each time point).

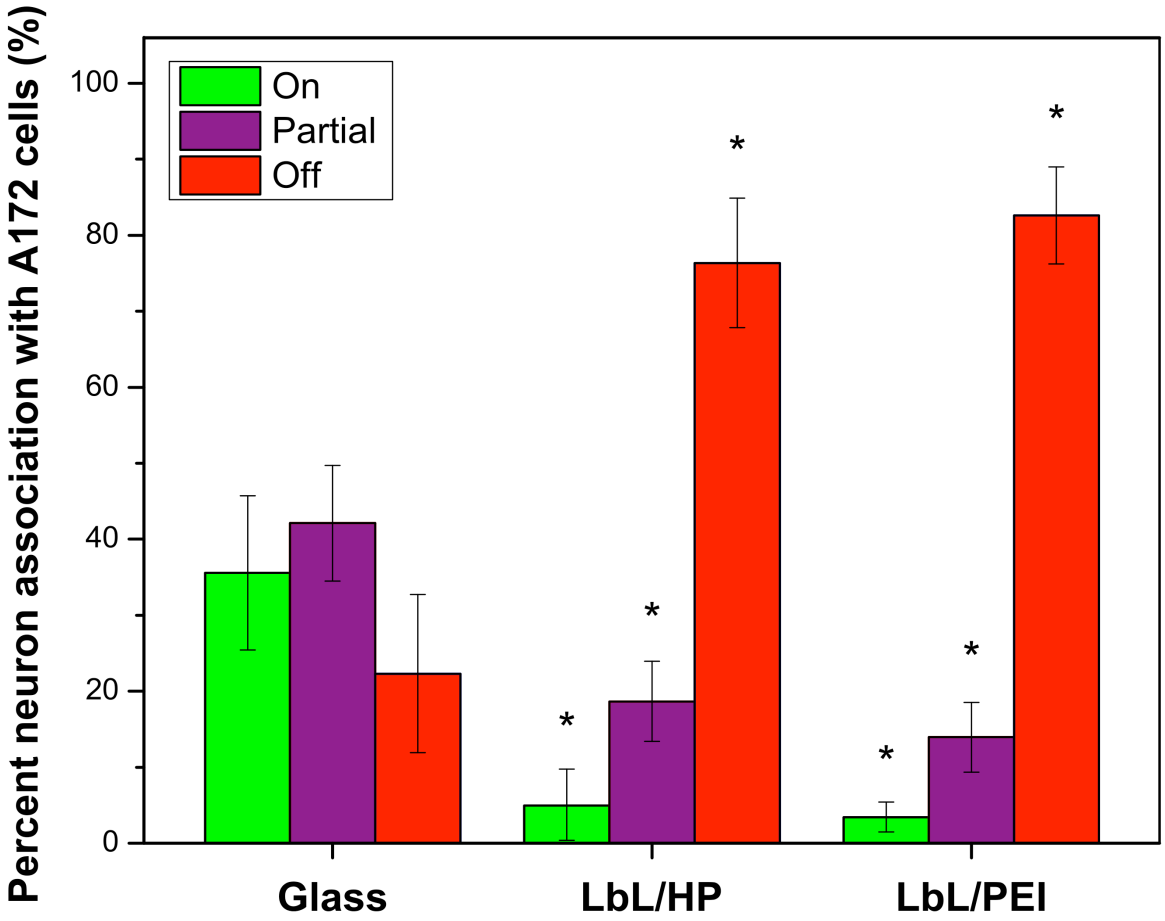


Figure 33 Percent primary chick cortical neuron association with A172 cells after 4 h co-culture (*p < 0.01, compared to glass for each condition).

significantly higher percentage of neurons associated on the substrate only and a significantly lower percentage of neuron partially or fully associated with A172 cells. This is most likely due to the cationic charge of HP and PEI substrates being favorable for neuron attachment [90, 101].

2.3.4 Conclusions

Since neurons and glial cells directly interact in the CNS, it is important to elucidate how cell-cell interaction can modulate cell and HP-modified substrate interaction. To our knowledge, no primary chick cortical neuron and A172 direct cell co-culture have previously been performed. Although only a proof of concept, this information has helped lay the foundation for more in depth co-culture studies and future in vivo studies. From this work it is evident that neuron and A172 interactions with the underlying substrate modulated their direct cell-cell involvement.

2.4 Conclusions and Future Work

From these studies, we have presented a simple and direct surface modification strategy to impart neural permissiveness to surfaces typically non-permissive to neurons. This highly desirable feature for neural interfacing applications was realized by the unique epoxy-amine clicked HP system that we have developed. The HP-modified surfaces are multifunctional imparting surface chemical cues, potential topographical and stiffness cues, and reservoirs for therapeutic molecules (discussed in further detail in chapter four) achieved in a single step for the first time. Both neuron-like PC12 cells and primary cortical neurons exhibited adhesion and differentiation confirming the HP neural permissive behavior. CNS inflammatory model cell types NIH 3T3 fibroblast, RAW 264.7 macrophage, and A172 astrocyte-like cells were not damaged by the HP-

modified surface. This could be a positive feature to help prevent negative effects of device micromotion by encouraging cellular integration on non-functional areas of the device. For future, more systematic investigations of macrophage responses to HP-modified surfaces, quantitative immunocytochemical staining will be employed to distinguish between M1 and M2 macrophages and emphasized together with other molecular-level characterizations, such as gene expression of common inflammatory markers. Additionally future research comparing the HP-modified substrates with cationically charged PEI substrates and uncharged topographically similar substrates will help illuminate which feature of the HP, charge or topography, more prominently influences the non-neuronal cellular responses, thus guiding us to refine this strategy toward more selective adhesion promoting outcomes. Other suggested future research would include cell-cell interaction of cortical and glial cells from an individual primary source. The findings of the completed and proposed studies taken together will help refine the neural implant HP surface modification strategy to ultimately advance performance, sensitivity, and longevity of neural devices.

CHAPTER THREE

GUIDED PARTICLE ADSORPTION FOR DIRECTIONAL NEURONAL GROWTH

3.1 Introduction

To provide sensitivity and long-term functionality to neural devices, it is imperative to direct neurons very close to or in contact with recording sites [120, 121]. Furthermore, for experimentation of neurons in culture, it is desirable to control the placement of cell attachment and growth. Taking advantage that native neural tissue develops with the help of contact guidance [156], polymer guidepost patterns in neural interfaces can improve assimilation of neurons onto specific areas, such as neural electrode recording sites. This has prompted several techniques to direct neuron adhesion and differentiation in a guided manner. For example methods printing patterns of cationic polymers have shown cell adhesion and neurite extension in line with patterned areas [20, 157]. Additionally, microgrooved substrate architecture width, height, and spacing have been shown to alter neurite growth rate, length, and trajectory [65, 127]. Topographical patterns with height dimension ranging from 100 nm [66] to 3 μm [60] have been implicated in studies investigating directional neurite formation and outgrowth.

A number of methods have sought to deposit such patterning onto planar surfaces. Unlike standard photolithography techniques, microfluidic and microcontact printing are desirable, as they are simple methods that do not require power or harsh solvents that could destroy sensitive printed materials [157-160]. Additionally, microextrusion printing is a highly accurate, simple, and tunable method that can

produce complex designs [161]. With its minimal toxicity of reagents, microextrusion printing is typically used in 2D and 3D cell patterning studies [162, 163].

This research investigates the application of topographical nanostructured HP patterns for directional neuronal adhesion and growth. It was hypothesized that HPs could be used as contact guidance cues to direct PC12 cell neurite outgrowth along the edge of stripe patterns. Although this was not the case for the chosen pattern width and spacing in these studies, PC12 cells were still able to preferentially adhere to HP-patterned regions of LbL-primed substrates.

3.2 Materials and Methods

3.2.1 Microfluidic Printing Technique

Microfluidic device template was fabricated by standard photolithography technique (Figure 34). Briefly, SU-8 negative photoresist film was adhered to a polished aluminum substrate by heat. Photomask pattern printed on transparency film was placed on top of a photoresist substrate and subject to UV light for 30 s, so that only transparent surfaces exposed to light were cured. All other uncured surfaces were dissolved by resist stripper chemical agents, leaving behind a raised surface of the template design. To develop the microfluidic device mold, PDMS curing agent to base (1:10) was added to the master template and cured in an oven at 60 °C for 1 h.

For HP printing, the inlet and exit of the mold was exposed, the mold was pressed onto LBL-primed surfaces, and 1 mg/mL HP solution in H_2O was added to the inlet and allowed to move through the stripped pattern to the outlet by capillary forces. After 10 min incubation, DI H_2O was added to the inlet to rinse out the HP solution, then the mold was removed. The HP-patterned surface was rinsed again with DI H_2O and

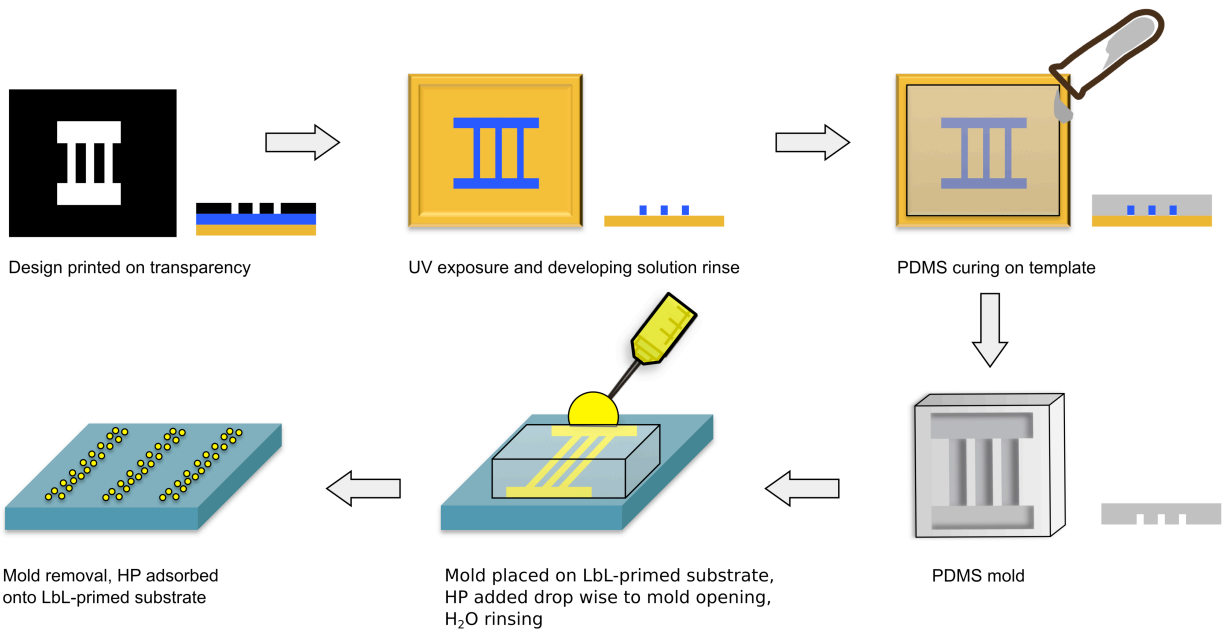


Figure 34 Schematic of microfluidic printing device fabrication process and technique.

allowed to air dry to make an HP and PSS-patterned surface. The surface HP pattern deposition was characterized by phase contrast and SEM.

3.2.2 Microcontact Printing Technique

Using a standard LP record as a master template, a PDMS curing agent to base (1:10) microcontact mold was produced (Figure 35). 1 mg/mL HP solution was added drop wise to the printing side of the mold, adsorbed for 10 min, removed, and the mold was allowed to air dry. This HP-modified side of the mold was gently pressed onto LbL-primed substrates for 2 min, removed, rinsed with DI H_2O, and allowed to air dry to make an HP and PSS-patterned surface. The surface HP pattern deposition was characterized by phase contrast and SEM. Additionally, the transfer of agents from the PDMS mold surface to the substrate was characterized by 1 mg/mL fluorescein isothiocyanate-bovine serum albumin (FITC-BSA) in 1X PBS.

3.2.3 Microextrusion Printing Technique

To produce the microextrusion ink, a solution of sodium alginate and 1X PBS was heated and stirred until well mixed. PSS in 1X PBS was then well mixed with this solution and filtered, yielding concentrations of 1.5 mg/mL sodium alginate and 1 mg/mL PSS. The pattern design was deposited with a microextruder extruding at speed 0.001 mg/mL with 30G flat tipped needle onto PEI-coated LbL-primed surfaces, allowed to adsorb for 10 min, rinsed with DI H_2O, incubated in 1 mg/mL HP solution for 10 min, again rinsed with DI H_2O, and allowed to air dry to make an HP and PEI-patterned surface (Figure 36). The surface HP pattern deposition was characterized by phase contrast and SEM.

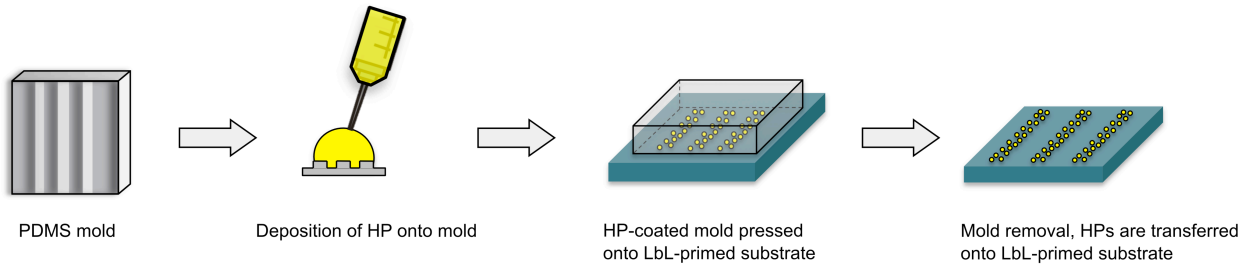


Figure 35 Schematic of microcontact printing device technique.

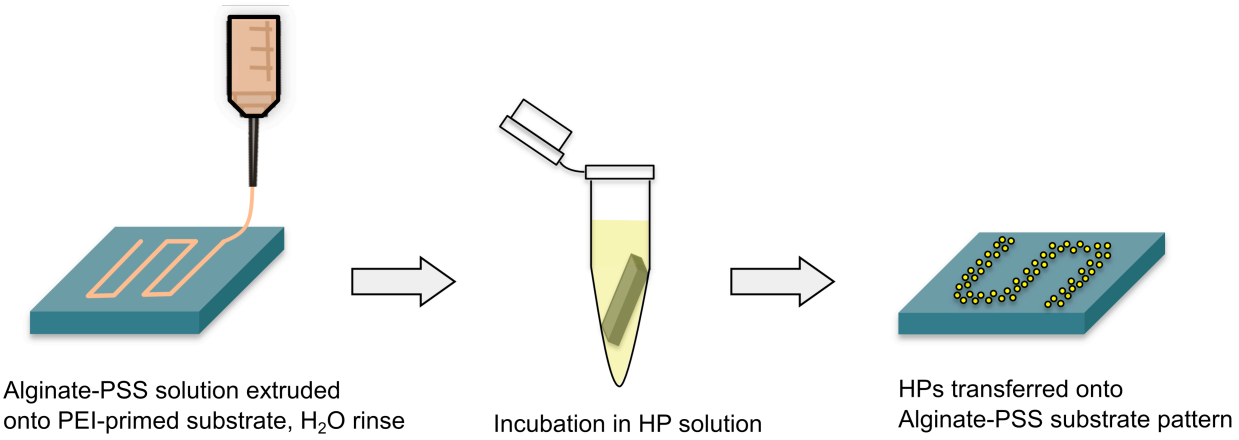


Figure 36 Schematic of microextrusion printing device technique.

3.2.4 PC12 Cell Culture

The PC12 cell line, from rat adrenal gland pheochromocytoma, was used at passages 11 – 15. The cells were maintained on T25 tissue culture flask in F-12K medium (ATCC) supplemented with 15% HS (Life Technologies), 2.5% FBS (Thermo Scientific), and 1% Anti/Anti (Life Technologies). To pass, cells were detached from flasks by mechanical force via pipetting and dispersed through a 22G x ¾ needle multiple times to acquire individual cells.

Adhesion and Differentiation Study: To evaluate how HP-patterning influences neuron adhesion and differentiation, PC12 cells were seeded at a density of either 10 000 cells/cm^2 or 40 000 cells/cm^2 onto HP-patterned glass substrates in a 35 mm dish and PLL-coated 35 mm dish control samples. Cells were allowed to attach for 24 h after which differentiation was induced by switching the medium to differentiation medium of supplemented F-12K culture medium with 1% HS, 0.2% FBS, 1% Anti/Anti, and 50 ng/mL 2.5 s NGF (BD Biosciences). Phase contrast images were taken every 24 h. After 72 h substrates were qualitatively assessed using SEM. Samples were washed with 1X PBS, fixed with 3% gluteraldehyde (Electron Microscopy Sciences, USA) for 24 h at 4 °C, and underwent processes of dehydration using a series of ascending grades of ethanol washes (25, 50, 75, and 100%). To ensure a thorough removal of water, dehydration was continued by either critical point drying or incubation in a series of 100% ethanol and HMDS mixtures at ratios of 2:1, 1:1, and 1:2, followed by complete evaporation in 100% HMDS [100]. Samples were sputter-coated with gold for 20 s at 20 mA before SEM imaging.

3.3 Results and Discussion

3.3.1 Microfluidic Printing Technique

The PDMS mold was used to construct an HP pattern in two different ways. In the first method, the PDMS mold was fabricated using standard photolithography technique, then used as a microfluidic chamber to deposit particles onto the substrate surface. The microfluidic patterning technique produced HP-patterned surfaces with uniform HP deposition but inconsistent line width (Figure 37A). The uniform HP adsorption is most likely due to the similar adsorption technique of HP solution incubated on LbL-primed surface, although not under fully submerged conditions [128]. The HP solution tended to seep under the mold-substrate contact region resulting in bulging of the stripes of the pattern and an inconsistent patterned line width. This is most likely due to the PDMS mold having insufficient contact strength with the underlying substrate as an oxygen plasma pretreatment, that is typically done to improve surface contact strength [164], was forgone due to the glass LbL treatment.

PC12 cells preferentially adhered to HP-patterned regions and not to underlying LbL-primed regions (Figure 37B). This is consistent with previous work where PC12 cells adhered to HP-modified surfaces and did not adhere to PSS-modified surfaces, which is most likely due to the cationic charge of the HPs [128]. The neurites of the differentiated PC12 cells did not have a preferred trajectory (Figure 37C). This may be due to the width of the stripe, which is a least an order of magnitude larger than most topographically patterned or polymer printed substrates that produce maximal neurite extension due to trajectory preference [165, 166].

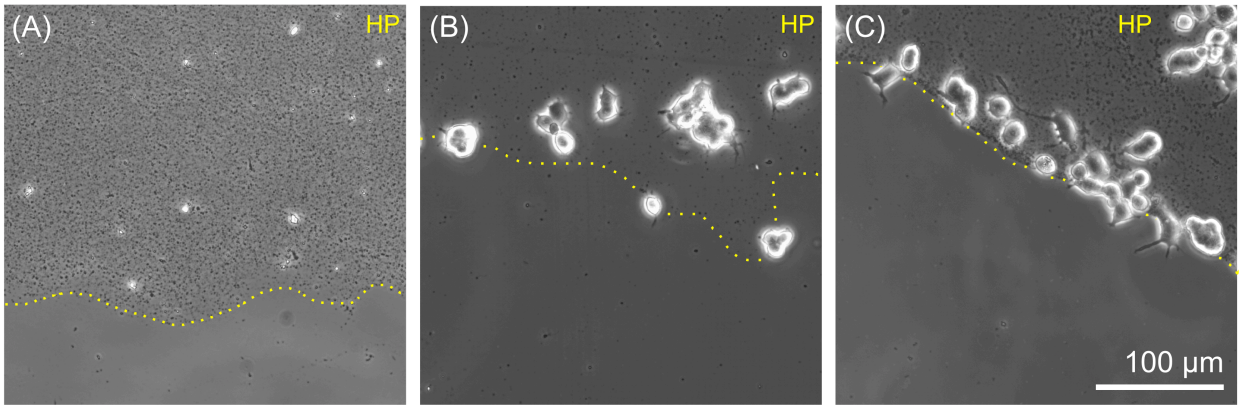


Figure 37 Microfluidic printing technique phase contrast images of (A) HP-patterned surface edge, (B) PC12 cells near HP-patterned surface edge after 24 h and (C) NGF-induced PC12 cells near HP-patterned surface edge after 72 h. Yellow dashed line signifies HP-pattern edge.

3.3.2 Microcontact Printing Technique

In the second method using the PDMS mold patterning technique, the PDMS mold was used as a microcontact printing device to deposit HPs onto the substrate surface. This method produced well-defined stripes when characterized with fluorescent BSA (Figure 38). However, occasionally the inside of the stripe pattern did not fully print onto the substrate (Figure 38B inset). This may be due to the slightly raised edges of the LP master template, where if insufficient contact pressure is pushed on the mold during printing, only the raised edges of the pattern print [167]. This method allowed for the HPs to be transferred from the mold to the LbL-primed substrate (Figure 38). Transfer of HPs in this way is most likely due to sufficient inking of the mold through hydrophobic-hydrophobic attractive forces of the PDMS and HPs [168]. The HPs were then transferred to the LbL-primed surface through electrostatic attractive forces during contact. Transfer of the pattern was inconsistent and produced areas of HP aggregation within the patterned areas (Figure 38C, Figure 39C inset). This may be a result of the raised edges of the mold pattern adsorbing HPs on their interior vertical surface, contributing to increased HP density near the pattern edge.

PC12 cells preferentially adhered to HP-printed regions over LbL-primed regions (Figure 39A). Again, this is likely due to the cationic nature of the HP-printed regions. After 72 h in vitro culture, PC12 cells did not fully differentiate on the HP-printed regions (Figure 39B). This may be due to the topography and/or charge of aggregated HP regions producing a steric hindrance effect, reducing neurite extension or preventing the neurite extension itself [169, 170]. Of the PC12 cells that did differentiate, neurites appeared to have no preference for extension direction, extending neurites on both the

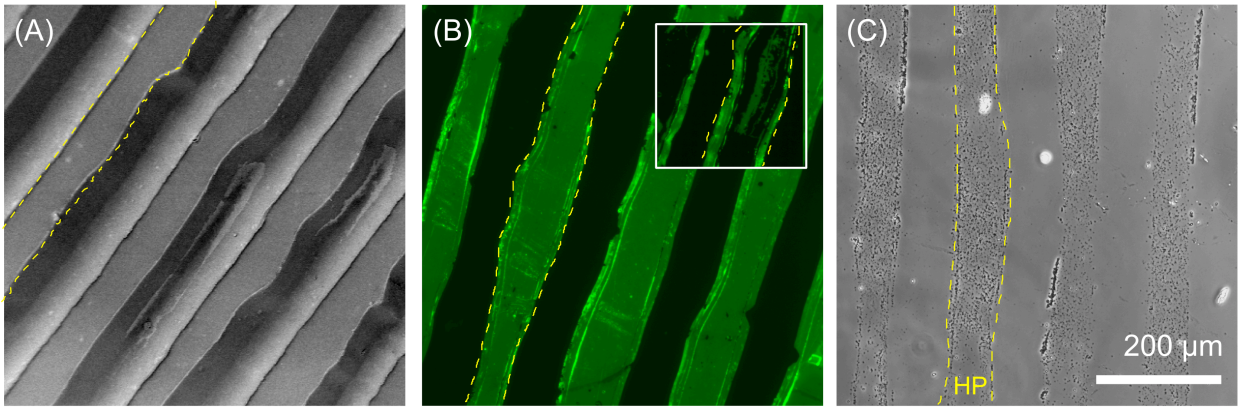


Figure 38 Microcontact printing technique (A) SEM image of LP record master template, (B) fluorescent image of FITC-BSA (green) patterned substrate, and (C) phase contrast image of HP-patterned substrate. Yellow dashed line signifies pattern edge.

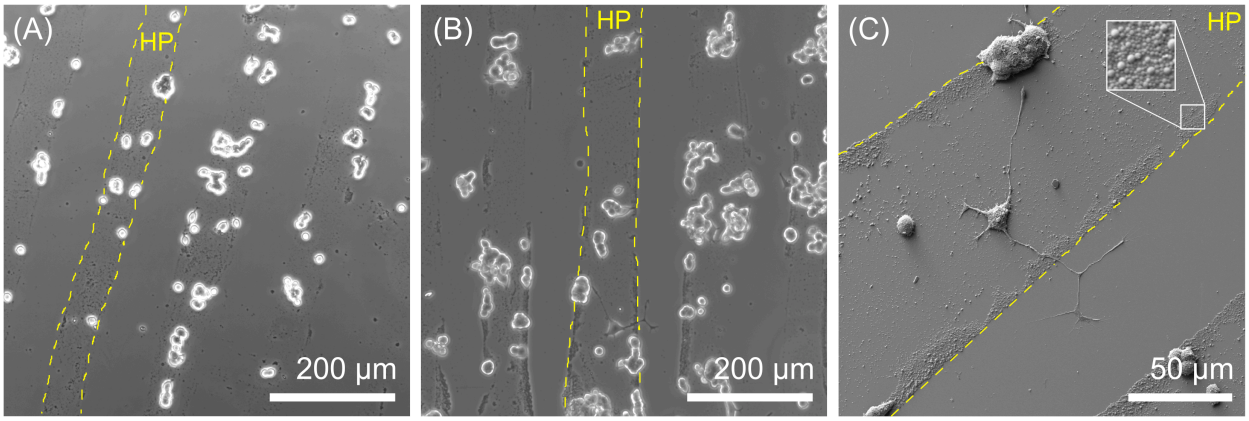


Figure 39 Microcontact printing technique (A) phase contrast image of PC12 cells on HP-patterned surface after 24 h and (B,C) NGF-induced PC12 cells on HP-patterned surface after 72 h. Yellow dashed line signifies HP-pattern edge.

HP and PSS substrate regions.

3.3.3 Microextrusion Printing Technique

Microextrusion printing technique provided a highly reproducible, consistent, and well-defined HP-printed pattern (Figure 40). The patterns can be easily changed through controlling the movement configuration of the platform that holds the substrate (Figure 40A). The width of the pattern, limited by the needle size, ink viscosity, extrusion speed, and platform speed, was minimized at roughly 400 μm (Figure 40B). As shown in Figure 40C, the HPs adsorbed uniformly onto the PSS-printed regions of the substrate due to the similar HP adsorption technique of substrates incubated fully submerged in HP solution [128].

PC12 cells adhered in equal amounts to both HP and PEI-adsorbed regions (Figure 41A-C). Again, this is likely due to the cationic nature of the both the HP and PEI polymer chemistry [90, 125, 128]. After 72 h in vitro culture, PC12 cells differentiated on both the HP and PEI regions (Figure 41D,E). Although only qualitatively assessed, it appeared that neurites extended favorably on both HP and PEI regions. When cells encountered an edge of one region, they appeared to have no preference for neurite trajectory (Figure 41D,E). It has been shown in previous research that PC12 cells differentiated to similar extents and grew similar length neurites on both HP and PEI-modified substrates [128].

3.4 Conclusions and Future Work

A number of techniques were used to guide HP deposition onto LbL-primed or PEI-coated LbL-primed substrates with varying success. Of these techniques, the microextrusion technique was the most reproducible and adjustable, that still provided

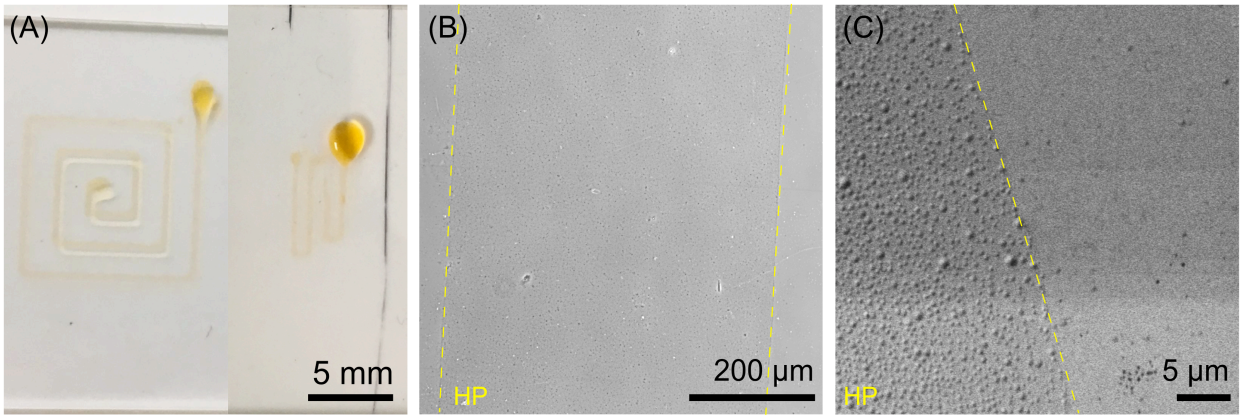


Figure 40 Microextrusion printing technique (A) photograph of patterned dyed alginate-PSS ink, (B) phase contrast image of HP-patterned surface edges, and (C) SEM image of HP-patterned surface edge. Yellow dashed line signifies HP-pattern edge.

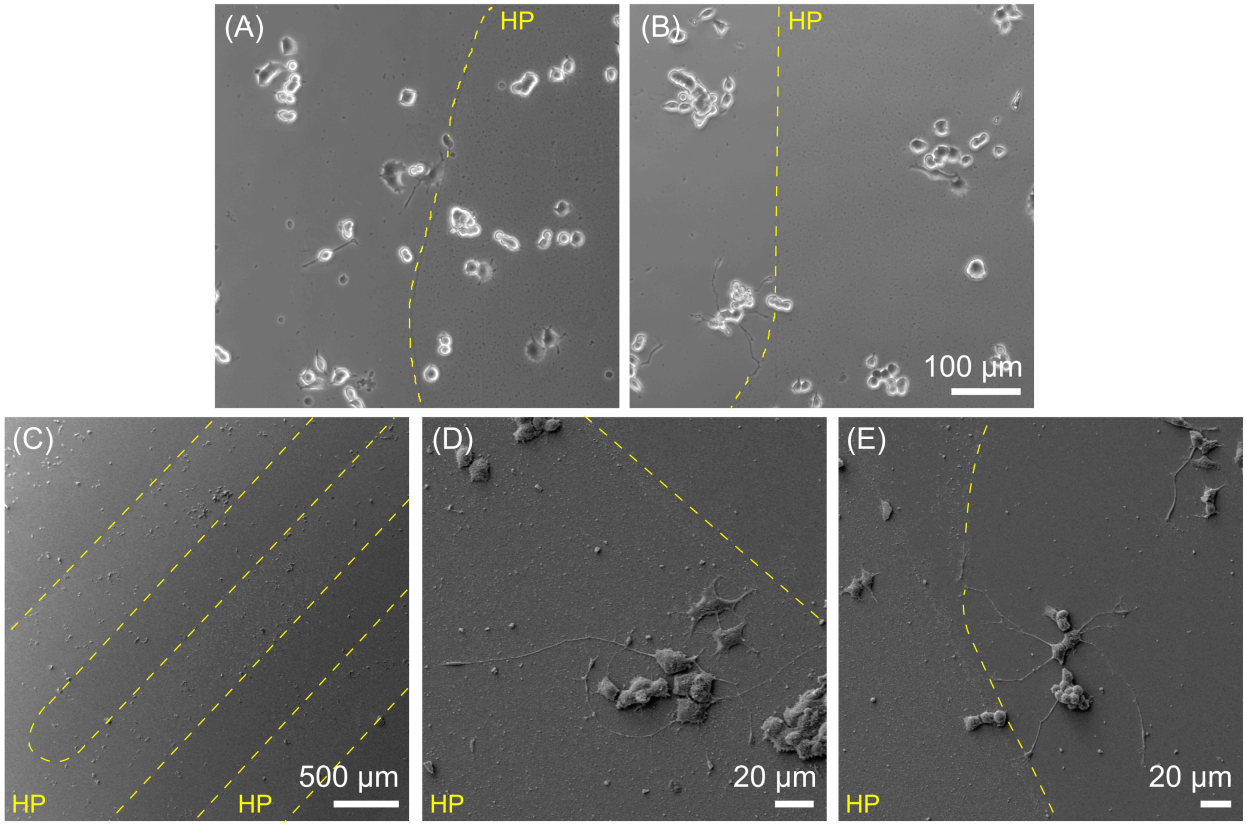


Figure 41 Microextrusion printing technique (A,B) phase contrast images of NGF-induced PC12 cells near HP-patterned surface edge after 72 h and (C,D,E) SEM images of NGF-induced PC12 cells near HP-patterned surface edge after 72 h. Yellow dashed line signifies HP-pattern edge.

consistent HP density deposition. HP-printed stripe width varied from 80 to 400 μm, depending on the technique used. PC12 cells were able to preferentially attach to HP-printed regions over LbL-primed regions, which could be useful for improving electrode functionality through guiding neuronal cells onto recording sites. After PC12 cell differentiation overtime, neurites did not have a favored trajectory possibly due the large width of space between HP-printed regions. For future experiments, more intricate photolithography and microextrusion techniques will be employed to reduce the HP stripe width and spacing. Upon successful generation of such a pattern, the HP density and surface coverage will be quantitatively determined with the goal of keeping these aspects similar to the unpatterned HP-modified substrates.

CHAPTER FOUR

CONTROLLED RELEASE OF THERAPEUTICS FROM SURFACE-ADSORBED HYDROGEL PARTICLES FOR LOCALIZED NEUROPROTECTION

4.1 Introduction

Neural devices have the potential to improve patient care and well being in a number or neurodegenerative disorders and traumatic brain injuries. With their ability to stimulate and record data from individual neurons in specific brain regions, they can provide additional insight into normal and diseased brain states [171]. For both situations to be realized, healthy neurons must be in close proximity to such devices for suitable cell-device communication [172]. While immediate device insertion into the brain physically damages neurons in the path of the device, neurons in the surrounding vicinity also suffer greatly [7]. This is due to a number of physiological circumstances, but most significantly, microglial activation. Reactive microglia can produce harmful pro-inflammatory cytokines and neurotoxic factors that can be directly toxic to neurons, act indirectly through synergistic interactions with other cytokines [11, 12] or act through interactions with other non-neuronal cells [13, 129]. The first event in microglial activation is the increase in production of ROS, such as H_2O_2 [10], which can lead to a host of other cytokine release prompting damage of neurons [7, 13, 14].

A number of therapeutic strategies have been investigated to reduce such adverse reactions of ROS towards improving neuron health near critical electrode communication zones. Strategies of particular interest employ the delivery of antioxidant agents. Local [26, 173] and systemic [27] delivery applications of antioxidants have

shown promise in reducing inflammatory responses short-term, but were not able to attenuate inflammatory responses long-term.

Besides imparting permissiveness towards typical neural device surfaces, HPs have a bonus reservoir function, which can be used to load therapeutic molecules like antioxidants. In particular, RES is an antioxidant present in grapes, wine, and berries, and has been linked to neural protective effects [174, 175] and reduced neural inflammation following an in vivo neural device implantation study [27]. The low bioavailability and rapid clearance of the free form of RES prompts the use of drug delivery mechanisms to provide its full benefits [176]. This study investigates the potential of surface-adsorbed HPs, loaded with RES, as a local reservoir for counteracting adverse effects from oxidative species.

4.2 Materials and Methods

4.2.1 Loading Capabilities of Free Hydrogel Particles

RES was dissolved at the concentration of 5 mM (1.14 mg/mL) in solvent of ethanol and 18.2 MΩ•cm ultrapure H_2O (1:1). Lyophilized HP (0.88 mg) was mixed with 1 mL RES solution and incubated on a shaker at 60 RPM for 4 h in the absence of light. After incubation, the solution was centrifuged at 21 kRCF for 10 min. Then 0.8 mL supernatant was replaced with fresh solvent and mixed. The centrifugation was repeated 5X to obtain 5 batches of supernatant. The supernatant was diluted 100X and the concentration of RES was quantified using a plate reader. The hydrodynamic diameter of the HPs was characterized using a Zetasizer nano-ZS system (Malvern Zetasizer Nanoseries, Malvern, UK).

The loaded amount of RES was calculated via subtracting accumulated amount of RES in supernatant from the original total amount. The loading efficiency was defined as the ratio between the loaded amount of RES and the mass of particles.

4.2.2 Loading Capabilities of Surface-Adsorbed Hydrogel Particles

Nile red-loaded sample preparation: Nile red, a hydrophobic dye, was used as a model drug to determine the potential of surface adsorbed HPs as reservoirs to accommodate therapeutic molecules. For the loading experiment, LbL/HP silicon substrates were incubated in nile red solution (0.1 mg/mL in DI water) at room temperature for 3 h, then rinsed with DI water and air-dried. The same process was applied on LbL/PEI silicon substrates, which were included as a control. The samples were characterized with a Zeiss Axio Observer A1 inverted fluorescent microscope (Zeiss, Germany) by capturing representative images using the same imaging parameters.

RES-loaded sample preparation: To prepare free RES and RES-loaded LbL/HP samples, RES (AstaTech, China) was sonicated covered from light at a concentration of 50 mM in a solvent of ethanol and 18.2 MΩ•cm ultrapure H_2O (1:1) until well mixed. To prepare RES-loaded LbL/HP samples, the day before cell seeding LbL/HP glass substrates were incubated in 50 mM RES solution on a mixing plate at 60 RPM protected from light for 4 h. Substrates were then rinsed 5X with solvent for 5 min each and air-dried in the hood overnight. The HP surfaces were characterized by SEM. In order to preserve surface morphology, the samples were examined directly without any conductive gold coating. For AFM characterization in air, silicon LbL/HP substrates with and without loaded RES were analyzed for topography in contact mode with an

AC240TSA-R3 (f = 70 kHz, k = 2 N/m) probe (Asylum Research, USA).

To study the water contact angle, droplets of DI H_2O (3 μL) were carefully placed on the treated substrates (n = 3), and measured using the half angle method.

4.2.3 Bioactivity of Free and Surface-Adsorbed Hydrogel Particles

Free HPs: The loaded RES amount was calculated following the aforementioned protocol, after which RES-loaded particles were concentrated for the bioactivity study. For comparison, a control group of solution with free RES was prepared at the same concentration of the RES in the particle solution. To determine the amount of active RES in the particles, 2,2-diphenyl-1-picrylhydrazyl (DPPH) solution in ethanol was mixed with the RES solution or RES-loaded particles at a 1:1 molar ratio. After 50 min incubation [177] in the absence of light, the solution was centrifuged to remove the particles, and the supernatant was taken for absorbance reading at the wavelength of 542 nm.

The bioactivity of RES was estimated from the consumed amount of DPPH in 50 min. The active percentage of RES in HPs was calculated via the ratio between the consumed amount of DPPH with particle solution and the consumed DPPH in the control group.

Surface-adsorbed HPs: Two pieces of wafers (1 cm x 1 cm) were put back-to-back vertically in one well of a 48-well plate. DPPH solution (100 μM in ethanol) was added at a volume of 1 mL. The reaction between RES and DPPH was allowed for 50 min in the absence of light. The DPPH concentration was obtained via the absorbance of solution collected at 540 nm using UV-vis spectrometer and a plate reader.

Stability: The stability of RES loaded in the particles in H_2O was investigated every 7 days for 4 weeks stored at 4 °C in the absence of light. The active percentage of RES was obtained following the procedure in the bioactivity study.

4.2.4 PC12 Cell Culture

The PC12 cell line, from rat adrenal gland pheochromocytoma, was used at passages 7 – 17. The cells were maintained on T25 tissue culture flask in F-12K medium (ATCC) supplemented with 15% HS (Life Technologies), 2.5% FBS (Thermo Scientific), and 1% Anti/Anti (Life Technologies). To pass, cells were detached from flasks by mechanical force via pipetting and dispersed through a 22G x ¾ needle multiple times to acquire individual cells.

Cell adhesion: To evaluate the influence RES loading of HP-modified substrates had on cellular adhesion, individual PC12 cells were acquired and seeded at a density of 20 000 cells/cm^2 onto the untreated LbL/HP glass substrates, solvent treated LbL/HP substrates, and RES-loaded LbL/HP substrates (n = 3) placed in a 35 mm dish. After 4 and 24 h, representative phase contrast images were taken on each sample using a Zeiss Axio Observer A1 inverted microscope (Zeiss, Germany). The number of attached cells on each sample was quantified.

50% H_2O_2 cell damage assay: A WST-1 (Roche applied science, USA) assay was used to assess cell metabolic activity. Individual PC12 cells were seeded at a density of 40 000 cells/cm^2 onto LbL/HP glass substrates (n = 4) placed per well in a 24-well plate. After a 24 h incubation at 37 °C, to keep conditions consistent for the "*Neuroprotective effect of RES"* cell study (details below), 2 cell-containing LbL/HP glass substrates and 2 LbL/HP glass substrates without cells were placed per well in a

24-well plate. Cell medium was removed and cells were treated with various concentrations of H_2O_2 (Fisher Scientific, USA) diluted in medium. After a 2 h incubation, cell-containing samples were transferred to individual wells in a 48-well plate containing 125 µL fresh medium. Next, 12.5 µL WST-1 reagent was added to each well, and incubated at 37 °C for 2 h protected from light. After mixing on a shaker for 1 min, 100 µL of each supernatant was transferred to a 96-well plate. Formazan, a chromogenic byproduct of cellular mitochondrial dehydrogenases of tetrazolium salt, was quantified using a plate reader to measure the solution absorbance at 440 nm against a blank control. The intensity of measured light absorption is directly correlated to the replication of genomic DNA and is therefore an indirect parameter regarding cell metabolic activity. Representative phase contrast images were taken for each sample using a Zeiss Axio Observer A1 inverted microscope (Zeiss, Germany) before beginning the WST-1 procedure.

Neuroprotective effect of RES: LbL/HP glass substrates were seeded with individual PC12 cells following procedures described in the previously mentioned "*50% H_2O_2 cell damage assay*". After 24 h incubation at 37 °C, medium was removed. For no treatment (-H_2O_2, -RES), 1.05 mM H_2O_2 treatment (+H_2O_2, -RES), and 1.05 mM H_2O_2 with 5.6 µm free RES treatment (+H_2O_2, +RES (free)), 2 cell-containing LbL/HP glass substrates and 2 LbL/HP glass substrates without cells were placed per well in a 24-well plate. For RES-loaded sample treatment (+H_2O_2, +RES (LbL/HP)), 2 cell-containing LbL/HP glass substrates and 2 RES-loaded LbL/HP glass substrates (+RES (LbL/HP)) without cells were placed per well in a 24-well plate upon which 1.05 H_2O_2 treatment was added. For (+H_2O_2, +RES (free)) treatment, free RES and H_2O_2 were well mixed

before addition to cell samples. All samples were incubated with the designated treatments in cell medium for 2 h at 37 °C, upon which the previously described WST-1 assay was performed.

DCF assay: 5-(and-6)-chloromethyl-2',7'-dichlorodihydrofluorescein diacetate, acetyl ester (CM-H_2DCFDA (DCF), Invitrogen, USA), a general oxidative stress indicator was used to visually indicate relative intracellular oxidative stress. Individual PC12 cells were seeded at a density of 40 000 cells/cm^2 onto LbL/HP glass substrates (n = 4) placed per well in a 24-well plate. After 24 h incubation at 37 °C, cell medium was removed and the cells were rinsed with 1X PBS + calcium + magnesium to remove any residual medium. DCF was diluted to 10 mM in 100% ethanol and serial diluted to a final concentration of 5 μM in 1X PBS + calcium + magnesium. 400 μL of DCF solution was added per well for 15 min at 37 °C, after which solution was removed and samples were allowed to recover in cell medium for 30 min at 37 °C in the absence of light. To investigate the neuroprotective effect, the RES study treatments were added as previously described and incubated with the samples for 2 h at 37 °C. The samples were rinsed with 1X PBS + calcium + magnesium and imaged in a glass bottom dish containing 1X PBS + calcium + magnesium with a Zeiss Axio Observer A1 inverted fluorescent microscope (Zeiss, Germany) under consistent imaging parameters.

4.2.5 Statistics

Data were analyzed by the one-way ANOVA using a Tukey's post-hoc test (SPSS statistics software). Differences were considered significant for $p < 0.05$. All data were reported as mean ± standard deviation.

4.3 Results and Discussion

4.3.1 Loading Capabilities of Surface-Adsorbed Hydrogel Particles

Not only can the cationic HPs adsorb onto planar substrates and improve neuron adhesion as well as support neurite outgrowth, the drug carrier function of these HPs can also be capitalized. In our previous work, we demonstrated that such HPs in suspension can readily encapsulate hydrophobic molecules, as evident from the successful loading of nile red dye as a model hydrophobic drug [32]. This attractive feature offers an unique opportunity for potential localized delivery of therapeutics that are hydrophobic in nature and beneficial for neural interfacing applications, for example, anti-inflammatory glucocorticoids [178, 179] and neuroprotective antioxidants [27, 180]. To ensure that this reservoir function is preserved even when these HPs are adsorbed on planar substrates, we carried out a loading test using nile red. As shown in Figure 42, after incubating the LbL/HP-modified silicon substrate in nile red solution, fluorescent signals were observed on the surface and the shape of the fluoresced areas resembled that of individual HPs. In contrast, negligible signal was detected on the LbL/PEI-modified control substrate following nile red incubation (Figure 42), suggesting that nile red encapsulation is neither due to nonspecific adsorption onto the underlying LbL precursor polymer layers nor due to a charge mediated effect, but largely due to hydrophobic interaction between the dye and the hydrophobic moieties of the adsorbed HPs. Based on this result, we can conclude that, even after adsorption to planar substrates, these HPs remain capable as reservoirs for hydrophobic molecules, thus expanding functionality of the HP-modified surfaces.

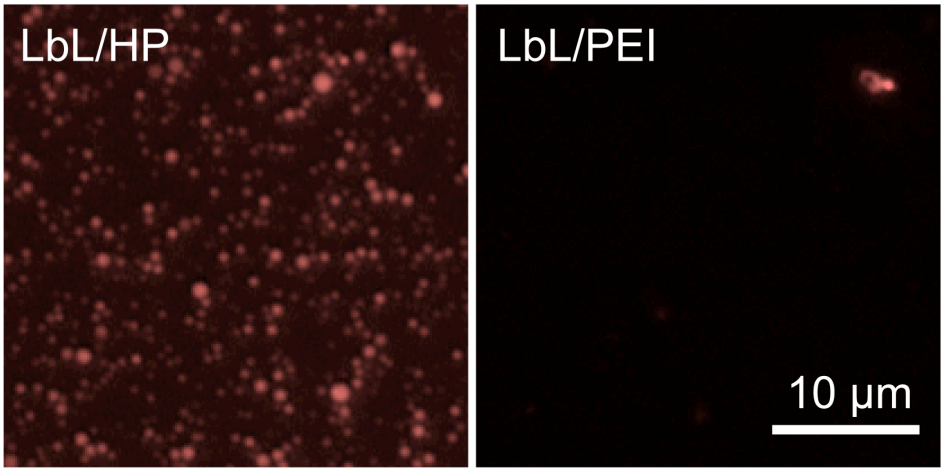


Figure 42 Fluorescent images of LbL/HP and LbL/PEI-modified planar silicon substrates after incubation in nile red solution.

4.3.2 Resveratrol Loading into Hydrogel Particles in Suspension

Prepared RES solution was successfully loaded to lyophilized HPs. The loading content was found to be 9.5%, based on the following equation:

*Drug loading content = [(wt. of RES in HPs)/(wt. of HPs)]*100*

The RES-loaded HPs were characterized by DLS. As shown in Figure 43 the hydrodynamic size of the HPs increased after RES loading. This particle size increase, likely due to hydrophobic particle and hydrophobic drug loading interaction weakening the interactions between polymer chains resulting in the swelling of the HPs, has been seen before but is not totally understood [181, 182]. RES is an amphiphilic molecule with hydrophobic aromatic rings and hydrophilic phenolic hydroxyl groups (Figure 44). In addition to the proposed hydrophobic interaction loading mechanism, research has suggested that ionic interactions of the RES and polymer particle hydroxyl or amine functional groups could contribute to RES loading [183].

The RES loaded into HPs remained bioactive and was able to scavenge free radicals, confirming its antioxidant capability (Figure 45). This effect was not due to the particles themselves. The reduced amount of scavenged DPPH free radical of the RES-loaded HPs compared to free RES does not necessarily mean there was a reduced amount of bioactive RES. The RES-DPPH reaction may take place outside of the HP, as the DPPH solvent, ethanol, may facilitate the extraction of RES to outside of the HP [184]. This extraction step could lead to the reaction taking place in a time dependent manner.

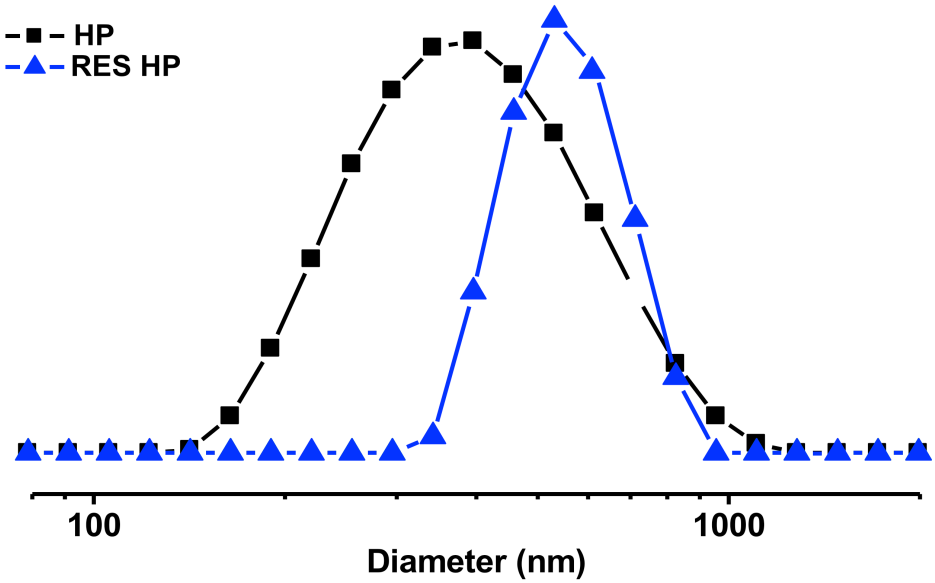


Figure 43 Intensity-average hydrodynamic size distribution of blank (HP) and RES-loaded HPs (RES HP) in water.

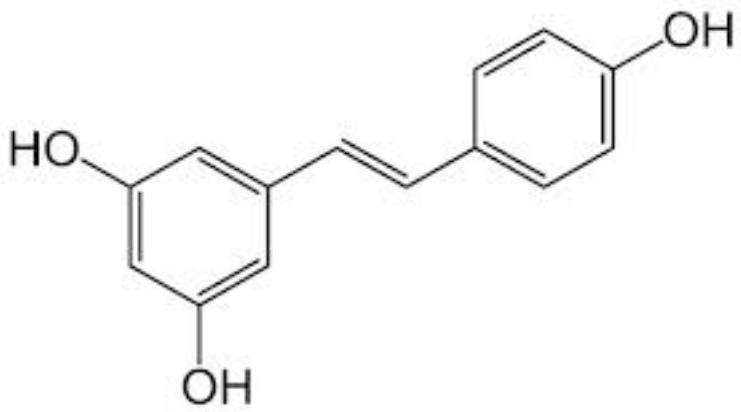


Figure 44 Chemical structure of RES.

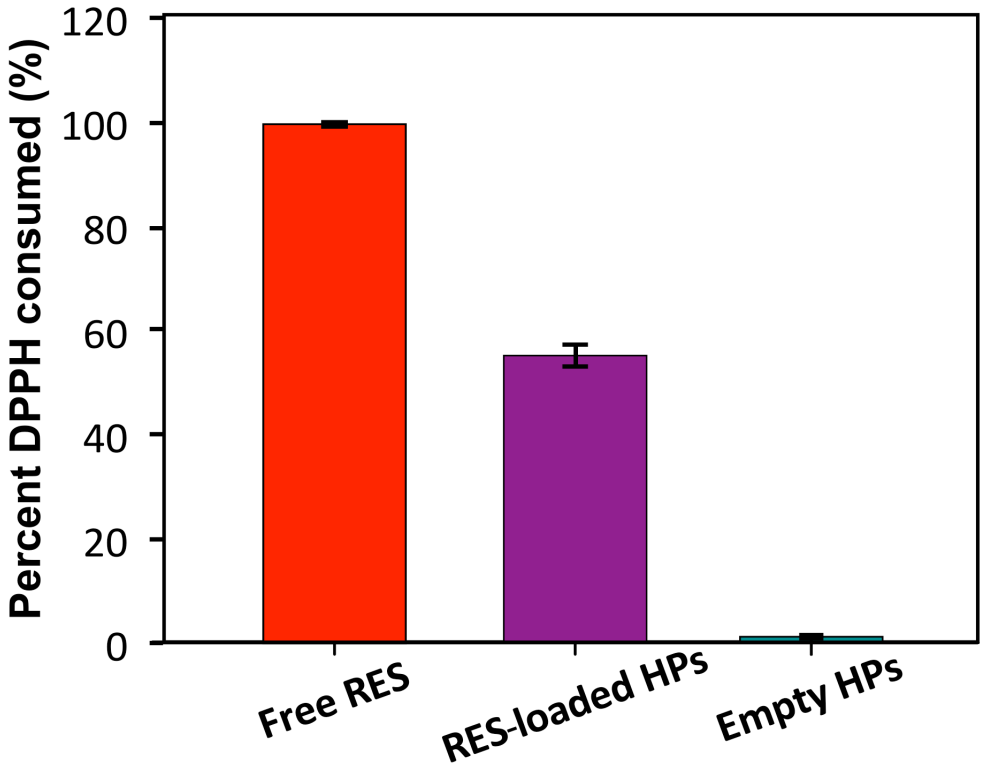


Figure 45 Activity of RES-loaded HPs and controls reacted with DPPH.

The decay of RES radical scavenging ability was significantly slower than that of free RES during the 4-week study only during the 1-week time point (Figure 46). This agrees with conclusions based on a review of research suggesting encapsulation of polyphenols in carriers has lead to improved molecule stability and bioavailability [185].

4.3.3 Characterization of Resveratrol-Loaded Surface-Adsorbed Hydrogel Particles

Using SEM (Figure 47) and AFM (Figure 48) it was found that the RES loading procedure did not compromise HP adsorption or HP morphology on the LbL-primed surface. Additionally, the activity of the RES loaded into the LbL/HP surface was maintained (Figure 49). This effect was not attributed to the particle or LbL-primed surface, as the unloaded LbL/HP control surface did not consume any free radicals. Based on prior calculations of the density of particles on the surface [128], the amount of moles of RES loaded into the LbL/HP surface was found to be 4.5 nmol/cm^2. This calculated amount was utilized when determining the amount of free RES for treatments in subsequent cell studies.

4.3.4 Surface Interaction of Neuron and Resveratrol-Loaded Hydrogel Particles

RES loading and solvent used in the RES loading procedure did not alter macroscopic hydrophilicity of HP-modified substrates (Figure 50). It was not further investigated whether RES was present on the outside surface of HPs. Regardless, we believe RES loading was not cytotoxic towards cells, as PC12 cell adhesion and growth was not significantly affected by RES loading or solvents (Figure 51). This is an important quality when considering the potential of HPs for surface modification of

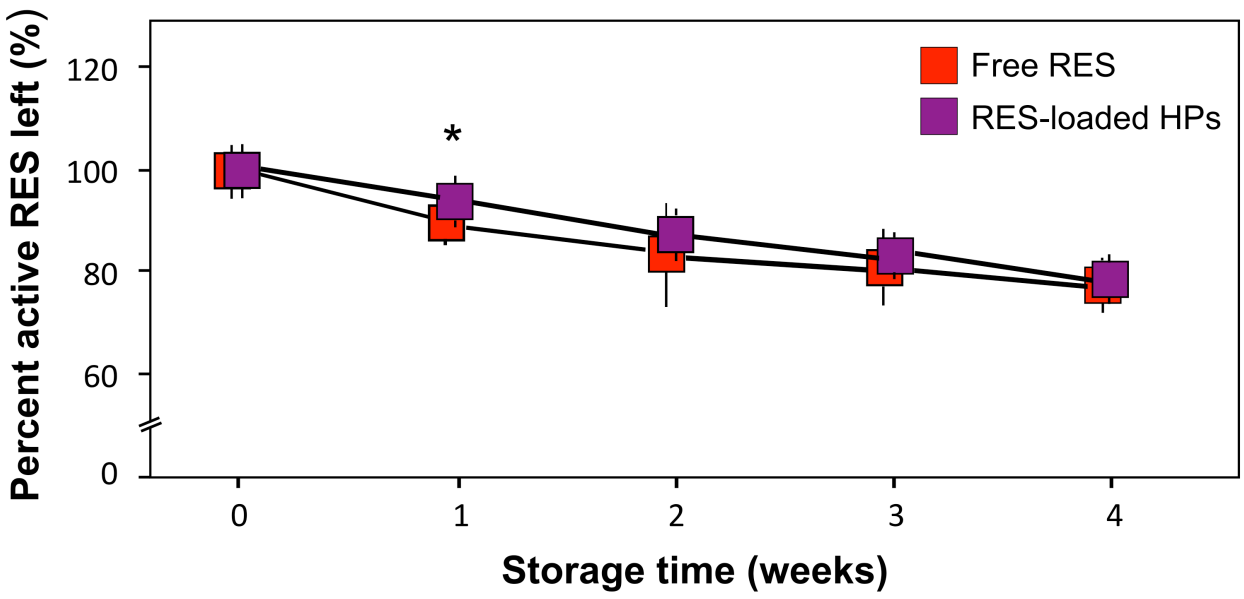


Figure 46 Stability of free RES and RES loaded to HPs over time (*$p < 0.05$, comparison between samples at each time point).

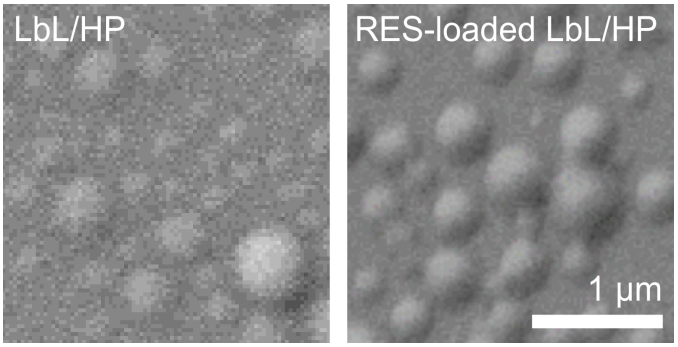


Figure 47 Representative scanning electron micrographs of unloaded LbL/HP and RES-loaded LbL/HP substrates.

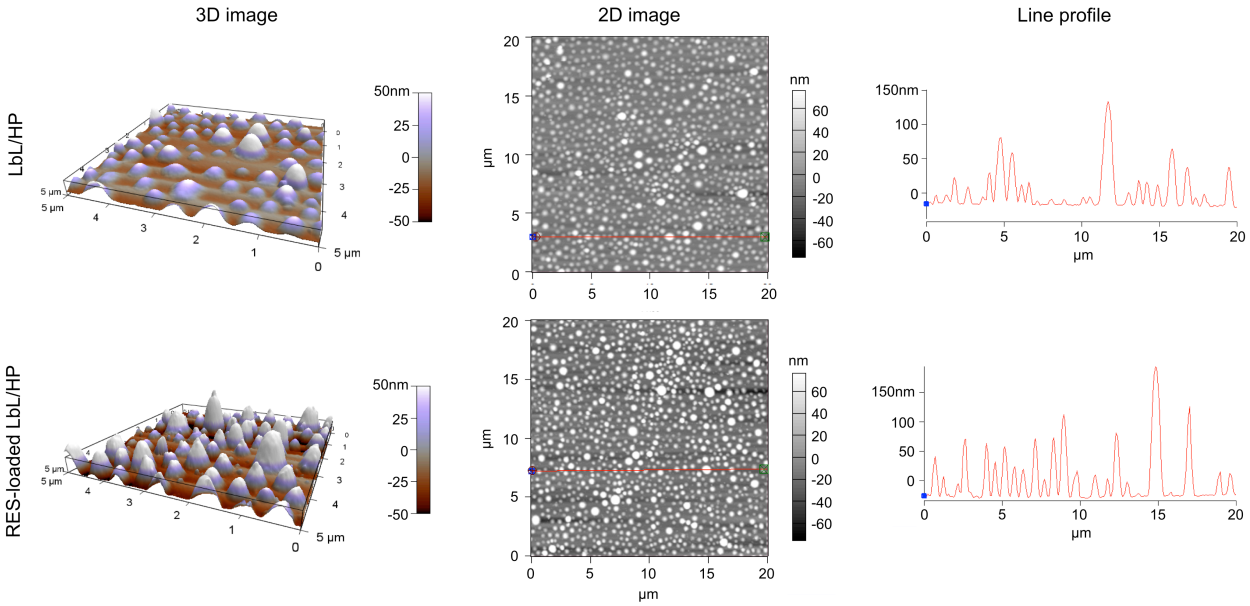


Figure 48 Representative 3D and 2D topographical images of silicon LbL/HP and RES-loaded LbL/HP substrates with line profile analysis (line profile analysis corresponds to the 2D image red line).

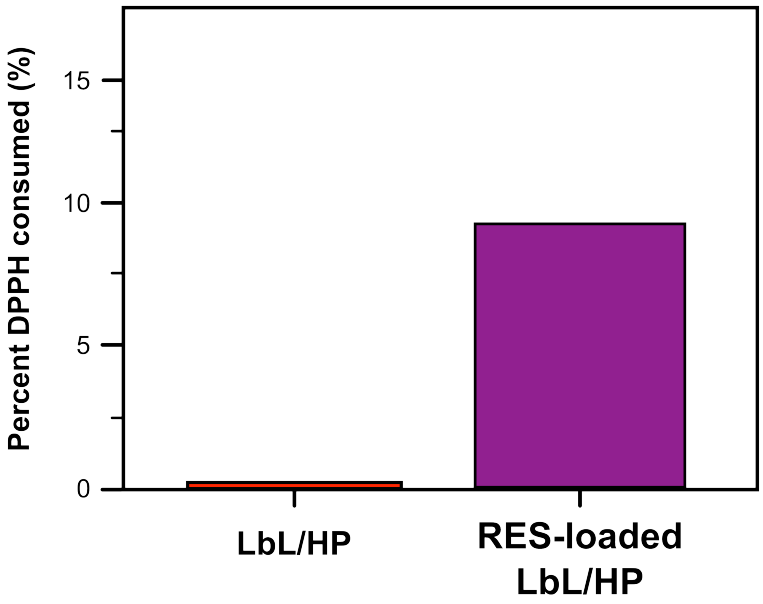


Figure 49 Activity of unloaded LbL/HP and RES-loaded LbL/HP substrates.

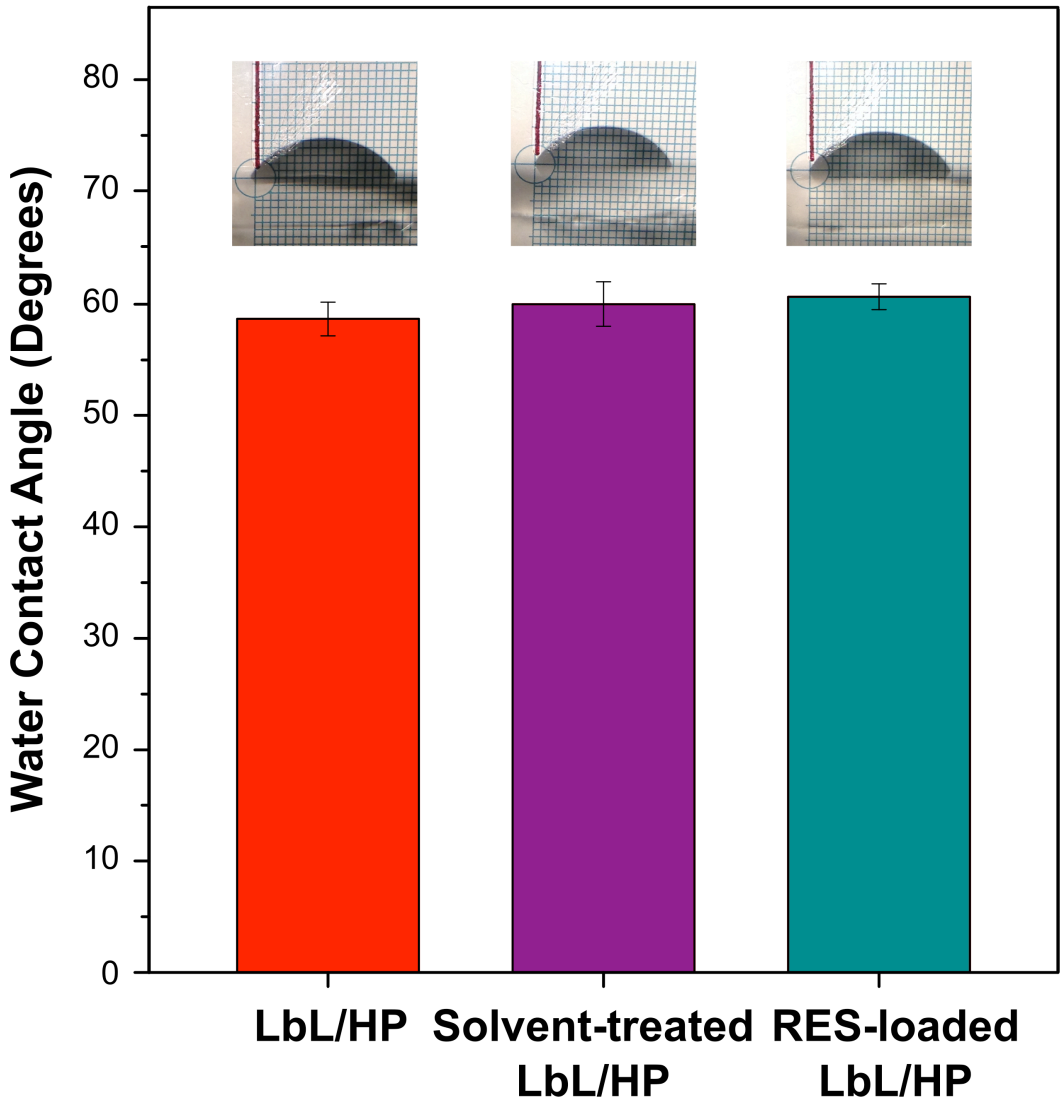


Figure 50 Water contact angle measurements and representative photographs (side view) of water droplets on RES-loaded LbL/HP and control substrates.

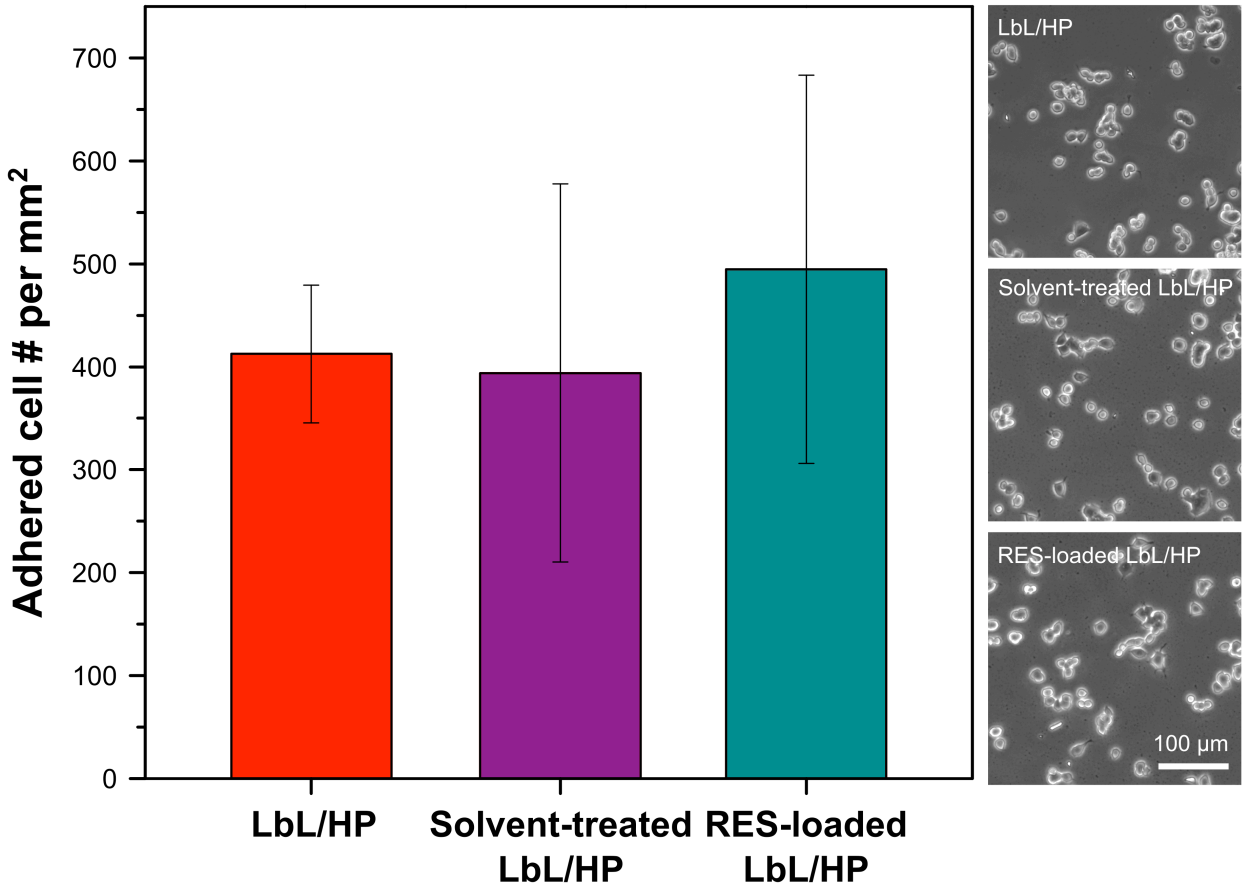


Figure 51 Representative phase contrast images of PC12 cell adhesion and quantitative adherent cell density on RES-loaded LbL/HP surfaces and controls after 24 h.

neural devices, where direct cell-device interaction is preferred. Interestingly, the solvent and RES treated groups had larger cell adhesion variation than untreated samples. This could be attributed to the exposure of the treated samples to ethanol, which the solvent contained.

4.3.5 Neuroprotective Effect of Resveratrol-Loaded Surface-Adsorbed Hydrogel Particles

PC12 cells were used to examine whether RES-loaded, HP-modified substrates were able to exert neuroprotection. First, a protocol to induce 50% cell damage was developed. Specifically, it was calculated by a WST-1 assay that 1.05 mM H_2O_2 led to 50% cell damage as determined by incubation of PC12 cells in the presence of various H_2O_2 concentrations for 2 h (Figure 52). This oxidative concentration was chosen for subsequent RES cell studies. Phase contrast imaging showed the PC12 cells became smaller and rounder as H_2O_2 concentration increased (Figure 52). This is in agreement with other studies, showing damaged PC12 cells typically present this phenotype [186, 187]. Exposure of LbL/HP to H_2O_2 for 2 h did not remove the adsorbed HPs from the surface (Figure 52 inset). As the proposed mechanism for H_2O_2 HP triggered release is due to reduction of HP crosslinking points from breakage of the 1,2-glycol linkage [32], the electrostatic interactions between the anionically charged LbL-primed surface and cationically charged amine groups of the HPs are most likely unaffected.

Although RES pre-treatment has shown to impart favorable short-term neuroprotective effects from oxidative damage [27, 186, 188], a simultaneous treatment of RES and H_2O_2 was chosen due to its similarities with the application specific purposes of the HP-modified surface design. The antioxidant activity of RES-loaded

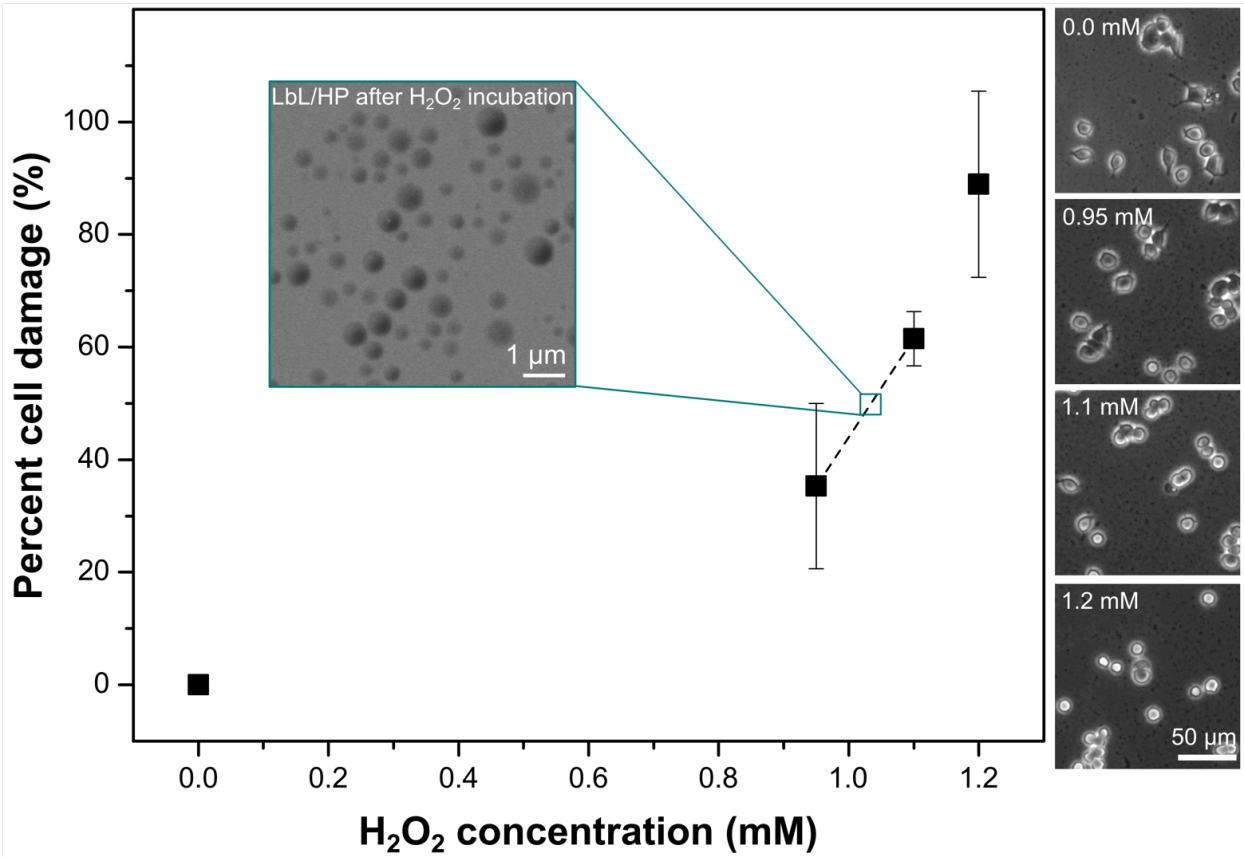


Figure 52 Percent PC12 cell damage as a function of H_2O_2 concentration with representative phase contrast images. Scanning electron microscope image of LbL/HP substrate incubated in 1.05 mM H_2O_2 for 2 h (inset).

LbL/HP substrates was then investigated. PC12 cells cultured with RES-loaded LbL/HP samples were statistically comparable to the non-treated control (Figure 53). Phase contrast images show comparable cell morphology of polygonal shaped PC12 cells with small extensions, which is consistent with healthy PC12 cell morphology, among the non-treated (-H_2O_2; -RES), free RES (+H_2O_2; +RES (free)), and RES-loaded LbL/HP (+H_2O_2; +RES (LbL/HP)) samples (Figure 53), whereas the H_2O_2 only treatment (+H_2O_2; -RES) had more rounded shaped cells, which is consistent with physically stressed PC12 cells [189]. It is possible that some of the oxidative molecules were mitigated by HPs themselves, nonetheless this was controlled for in the experimental setup.

Fluorescent imaging and quantification of DCF labeled PC12 cells showed free RES treatment (+H_2O_2, +RES (free)) promoted reduced intracellular oxidative species compared to the other treatment groups (Figure 54). Although metabolically comparable to the non-treated control (-H_2O_2; -RES), cells cultured with H_2O_2 and RES-loaded LbL/HP substrates (+H_2O_2; +RES (LbL/HP)) showed a comparable oxidative stress to cells treated with only H_2O_2 (+H_2O_2; -RES). This is unlike other research outcomes where the presence of intracellular oxidative species was directly correlated to the metabolic health of cells with RES treatment [186, 189, 190]. It is important to mention that in such previous studies all samples were pre-incubated with the antioxidant treatment, H_2O_2 concentrations were at least less than half of the concentration used in this study, and stressor incubation times ranged from brief times of 30 min [190] to significantly longer times up to 24 h [189], which accounted for many differences compared to our methods. Another contributing factor may be the proportion of RES moles to H_2O_2 moles, which was about 30% lower in our study compared to previous

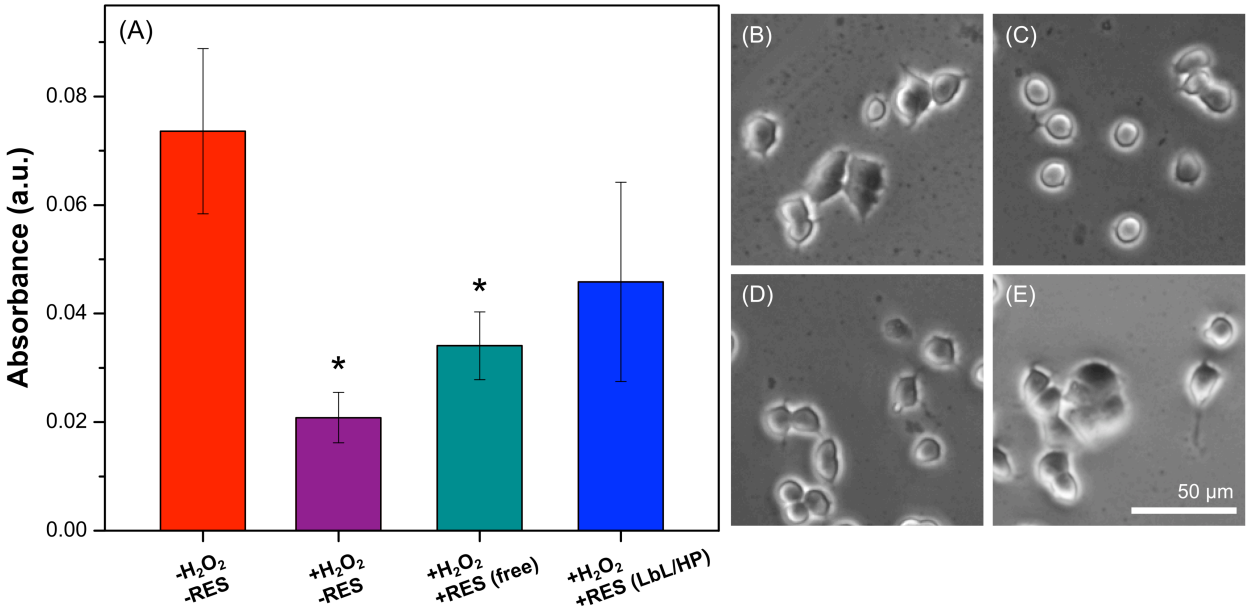


Figure 53 (A) Quantification of metabolically active PC12 cells after treatment for 2 h. Representative phase contrast images of cell morphology (B) -H_2O_2; -RES, (C) +H_2O_2; -RES, (D) +H_2O_2; +RES (free), (E) +H_2O_2; +RES (LbL/HP). (*$p < 0.05$, compared to no treatment).

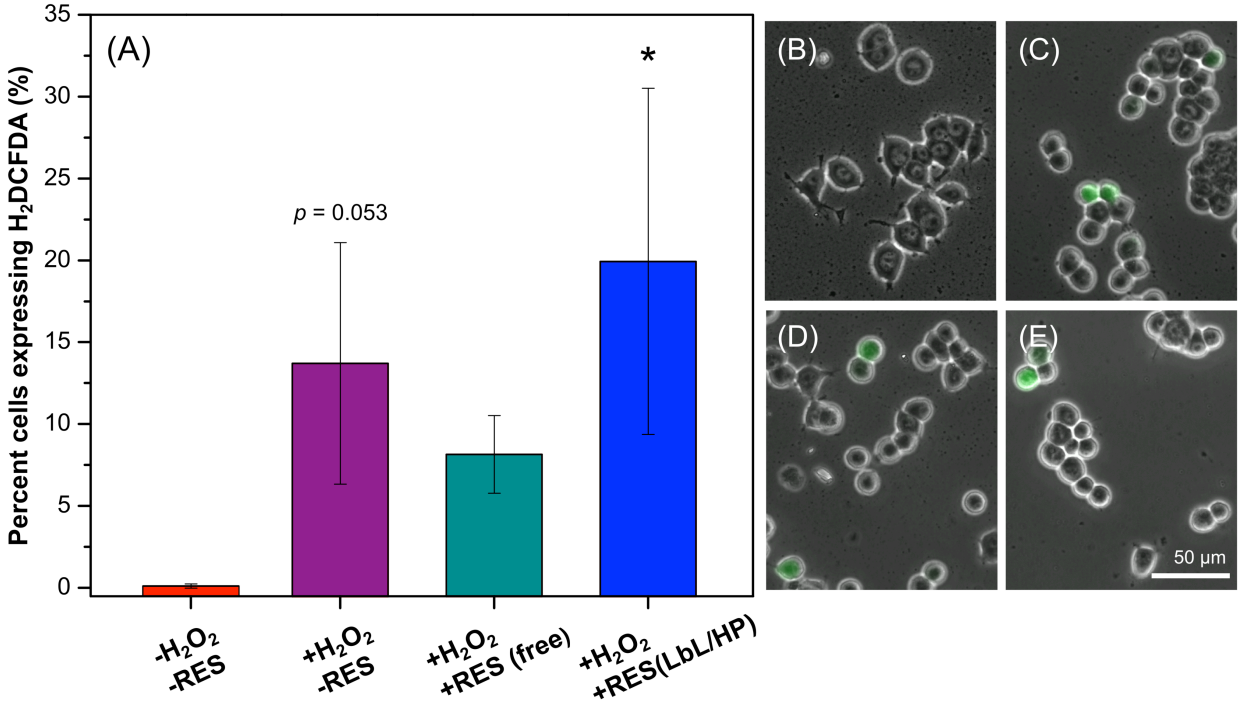


Figure 54 (A) Quantification PC12 cells presenting DCF signal after treatment for 2 h. Representative fluorescent (DCF: green) and phase contrast overlaid images of cells (B) -H_2O_2; -RES, (C) +H_2O_2; -RES, (D) +H_2O_2; +RES (free), (E) +H_2O_2; +RES (LbL/HP). (*$p < 0.05$, compared to no treatment).

research that evaluated the scavenging activity of RES with H_2O_2 to be 19.5% [191].

4.4 Conclusions and Future Work

In this research, we have presented a new functionality of loading neuroprotective agents of RES to our already multifunctional HP surface modification system. The loading mechanism of RES for free and surface-adsorbed HPs most likely takes advantage of the HP hydrophobic domains and amine and hydroxyl moieties. The loaded RES-HP complex was stable and remained bioactive over several weeks, which is an important aspect for scalable production of the strategy in the future. When prompted by an oxidative trigger, RES-loaded HPs can protect PC12 neuron-like cells' metabolic activity and promote healthy cell morphology. However under such a condition, intracellular oxidative species were still detected in cells. Elucidating the exact cause of this remains to be seen, although it may be due in part to treatment conditions of a high H_2O_2 oxidative trigger concentration over a short culture period, which was not typical of related DCF studies where cell metabolic health was consistent with DCF expression. Future research will investigate the protective mechanism of the RES-loaded HPs to counteract oxidative species, whether it be by a scavenging or release action.

CHAPTER FIVE

CONCLUSIONS AND RECOMMENDATIONS

HP-modified planar substrates were fabricated and characterized for their multiple combined unique properties. Interaction of HPs adsorbed onto planar substrates with CNS cell types including neurons and those involved in inflammatory stab models like fibroblasts, astrocytes, and macrophages were investigated. Cell interactions such as viability, adhesion, proliferation, morphology, and protein expression and secretion were qualitatively and quantitatively determined. The ability to pattern surfaces with HPs, characterization of such surfaces, and subsequent neural cell interactions were studied. RES antioxidant molecule loading capacity, stability, attenuation of oxidative stimuli, and function in promoting cell health were examined using free and surface-adsorbed HPs. The common goal of these objectives was to establish practicability of a multi-functional polymeric system for neuro-integrative materials.

The specific conclusions in this dissertation are listed below:

1. Polyetheramine based HPs were successfully used to modify solid planar surfaces through electrostatic interactions with a precursor film of alternating polyelectrolyte solutions. These surface-adsorbed particles were not removed under simulated implantation conditions.

2. The physical properties of the HP-modified surfaces, including surface density per fabrication conditions and wettability, were characterized.

3. The HP-modified planar surfaces were not cytotoxic towards cells.

4. The HP-modified planar substrates imparted favorable neural cell adhesive

properties and supported neural cell differentiation.

5. The HP-modified planar substrates supported CNS inflammatory cell type cell adhesion and proliferation.

6. The HPs adsorbed onto planar substrates were not phagocytosed by macrophages.

7. Direct cortical neuron and A172 cell-cell involvement was modulated due to underlying substrate modifications.

8. The HPs could be adsorbed onto planar substrates in a guided manner and neural cells exclusively preferentially adhered to HP-patterned regions over underlying LbL-primed regions.

9. RES therapeutic molecule loading, stability, bioactivity, and oxidative stress attenuation was capable in free and surface-adsorbed HPs.

10. Surface-adsorbed HPs loaded with RES did not affect PC12 cell adhesion.

11. RES loaded into HP-modified surfaces was able to reduce effects imposed by the oxidative agent H_2O_2.

Based on the above conclusions in this dissertation, the following future work is proposed:

1. Comparison of HP-modified substrates with cationically charged PEI substrates and uncharged topographically similar substrates will help illuminate which feature of the HP, charge or topography, more prominently influences the non-neuronal cellular responses.

2. AFM analysis of surface-adsorbed HPs under physiological hydrated conditions will reveal the particle modulus that is sensed by adhered cells and guide

experiments to tailor the HP stiffness and cell interactions.

3. Quantitative immunocytochemical staining to distinguished between pro-inflammatory (M1) and pro-healing (M2) macrophages will be emphasized together with other molecular-level characterizations, such as gene expression of common inflammatory markers, to determine reactivity of microglia to surface-adsorbed HPs.

4. Cell-cell interaction of cortical and glial cells from an individual primary source and in vivo cortical implantation to investigate glial scarring in mouse models will help illuminate potential long-term use of HP-surface modification for neural devices.

5. For future HP patterning experiments, more intricate photolithography and microextrusion techniques will be employed to reduce the HP stripe width and spacing.

6. Future research will investigate the protective mechanism of the RES-loaded HPs to counteract oxidative species, whether it be by a scavenging or release action.

LIST OF REFERENCES

[1] Schwartz AB, Cui XT, Weber DJ, Moran DW. Brain-controlled interfaces: movement restoration with neural prosthetics. Neuron. 2006;52:205-20.
[2] Gage GJ, Stoetzner CR, Richner T, Brodnick SK, Williams JC, Kipke DR. Surgical implantation of chronic neural electrodes for recording single unit activity and electrocorticographic signals. Journal of visualized experiments : JoVE. 2012:1-4.
[3] Kim Y-T, Hitchcock RW, Bridge MJ, Tresco PA. Chronic response of adult rat brain tissue to implants anchored to the skull. Biomaterials. 2004;25:2229-37.
[4] Cui X, Wiler J, Dzaman M, Altschuler RA, Martin DC. In vivo studies of polypyrrole/peptide coated neural probes. Biomaterials. 2003;24:777-87.
[5] Niclou S, Franssen E, Ehlert E, Taniguchi M, Verhaagen J. Meningeal cell-derived semaphorin 3A inhibits neurite outgrowth. Mol Cell Neurosci. 2003;24:902-12.
[6] Ness R, David S. Leptomeningeal cells modulate the neurite growth promoting properties of astrocytes in vitro. Glia. 1997;19:47-57.
[7] McConnell GC, Rees HD, Levey AI, Gutekunst CA, Gross RE, Bellamkonda RV. Implanted neural electrodes cause chronic, local inflammation that is correlated with local neurodegeneration. Journal of neural engineering. 2009;6:1-12.
[8] Sofroniew MV. Molecular dissection of reactive astrogliosis and glial scar formation. Trends in neurosciences. 2009;32:638-47.
[9] Ladeby R, Wirenfeldt M, Garcia-Ovejero D, Fenger C, Dissing-Olesen L, Dalmau I, et al. Microglial cell population dynamics in the injured adult central nervous system. Brain research Brain research reviews. 2005;48:196-206.
[10] Twig G, Jung S-K, Messerli MA, Smith PJS, Shirihai OS. Real-time detection of reactive oxygen intermediates from single microglial cells. Biol Bull. 2001;261-262.
[11] Jeohn G-H, Kong L-Y, Wilson B, Hudson P, Hong J-S. Synergistic neurotoxic effects of combined treatments with cytokines in murine primary mixed neuron/glia cultures. J Neuroimmunol. 1998;85:1-10.
[12] Chao C, Molitor T, Hu S. Neuroprotective role of IL-4 against activated microglia. J Immunol. 1993;151:1473-81.
[13] Block ML, Hong JS. Microglia and inflammation-mediated neurodegeneration: multiple triggers with a common mechanism. Prog Neurobiol. 2005;76:77-98.
[14] Polikov VS, Tresco PA, Reichert WM. Response of brain tissue to chronically implanted neural electrodes. Journal of neuroscience methods. 2005;148:1-18.
[15] Wang P, Liu Q. Cell-based biosensors: principles and applications: Artech House; 2009.
[16] Georges PC, Miller WJ, Meaney DF, Sawyer ES, Janmey PA. Matrices with Compliance Comparable to that of Brain Tissue Select Neuronal Over Glial Growth in Mixed Cortical Cultures. Biophysical journal. 2006;90:3012-8.
[17] Yu LMY, Leipzig ND, Shoichet MS. Promoting neuron adhesion and growth. Mater Today. 2008;11:36-43.
[18] Luckenbill-Edds L. Laminin and the mechanism of neuronal outgrowth. Brain Research Reviews. 1997;23:1-27.
[19] Saneinejad S, Shoichet MS. Patterned glass surfaces direct cell adhesion and process outgrowth of primary neurons of the central nervous system. Journal of Biomedical Materials Research. 1998;42:13-9.
[20] Clark P, Britland S, Connolly P. Growth cone guidance and neuron morphology on micropatterned laminin surfaces. Journal of Cell Science. 1993;105:203-12.

[21] He W, Bellamkonda RV. Nanoscale neuro-integrative coatings for neural implants. Biomaterials. 2005;26:2983-90.
[22] Ruardij TG, Goedbloed MH, Rutten WLC. Adhesion and patterning of cortical neurons on polyethylenimine- and fluorocarbon-coated surfaces. IEEE Transactions on Biomedical Engineering. 2000;47:1593-9.
[23] Liu BF, Ma J, Xu QY, Cui FZ. Regulation of charged groups and laminin patterns for selective neuronal adhesion. Colloids and Surfaces B: Biointerfaces. 2006;53:175–8.
[24] Lakard S, Herlem G, A Propperb AK, Michel G, Vallès-Villarreal N, Gharbi T, et al. Adhesion and proliferation of cells on new polymers modified biomaterials. Bioelectrochemistry. 2004;62:19–27.
[25] Roach P, Parker T, Gadegaard N, Alexander MR. Surface strategies for control of neuronal cell adhesion: a review. Surface Science Reports. 2010;65:145-73.
[26] Potter KA, Jorfi M, Householder KT, Foster EJ, Weder C, Capadona JR. Curcumin-releasing mechanically adaptive intracortical implants improve the proximal neuronal density and blood-brain barrier stability. Acta biomaterialia. 2014;10:2209-22.
[27] Potter KA, Buck AC, Self WK, Callanan ME, Sunil S, Capadona JR. The effect of resveratrol on neurodegeneration and blood brain barrier stability surrounding intracortical microelectrodes. Biomaterials. 2013;34:7001-15.
[28] Gutowski SM, Templeman KL, South AB, Gaulding JC, Shoemaker JT, LaPlaca MC, et al. Host response to microgel coatings on neural electrodes implanted in the brain. Journal of biomedical materials research Part A. 2014;102:1486-99.
[29] Cui X, Lee VA, Raphael Y, Wiler JA, Hetke JF, Anderson DJ, et al. Surface modification of neural recording electrodes with conducting polymer/biomolecule blends. J Biomed Mater Res. 2000;56:261-72.
[30] Rao L, Zhou H, Li T, Li C, Duan YY. Polyethylene glycol-containing polyurethane hydrogel coatings for improving the biocompatibility of neural electrodes. Acta biomaterialia. 2012;8:2233-42.
[31] Kojima C, Fusaoka-Nishioka E, Imai T, Nakahira A, Onodera H. Dendrigraft polylysine coated-poly(glycolic acid) fibrous scaffolds for hippocampal neurons. Journal of biomedical materials research Part A. 2016;104:2744-50.
[32] Tang S, Shi Z, Cao Y, He W. Facile aqueous-phase synthesis of multi-responsive nanogels based on polyetheramines and bisepoxide. J Mater Chem B. 2013;1:1628-34.
[33] Bettinger CJ, Langer R, Borenstein JT. Engineering substrate topography at the micro- and nanoscale to control cell function. Angewandte Chemie. 2009;48:5406-15.
[34] Mitragotri S, Lahann J. Physical approaches to biomaterial design. Nature Materials. 2008;8:15-23.
[35] Champion JA, Walker A, Mitragotri S. Role of particle size in phagocytosis of polymeric microspheres. Pharmaceutical research. 2008;25:1815-21.
[36] Tabata Y, Ikada Y. Effect of the size and surface charge of polymer microspheres on their phagocytosis by macrophage. Biomaterials. 1988;9:356-62.
[37] Oh JK, Drumright R, Siegwart DJ, Matyjaszewski K. The development of microgels/nanogels for drug delivery applications. Progress in Polymer Science. 2008;33:448-77.
[38] Boehler C, Stieglitz T, Asplund M. Nanostructured platinum grass enables superior impedance reduction for neural microelectrodes. Biomaterials. 2015;67:346-53.
[39] Chapman CA, Chen H, Stamou M, Biener J, Biener MM, Lein PJ, et al. Nanoporous

gold as a neural interface coating: effects of topography, surface chemistry, and feature size. ACS applied materials & interfaces. 2015;7:7093-100.
[40] Vinogradov SV, Bronich TK, Kabanov AV. Nanosized cationic hydrogels for drug delivery: preparation, properties and interactions with cells. Adv Drug Delivery Rev. 2002;54:135–47.
[41] Fujii A, Maruyama T, Sotani T, Ohmukai Y, Matsuyama H. pH-responsive behavior of hydrogel microspheres altered by layer-by-layer assembly of polyelectrolytes. Colloids and Surfaces A: Physicochemical and Engineering Aspects. 2009;337:159–63.
[42] Cheng G, Mi L, Cao Z, Xue H, Yu Q, Carr L, et al. Functionalizable and ultrastable zwitterionic nanogels. Langmuir : the ACS journal of surfaces and colloids. 2010;26:6883–6.
[43] Tang S, Huang L, Shi Z, He W. Water-based synthesis of cationic hydrogel particles: effect of the reaction parameters and in vitro cytotoxicity study. J Mater Chem B. 2015;3:2842-52.
[44] Hoffman AS. Hydrogels for biomedical applications. Advanced Drug Delivery Reviews. 2002;54:3-12.
[45] Lacour SP, Benmerah S, Tarte E, FitzGerald J, Serra J, McMahon S, et al. Flexible and stretchable micro-electrodes for in vitro and in vivo neural interfaces. Medical & biological engineering & computing. 2010;48:945-54.
[46] Bajpai AK, Shukla SK, Bhanu S, Kankane S. Responsive polymers in controlled drug delivery. Progress in Polymer Science. 2008;33:1088-118.
[47] Vinogradov SV, Bronich TK, Kabanov AV. Nanosized cationic hydrogels for drug delivery: preparation, properties and interactions with cells. Adv Drug Delivery Rev. 2002;54:135-47.
[48] Xia Y, Yin X, Burke NAD, Stöver HDH. Thermal response of narrow-disperse poly(N-isopropylacrylamide) prepared by atom transfer radical polymerization. Macromolecules. 2005;38:5937–43.
[49] Pelton RH, Chibante P. Preparation of aqueous latices with N-isopropylacrylamide. Colloids and Surfaces. 1986;20:247–56.
[50] Dupin D, Fujii S, Armes SP, Reeve P, Baxter SM. Efficient synthesis of sterically stabilized pH-responsive microgels of controllable particle diameter by emulsion polymerization. Langmuir : the ACS journal of surfaces and colloids. 2006;22:3381–7.
[51] Napoli A, Valentini M, Tirelli N, Müller M, Hubbell JA. Oxidation-responsive polymeric vesicles. Nature Materials. 2004;3:183 -9.
[52] Dupin D, Fujii S, Armes SP. Efficient synthesis of sterically stabilized pH-responsive microgels of controllable particle diameter by emulsion polymerization. Langmuir : the ACS journal of surfaces and colloids. 2006;22:3381-7.
[53] Raemdonck K, Demeester J, De Smedt S. Advanced nanogel engineering for drug delivery. Soft Matter. 2009;5:707-15.
[54] McGillicuddy FC, Lynch I, Rochev YA, Burke M, Dawson KA, Gallagher WM, et al. Novel "plum pudding" gels as potential drug-eluting stent coatings: controlled release of fluvastatin. Journal of biomedical materials research Part A. 2006;79:923-33.
[55] Jessell TM. Adhesion molecules and the hierarchy of neural development. Neuron. 1988;1:3–13.
[56] Goodman CS. Mechanisms and molecules that control growth cone guidance. Annu Rev Neurosci. 1996;19:341-77.

[57] Hoffman-Kim D, Mitchel JA, Bellamkonda RV. Topography, cell response, and nerve regeneration. Annual review of biomedical engineering. 2010;12:203-31.
[58] Curtis A, Wilkinson C. Topographical control of cells. Biomaterials. 1997;18:1573-83.
[59] Palka J, Whitlock KE, Murray MA. Guidepost cells. Current Opinion in Neurobiology. 1992;2:48-54.
[60] Micholt L, Gartner A, Prodanov D, Braeken D, Dotti CG, Bartic C. Substrate topography determines neuronal polarization and growth in vitro. PloS one. 2013;8:1-14.
[61] Dowell-Mesfin NM, Abdul-Karim MA, Turner AMP, Schanz S, Craighead HG, Roysam B, et al. Topographically modified surfaces affect orientation and growth of hippocampal neurons. Journal of neural engineering. 2004;1:78-90.
[62] Bugnicourt G, Brocard J, Nicolas A, Villard C. Nanoscale surface topography reshapes neuronal growth in culture. Langmuir : the ACS journal of surfaces and colloids. 2014;30:4441–9.
[63] Kundu A, Micholt L, Friedrich S, Rand DR, Bartic C, Braeken D, et al. Superimposed topographic and chemical cues synergistically guide neurite outgrowth. Lab on a Chip. 2013;13:3070-81.
[64] Turner AMP, Dowell N, Turner SWP, Kam L, Turner JN, Craighead HG, et al. Attachment of astroglial cells to microfabricated pillar arrays of different geometries. Journal of Biomeical Materials Research. 2000;51:430-41.
[65] Su WT, Liao YF, Wu TW, Wang BJ, Shih YY. Microgrooved patterns enhanced PC12 cell growth, orientation, neurite elongation, and neuritogenesis. J Biomed Mater Res, Part A. 2013;101:185-94.
[66] Johansson F, Carlberg P, Danielsen N, Montelius L, Kanje M. Axonal outgrowth on nano-imprinted patterns. Biomaterials. 2006;27:1251-8.
[67] Peng J, Zhao D, Tang X, Tong F, Guan L, Wang Y, et al. Cool microcontact printing to fabricate thermosensitive microgel patterns. Langmuir : the ACS journal of surfaces and colloids. 2013;29:11809-14.
[68] Xia Y, Tang Y, Wu H, Zhang J, Li Z, Pan F, et al. Fabrication of patterned thermoresponsive microgel strips on cell-adherent background and their application for cell sheet recovery. ACS applied materials & interfaces. 2017;9:1255-62.
[69] Schmidt CE, Leach JB. Neural tissue engineering: strategies for repair and regeneration. Annual review of biomedical engineering. 2003;5:293-347.
[70] Leach JB, Brown XQ, Jacot JG, Dimilla PA, Wong JY. Neurite outgrowth and branching of PC12 cells on very soft substrates sharply decreases below a threshold of substrate rigidity. Journal of neural engineering. 2007;4:26-34.
[71] Lyon LA, Meng Z, Singh N, Sorrell CD, John AS. Thermoresponsive microgel-based materials. Chemical Society Reviews. 2009;38:865-74.
[72] Kohli E, Han HY, Zeman AD, Vinogradov SV. Formulations of biodegradable Nanogel carriers with 5'-triphosphates of nucleoside analogs that display a reduced cytotoxicity and enhanced drug activity. Journal of controlled release : official journal of the Controlled Release Society. 2007;121:19-27.
[73] Spira ME, Hai A. Multi-electrode array technologies for neuroscience and cardiology. Nature Nanotechnology. 2013;8:83-94.
[74] Buzsaki G. Large-scale recording of neuronal ensembles. Nat Neurosci.

2004;7:446-51.
[75] Rutten WL. Selective electrical interfaces with the nervous system. Annu Rev Biomed Eng. 2002;4:407-52.
[76] Jackson A, Zimmermann JB. Neural interfaces for the brain and spinal cord--restoring motor function. Nat Rev Neurol. 2012;8:690-9.
[77] Fattahi P, Yang G, Kim G, Abidian MR. A review of organic and inorganic biomaterials for neural interfaces. Adv Mater. 2014;26:1846-85.
[78] Olsen SR, Bortone DS, Adesnik H, Scanziani M. Gain control by layer six in cortical circuits of vision. Nature. 2012;483:47-52.
[79] Hochberg LR, Serruya MD, Friehs GM, Mukand JA, Saleh M, Caplan AH, et al. Neuronal ensemble control of prosthetic devices by a human with tetraplegia. Nature. 2006;442:164-71.
[80] Gunasekera B, Saxena T, Bellamkonda R, Karumbaiah L. Intracortical recording interfaces: current challenges to chronic recording function. ACS Chem Neurosci. 2015;6:68-83.
[81] Grill WM, Norman SE, Bellamkonda RV. Implanted neural interfaces: biochallenges and engineered solutions. Annu Rev Biomed Eng. 2009;11:1-24.
[82] Spataro L, Dilgen J, Retterer S, Spence AJ, Isaacson M, Turner JN, et al. Dexamethasone treatment reduces astroglia responses to inserted neuroprosthetic devices in rat neocortex. Exp Neurol. 2005;194:289-300.
[83] Gutowski SM, Shoemaker JT, Templeman KL, Wei Y, Latour RA, Jr., Bellamkonda RV, et al. Protease-degradable PEG-maleimide coating with on-demand release of IL-1Ra to improve tissue response to neural electrodes. Biomaterials. 2015;44:55-70.
[84] He W, McConnell GC, Schneider TM, Bellamkonda RV. A novel anti-inflammatory surface for neural electrodes. Adv Mater. 2007;19:3529-33.
[85] Cao Y, He W. Synthesis and characterization of glucocorticoid functionalized poly(N-vinyl pyrrolidone)-a versatile prodrug for neural interface. Biomacromolecules. 2010;11:1298-307.
[86] Abidian MR, Corey JM, Kipke DR, Martin DC. Conducting-polymer nanotubes improve electrical properties, mechanical adhesion, neural attachment, and neurite outgrowth of neural electrodes. Small. 2010;6:421-9.
[87] Azemi E, Lagenaur CF, Cui XT. The surface immobilization of the neural adhesion molecule L1 on neural probes and its effect on neuronal density and gliosis at the probe/tissue interface. Biomaterials. 2011;32:681-92.
[88] Roach P, Parker T, Gadegaard N, Alexander MR. Surface strategies for control of neuronal cell adhesion: a review. Surf Sci Rep. 2010;65:145-73.
[89] Yavin E, Yavin Z. Attachment and culture of dissociated cells from rat embryo cerebral hemispheres on polylysine-coated surface. J Cell Biol. 1974;62:540-6.
[90] Ruegg UT, Hefti F. Growth of dissociated neurons in cuture dishes with synthetic polymeric amines. Neurosci Lett. 1984;49:319-24.
[91] Mehrishi JN. Molecular aspects of the mammalian cell surface. Prog Biophys Mol Biol. 1972;25:1-68.
[92] Dowell-Mesfin NM, Abdul-Karim MA, Turner AM, Schanz S, Craighead HG, Roysam B, et al. Topographically modified surfaces affect orientation and growth of hippocampal neurons. J Neural Eng. 2004;1:78-90.
[93] Hai A, Dormann A, Shappir J, Yitzchaik S, Bartic C, Borghs G, et al. Spine-shaped

gold protrusions improve the adherence and electrical coupling of neurons with the surface of micro-electronic devices. J R Soc, Interface. 2009;6:1153-65.
[94] Simitzi C, Efstathopoulos P, Kourgiantaki A, Ranella A, Charalampopoulos I, Fotakis C, et al. Laser fabricated discontinuous anisotropic microconical substrates as a new model scaffold to control the directionality of neuronal network outgrowth. Biomaterials. 2015;67:115-28.
[95] Raffa V, Pensabene V, Menciassi A, Dario P. Design criteria of neuron/electrode interface. The focused ion beam technology as an analytical method to investigate the effect of electrode surface morphology on neurocompatibility. Biomed Microdevices. 2007;9:371-83.
[96] Johnson CA, Lenhoff AM. Adsorption of charged latex particles on mica studied by atomic force microscopy. J Colloid Interface Sci. 1996;179:587-99.
[97] Kim M-H, Park M, Kang K, Choi IS. Neurons on nanometric topographies: insights into neuronal behaviors in vitro. Biomater Sci. 2014;2:148-55.
[98] Chen Z-J, Gillies GT, Broaddus WC, Prabhu SS, Fillmore H, Mitchell RM, et al. A realistic brain tissue phantom for intraparenchymal infusion studies. J Neurosurg. 2004;101:314-22.
[99] Leach JB, Brown XQ, Jacot JG, Dimilla PA, Wong JY. Neurite outgrowth and branching of PC12 cells on very soft substrates sharply decreases below a threshold of substrate rigidity. J Neural Eng. 2007;4:26-34.
[100] Huang L, Zhang T, Liaw PK, He W. Macrophage responses to a Zr-based bulk metallic glass. J Biomed Mater Res, Part A. 2014;102:3369-78.
[101] Sensenbrenner M, Maderspach K, Latzkovits L, Jaros GG. Neuronal cells from chick embryo cerebral hemispheres cultivated on polylysine-coated surfaces. Dev Neurosci. 1978;1:90-101.
[102] Letourneau PC. Possible roles for cell-to-substratum adhesion in neuronal morphogenesis. Dev Biol. 1975;44:77-91.
[103] Decher G, Hong J-D. Buildup of ultrathin multilayer films by a self-assembly process, 1 consecutive adsorption of anionic and cationic bipolar amphiphiles on charged surfaces. Macromolecular Symposia. 1991;46:321-7.
[104] Adamczyk Z, Siwek B, Zembala M, Belouschek P. Kinetics of localized adsorption of colloid particles. Adv Colloid Interface Sci. 1994;48:151-280.
[105] Hanarp P, Sutherland DS, Gold J, Kasemo B. Influence of polydispersity on adsorption of nanoparticles. J Colloid Interface Sci. 2001;241:26-31.
[106] Lampin M, Warocquier-Clerout R, Legris C, Degrange M, Sigot-Luizard MF. Correlation between substratum roughness and wettability, cell adhesion, and cell migration. J Biomed Mater Res. 1997;36:99-108.
[107] Fujimoto K, Takahashi T, Miyaki M, Kawaguchi H. Cell activation by the micropatterned surface with settling particles. J Biomater Sci, Polym Ed. 1997;8:879-91.
[108] Chen J, Luo G, Cao W. The study of layer-by-layer ultrathin films by the dynamic contact angle method. J Colloid Interface Sci. 2001;238:62-9.
[109] Bledi Y, Domb AJ, Linial M. Culturing neuronal cells on surfaces coated by a novel polyethyleneimine-based polymer. Brain Res Protoc. 2000;5:282-9.
[110] Vancha AR, Govindaraju S, Parsa KV, Jasti M, Gonzalez-Garcia M, Ballestero RP. Use of polyethyleneimine polymer in cell culture as attachment factor and lipofection enhancer. BMC Biotechnol. 2004;4:1-12.

[111] Song HK, Toste B, Ahmann K, Hoffman-Kim D, Palmore GT. Micropatterns of positive guidance cues anchored to polypyrrole doped with polyglutamic acid: a new platform for characterizing neurite extension in complex environments. Biomaterials. 2006;27:473-84.
[112] Mattila PK, Lappalainen P. Filopodia: molecular architecture and cellular functions. Nat Rev Mol Cell Biol. 2008;9:446-54.
[113] Bain LE, Collazo R, Hsu SH, Latham NP, Manfra MJ, Ivanisevic A. Surface topography and chemistry shape cellular behavior on wide band-gap semiconductors. Acta biomaterialia. 2014;10:2455-62.
[114] Benoit M, Gabriel D, Gerisch Gn, Gaub HE. Discrete interactions in cell adhesion measured by single-molecule force spectroscopy. Nat Cell Biol. 2000;2:313-7.
[115] Beaussart A, El-Kirat-Chatel S, Sullan RM, Alsteens D, Herman P, Derclaye S, et al. Quantifying the forces guiding microbial cell adhesion using single-cell force spectroscopy. Nature protocols. 2014;9:1049-55.
[116] Limousin P, Krack P, Pollak P, Benazzouz A, Ardouin C, Hoffmann D, et al. Electrical stimulation of the subthalamic nucleus in advanced parkinson's disease. N Engl J Med. 1998;339:1105-11.
[117] The Deep-Brain Stimulation for Parkinson's Disease Study Group. Deep-brain stimulation of the subthalamic nucleus or the pars interna of the globus pallidus in parkinson's disease. N Engl J Med. 2001;345:956-63.
[118] Boon P, Vonck K, De Herdt V, Van Dycke A, Goethals M, Goossens L, et al. Deep brain stimulation in patients with refractory temporal lobe epilepsy. Epilepsia. 2007;48:1551-60.
[119] Mayberg HS, Lozano AM, Voon V, McNeely HE, Seminowicz D, Hamani C, et al. Deep brain stimulation for treatment-resistant depression. Neuron. 2005;45:651-60.
[120] Bieberich E, Guiseppi-Elie A. Neuronal differentiation and synapse formation of PC12 and embryonic stem cells on interdigitated microelectrode arrays. Biosens Bioelectron. 2004;19:923-31.
[121] Bove M, Grattarola M, Martinoia S, Verreschi G. Interfacing cultured neurons to planar substrate microelectrodes: characterization of the neuron-to-microelectrode junction. Bioelectrochem Bioenerg. 1995;38:255-65.
[122] Khan SP, Auner GG, Newaz GM. Influence of nanoscale surface roughness on neural cell attachment on silicon. Nanomed Nanotech Biol Med. 2005;1:125-9.
[123] Schlie-Wolter S, Deiwick A, Fadeeva E, Paasche G, Lenarz T, Chichkov BN. Topography and coating of platinum improve the electrochemical properties and neuronal guidance. ACS applied materials & interfaces. 2013;5:1070-7.
[124] Kolarcik CL, Luebben SD, Sapp SA, Hanner J, Snyder N, Kozai TDY, et al. Elastomeric and soft conducting microwires for implantable neural interfaces. Soft Matter. 2015;11:4847-61.
[125] Mehrishi JN. Molecular aspects of the mammalian cell surface. Prog Biophys Mol Biol. 1972;25:1-68.
[126] Hai A, Dormann A, Shappir J, Yitzchaik S, Bartic C, Borghs G, et al. Spine-shaped gold protrusions improve the adherence and electrical coupling of neurons with the surface of micro-electronic devices. Journal of the Royal Society, Interface / the Royal Society. 2009;6:1153-65.
[127] Rajnicek AM, Britland S, McCaig CD. Contact guidance of CNS neurites on

grooved quartz: influence of groove dimensions, neuronal age and cell type. J Cell Sci. 1997;110:2905-13.
[128] Morin EA, Tang S, Rogers KL, He W. Facile use of cationic hydrogel particles for surface modification of planar substrates toward multifunctional neural permissive surfaces: an in vitro investigation. ACS applied materials & interfaces. 2016;8:5737-45.
[129] Barone F, Arvin B, White R, Miller A, Webb C, Willette R, et al. Tumor necrosis factor-α a mediator of focal ischemic brain injury. Stroke. 1997;28:1233-44.
[130] Webb K, Hlady V, Tresco PA. Relative importance of surface wettability and charged functional groups on NIH 3T3 fibroblast attachment, spreading, and cytoskeletal organization. J Biomed Mater Res. 1998;41:422-30.
[131] Kim SH, Ha HJ, Ko YK, Yoon SJ, Rhee JM, Kim MS, et al. Correlation of proliferation, morphology and biological responses of fibroblasts on LDPE with different surface wettability. J Biomater Sci Polymer Edn. 2007;18:609-22.
[132] Gilletti A, Muthuswamy J. Brain micromotion around implants in the rodent somatosensory cortex. Journal of neural engineering. 2006;3:189-95.
[133] Lee H, Bellamkonda RV, Sun W, Levenston ME. Biomechanical analysis of silicon microelectrode-induced strain in the brain. Journal of neural engineering. 2005;2:81-9.
[134] Potter KA, Buck AC, Self WK, Capadona JR. Stab injury and device implantation within the brain results in inversely multiphasic neuroinflammatory and neurodegenerative responses. Journal of neural engineering. 2012;9:1-14.
[135] Raivich G, Bohatschek M, Kloss CUA, Werner A, Jones LL, Kreutzberg GW. Neuroglial activation repertoire in the injured brain: graded response, molecular mechanisms and cues to physiological function. Brain Res Rev. 1999;30:77-105.
[136] Weldon DT, Rogers SD, Ghilardi JR, Finke MP, Cleary JP, O'Hare E, et al. Fibrillar beta-amyloid induces microglial phagocytosis, expression of inducible nitric oxide synthase, and loss of a select population of neurons in the rat CNS in vivo. J Neurosci. 1998;18:2161-73.
[137] Giulian D, Chen J, Ingeman JE, George JK, Noponen M. The role of mononuclear phagocytes in wound healing after traumatic injury to adult mammalian brain. J Neurosci. 1989;9:4416-29.
[138] Saxena T, Karumbaiah L, Gaupp EA, Patkar R, Patil K, Betancur M, et al. The impact of chronic blood–brain barrier breach on intracortical electrode function. Biomaterials. 2013;34:4703-13.
[139] Ma J, Liu L, Che G, Yu N, Dai F, You Z. The M1 form of tumor-associated macrophages in non-small cell lung cancer is positively associated with survival time. BMC Cancer. 2010;10:1-9.
[140] Campa VM, Iglesias JM, Carcedo MT, Rodriguez R, Riera J, Ramos S, et al. Polyinosinic acid induces TNF and NO production as well as NF-kappaB and AP-1 transcriptional activation in the monocyte-macrophage cell line RAW 264.7. Inflammation Research. 2005;54:328-37.
[141] Neacsu P, Mazare A, Cimpean A, Park J, Costache M, Schmuki P, et al. Reduced inflammatory activity of RAW 264.7 macrophages on titania nanotube modified Ti surface. The international journal of biochemistry & cell biology. 2014;55:187-95.
[142] Porcheray F, Viaud S, Rimaniol AC, Leone C, Samah B, Dereuddre-Bosquet N, et al. Macrophage activation switching: an asset for the resolution of inflammation. Clinical and experimental immunology. 2005;142:481-9.

[143] Colucci-Guyon E, Tinevez JY, Renshaw SA, Herbomel P. Strategies of professional phagocytes in vivo: unlike macrophages, neutrophils engulf only surface-associated microbes. J Cell Sci. 2011;124:3053-9.
[144] Gil YG, Kang MK. Capsaicin induces apoptosis and terminal differentiation in human glioma A172 cells. Life sciences. 2008;82:997-1003.
[145] Duffy PE, Huang Y-Y, Rapport MM. The relationship of glial fibrillary acidic protein to the shape, motility, and differentiation of human astrocytoma cells. Exp Cell Res. 1982;139:145-57.
[146] Davis RL, Dertien J, Syapin PJ. Ethanol-induced modulation of inducible nitric-oxide synthase activity in human A172 astrocytoma cells. Alcoholism, clinical and experimental research. 2002;26:1404-11.
[147] Volterra A, Meldolesi J. Astrocytes, from brain glue to communication elements: The revolution continues. Nat Rev Neurosci. 2005;6:626-40.
[148] Allaman I, Belanger M, Magistretti PJ. Astrocyte-neuron metabolic relationships: for better and for worse. Trends in neurosciences. 2011;34:76-87.
[149] Nedergaard M. Direct Signaling from Astrocytes to Neurons in Cultures of Mammalian Brain Cells. Science. 1994;263:1768-71.
[150] Hama H, Hara C, Yamaguchi K, Miyawaki A. PKC signaling mediates global enhancement of excitatory synaptogenesis in neurons triggered by local contact with astrocytes. Neuron. 2004;41:405-15.
[151] Costa S, Planchenault T, Charriere-Bertrand C, Mouchel Y, Fages C, Juliano S, et al. Astroglial permissivity for neuritic outgrowth in neuron-astrocyte cocultures depends on regulation of laminin bioavailability. Glia. 2002;37:105-13.
[152] Spoerri PE. Neurotrophic effects of GABA in cultures of embryonic chick brain and retina. Synapse. 1988;2:11-22.
[153] Brewer GJ. Regeneration and proliferation of embryonic and adult rat hippocampal neurons in culture. Experimental Neurology. 1999;159:237-47.
[154] Lelong I, Petegnief V, Rebel G. Neuronal cells mature faster on polyethyleneimine coated plates than on polylysine coated plates. J Neurosci Res. 1992;32:562-8.
[155] Takano H, Sul J-Y, Mazzanti ML, Doyle RT, Haydon PG, Porter MD. Micropatterned substrates: approach to probing intercellular communication pathways. Anal Chem. 2002:4640-6.
[156] Rutishauser U, Jessell TM. Cell adhesion molecules in vertebrate neural development. Physiol Rev. 1988;68:819-57.
[157] James CD, Davis R, Meyer M, Turner A, Turner S, Withers G, et al. Aligned microcontact printing of micrometer-scale poly-L-Lysine structures for controlled growth of cultured neurons on planar microelectrode arrays. IEEE Trans Biomed Eng. 2000;47:17-21.
[158] Alom Ruiz S, Chen CS. Microcontact printing: A tool to pattern. Soft Matter. 2007;3:168-77.
[159] Csucs G, Michel R, Lussi JW, Textor M, Danuser G. Microcontact printing of novel co-polymers in combination with proteins for cell-biological applications. Biomaterials. 2003;24:1713-20.
[160] Rhee SW, Taylor AM, Tu CH, Cribbs DH, Cotman CW, Jeon NL. Patterned cell culture inside microfluidic devices. Lab Chip. 2005;5:102-7.
[161] Bruneaux J, Therriault D, Heuzey M-C. Micro-extrusion of organic inks for direct-

write assembly. Journal of Micromechanics and Microengineering. 2008;18:1-11.
[162] Vozzi G, Previti A, DeRossi D, Ahluwalia A. Microsyringe-based deposition of two-dimensional and three-dimensional polymer scaffolds with a well-defined geometry for application to tissue engineering. Tissue Eng. 2002;8:1089-98.
[163] Murphy SV, Atala A. 3D bioprinting of tissues and organs. Nature biotechnology. 2014;32:773-85.
[164] Bhattacharya S, Datta A, Berg JM, Gangopadhyay S. Studies on surface wettability of poly(dimethyl) siloxane (PDMS) and glass under oxygen-plasma treatment and correlation with bond strength. Journal of Microelectromechanical Systems. 2005;14:590-7.
[165] Kam L, Shain W, Turner JN, Bizios R. Axonal outgrowth of hippocampal neurons on micro-scale networks of polylysine-conjugated laminin. Biomaterials. 2001;22:1049-54.
[166] Mahoney MJ, Chen RR, Tan J, Saltzman WM. The influence of microchannels on neurite growth and architecture. Biomaterials. 2005;26:771-8.
[167] Hui CY, Jagota A, Lin YY, Kramer EJ. Constraints on microcontact printing imposed by stamp deformation. Langmuir : the ACS journal of surfaces and colloids. 2002;18:1394-407.
[168] Lee S, Iten R, Muller M, Spencer ND. Influence of molecular architecture on the adsorption of poly(ethylene oxide)-poly(propylene oxide)-poly(ethylene oxide) on PDMS surfaces and implications for aqueous lubrication. Macromolecules. 2004;37:8349-56.
[169] Cao Z, Gilbert RJ, He W. Simple agarose-chitosan gel composite system for enhanced neuronal growth in three dimensions. Biomacromolecules. 2009;10:2954–9.
[170] Li X, Macewan MR, Xie JD, Siewe D, Yuan X, Xia Y. Fabrication of density gradients of biodegradable polymer microparticles and their use in guiding neurite outgrowth. Adv Funct Mater. 2010;20:1632-7.
[171] Cogan SF. Neural stimulation and recording electrodes. Annual review of biomedical engineering. 2008;10:275-309.
[172] Henze DA, Borhegyi Z, Csicsvari J, Mamiya A, Harris KD, Buzsáki G. Intracellular features predicted by extracellular recordings in the hippocampus in vivo. Journal of Neurophysiology 2000;84:390-400
[173] Nguyen JK, Jorfi M, Buchanan KL, Park DJ, Foster EJ, Tyler DJ, et al. Influence of resveratrol release on the tissue response to mechanically adaptive cortical implants. Acta biomaterialia. 2016;29:81-93.
[174] Sun AY, Wang Q, Simonyi A, Sun GY. Resveratrol as a therapeutic agent for neurodegenerative diseases. Mol Neurobiol. 2010;41:375-83.
[175] Ravikumar M, Jain S, Miller RH, Capadona JR, Selkirk SM. An organotypic spinal cord slice culture model to quantify neurodegeneration. Journal of neuroscience methods. 2012;211:280-8.
[176] Augustin MA, Sanguansri L, Lockett T. Nano- and micro-encapsulated systems for enhancing the delivery of resveratrol. Annals of the New York Academy of Sciences. 2013;1290:107-12.
[177] Villano D, Fernandez-Pachon MS, Moya ML, Troncoso AM, Garcia-Parrilla MC. Radical scavenging ability of polyphenolic compounds towards DPPH free radical. Talanta. 2007;71:230-5.
[178] Kim DH, Martin DC. Sustained release of dexamethasone from hydrophilic

matrices using PLGA nanoparticles for neural drug delivery. Biomaterials. 2006;27:3031-7.
[179] Zhong Y, Bellamkonda RV. Dexamethasone-coated neural probes elicit attenuated inflammatory response and neuronal loss compared to uncoated neural probes. Brain Res. 2007;1148:15-27.
[180] Cao Y, He W. Water soluble antioxidant derivative poly(triethylene glycol methyl acrylate-co-α-tocopheryl acrylate) as a potential prodrug to enable localized neuroprotection. Acta Biomater. 2013;9:4558-68.
[181] Pan X, Yao P, Jiang M. Simultaneous nanoparticle formation and encapsulation driven by hydrophobic interaction of casein-graft-dextran and beta-carotene. Journal of colloid and interface science. 2007;315:456-63.
[182] Penalva R, Esparza I, Larraneta E, Gonzalez-Navarro CJ, Gamazo C, Irache JM. Zein-based nanoparticles improve the oral bioavailability of resveratrol and its anti-inflammatory effects in a mouse model of endotoxic shock. J Agric Food Chem. 2015;63:5603-11.
[183] Sanna V, Roggio AM, Siliani S, Piccinini M, Marceddu S, Mariani A, et al. Development of novel cationic chitosan-and anionic alginate-coated poly(D,L-lactide-co-glycolide) nanoparticles for controlled release and light protection of resveratrol. International journal of nanomedicine. 2012;7:5501-16.
[184] Kedare SB, Singh RP. Genesis and development of DPPH method of antioxidant assay. Journal of food science and technology. 2011;48:412-22.
[185] Fang Z, Bhandari B. Encapsulation of polyphenols--a review. Trends in Food Science & Technology. 2010;21:510-23.
[186] Jang J-H, Surh Y-J. Protective effects of resveratrol on hydrogen peroxide-induced apoptosis in rat pheochromocytoma (PC12) cells. Mutation Research. 2001;496:181-90.
[187] Luo H, Huang J, Liao WG, Huang QY, Gao YQ. The antioxidant effects of garlic saponins protect PC12 cells from hypoxia-induced damage. The British journal of nutrition. 2011;105:1164-72.
[188] Simao F, Matte A, Pagnussat AS, Netto CA, Salbego CG. Resveratrol preconditioning modulates inflammatory response in the rat hippocampus following global cerebral ischemia. Neurochemistry international. 2012;61:659-65.
[189] Crispo JA, Ansell DR, Piche M, Eibl JK, Khaper N, Ross GM, et al. Protective effects of polyphenolic compounds on oxidative stress-induced cytotoxicity in PC12 cells. Canadian journal of physiology and pharmacology. 2010;88:429-38.
[190] Hong H, Liu GQ. Protection against hydrogen peroxide-induced cytotoxicity in PC12 cells by scutellarin. Life sciences. 2004;74:2959-73.
[191] Gülçin İ. Antioxidant properties of resveratrol: A structure-activity insight. Innovative Food Science & Emerging Technologies. 2010;11:210-8.

VITA

Emily A. Morin was born and raised in Bristol, Tennessee the *Birthplace of Country Music* and home to the NASCAR fastest half-mile. In 2012, she obtained her Bachelor of Science degree in Biomedical Engineering from The University of Tennessee (Knoxville, TN). In August 2012, she began graduate school at the University of Tennessee under the guidance of Dr. Wei He in the Department of Mechanical, Aerospace, and Biomedical Engineering.